Transport of Motile Gyrotactic Microorganisms in Viscoelastic Fluids

By:

Muhammad Bilal Arain
Reg. No. 79-FBAS/PHDMA/S17

Department of Mathematics and Statistics
Faculty of Sciences
International Islamic University Islamabad
Pakistan
2022

Microorganisms
Fluid dynamics - Mathematical models
Viscoelasticity - " "
Gyrotaxis - " "
Biomathematics

Transport of Motile Gyrotactic Microorganisms in Viscoelastic Fluids

By:

Muhammad Bilal Arain
Reg. No. 79-FBAS/PHDMA/S17

Supervised By:

Dr. Ahmed Zeeshan

Department of Mathematics and Statistics
Faculty of Sciences
International Islamic University Islamabad
Pakistan
2022

Transport of Motile Gyrotactic Microorganisms in Viscoelastic Fluids

By:

Muhammad Bilal Arain
Reg. No. 79-FBAS/PHDMA/S17

A Dissertation

Submitted in Partial Fulfillment

of the Requirements for the Degree of

DOCTOR OF PHILOSOPHY

IN

MATHEMATICS

Supervised By:

Dr. Ahmed Zeeshan

Department of Mathematics and Statistics
Faculty of Sciences
International Islamic University Islamabad
Pakistan
2022

Author's Declaration

I, **Muhammad Bilal Arain** Reg. No. **79-FBAS/PHDMA/S17** hereby state that my Ph.D. thesis, entitled: **Transport of Motile Gyrotactic Microorganisms in Viscoelastic Fluids** is my own work and has not been submitted previously by me for taking any degree from this university, **International Islamic University, Sector H-10, Islamabad, Pakistan** or anywhere else in the country/world.

At any time if my statement is found to be incorrect even after my Graduation, the university has the right to withdraw my Ph.D. degree.

Name of Student: **(Muhammad Bilal Arain)**
Reg. No. **79-FBAS/PHDMA/S17**
Dated: **23/12/2022**

Plagiarism Undertaking

I solemnly declare that research work presented in the thesis, entitled: **Transport of Motile Gyrotactic Microorganisms in Viscoelastic Fluids** is solely my research work with no significant contribution from any other person. Small contribution/help wherever taken has been duly acknowledged and that complete thesis has been written by me.

I understand the zero tolerance policy of the HEC and University, **International Islamic University, Sector H-10, Islamabad, Pakistan** towards plagiarism. Therefore, I as an Author of the above titled thesis declare that no portion of my thesis has been plagiarized and any material used as reference is properly referred/cited.

I undertake that if I am found guilty of any formal plagiarism in the above titled thesis even after award of Ph.D. degree, the university reserves the rights to withdraw/revoke my Ph.D. degree and that HEC and the University has the right to publish my name on the HEC/University Website on which names of students are placed who submitted plagiarized thesis.

Student/Author Signature: 

Name: **(Muhammad Bilal Arain)**

Certificate of Approval

This is to certify that the research work presented in this thesis, entitled: **Transport of Motile Gyrotactic Microorganisms in Viscoelastic Fluids** was conducted by **Mr. Muhammad Bilal Arain,** Reg. No. **79-FBAS/PHDMA/S17** under the supervision of **Dr. Ahmed Zeeshan.** No part of this thesis has been submitted anywhere else for any other degree. This thesis is submitted to the **Department of Mathematics & Statistics, FBAS, IIU, Islamabad** in partial fulfillment of the requirements for the degree of **Doctor of Philosophy in Mathematics, Department of Mathematics & Statistics, Faculty of Basic & Applied Sciences, International Islamic University, Sector H-10, Islamabad, Pakistan.**

Student Name: Muhammad Bilal Arain **Signature:** _____

Examination Committee:

a) **External Examiner 1:**
Name/Designation/Office Address **Signature:** _____

Prof. Dr. Masood Khan
Department of Mathematics,
QAU, Islamabad

b) **External Examiner 2:**
Name/Designation/Office Address) **Signature:** _____

Dr. Maryiam Javed
Associate Professor,
Department of Applied Mathematics & Statistics,
Institute of Space and Technology, Islamabad, Pakistan.

c) **Internal Examiner:**
Name/Designation/Office Address) **Signature:** _____

Dr. Rahmat Ellahi
Associate Professor

Supervisor Name:
Dr. Ahmed Zeeshan **Signature:** _____

Name of HOD:
Prof. Dr. Nasir Ali **Signature:** _____

Name of Dean:
Prof. Dr. Muhammad Irfan Khan **Signature:** _____

Dedication

This thesis is dedicated

to

all those who prayed for me.

Acknowledgements

I am highly grateful to my Allah who encouraged and showed me a way for completing my PhD. Allah Almighty helped me overcome all the hurdles emerging during the whole span of the study. I am also thankful to my Holy Prophet (SAW) who is a source of benediction for all humans. He (SAW) preaching inspires us to inquire and search the universe under the direction of Allah. Several other kindhearted scholars guided me to complete this uphill task. I desire to applaud their help, but insufficient space hurdles me. I believe they would understand the situation. I offer heartfelt thanks to my supervisor, Dr. Ahmed Zeeshan who facilitated me to commence my research. I found Dr. Ahmed Zeeshan a very generous person in answering my queries. It would be unfair if I ignore the cooperation extended to me by Dr. Muhammad Mubashir Bhatti, my co-supervisor. It's an honor for me to offer deep respect to my teachers Prof. Dr. Nasir Ali, Prof. Dr. Tariq Javed, Prof. Dr. Muhammad Sajid, Prof. Dr. Arshad Zia, Dr. Ahmer Mehmood, Dr. Rahmat Ellahi, and Mr. Niaz Ahmed who enabled me mustered y courage and achieved the target. I also present warm thanks to my friends Mr. Shahid Nadeem, Mr. Khawaja Tariq Mehmood, Dr. Nasir Shahzad, Mr. Waqas Nazeer, Dr. Nauman Ejaz, Mr. Muhammad Imran Khan, Mr. Amad-ur-Rehman, Mr. Zeeshan Pervaiz, Mr. Muhammad Awais, Mr. Igrar Raza how assisted me in this journey. I, with humble obedience, appreciate the role of my parents who provided the basis for my career. The prays of my colleagues, and students did wonders in accomplishing my PhD. A huge credit also goes to HEC for awarding me Indigenous scholarship which enabled me to display my potential.

Muhammad Bilal Arain

Preface

Bioconvection occurs because microorganisms, which are denser than water, swims in one direction on average results in change of density in the fluid. The microorganisms which move against the gravity are called gyrotactic microorganisms, these organisms rise upwards in a fluid. When the upper surface of the suspensions becomes too dense due to the accumulation of microorganisms, it becomes unstable, and microorganisms fall to generate bioconvection. The pattern continues since these fallen organism tries to return to the top surface. Bottom-heavy alga and some oxytactic bacteria are two forms of up swimming microorganisms widely used in bioconvection investigations. Although their bioconvection patterns are extremely similar, their orientation processes are not.

Asymmetric mass distribution causes bottom-heavy microorganisms to swim upward in motionless water. When such microorganisms are in a flow field, the swimming direction is governed by the balance of torques caused by shear flow viscous drag and gravity acting on the cell. Cells tend to swim towards regions of downwelling fluid, which is known as gyrotaxis. Experiments using oxytactic bacteria on bioconvection are carried out in a chamber with the upper level of suspensions open. These bacteria use oxygen and swim up to higher oxygen concentrations. Theoretical models for both bottom-heavy alga and oxytactic bacteria are available. Numerical simulations of bioconvection are also carried out by several researchers.

Dillon et al. [1] developed a microscale model of bacterial swimming in 1995, which portrays microorganisms as individual germs. This model takes into account with various geometries such as flagellar rotation, hydrodynamic interaction of swimming bacteria, and microbial absorption. He also simulated this model, but due of the complex geometry included in this model, only a few microorganisms were depicted in the simulation.

A particle model of chemotaxis was proposed by Hopkins and Fauci [2]. They described microorganisms as discrete particles while ignoring the geometry (such as flagellar motion). They were able to simulate numerous particles using this simplified definition of microorganisms. It was also assumed that dilute fluids were homogeneous and incompressible.

It is noticed that there is no addition to the research of viscoelastic fluid flow between rotating circular plates filled with microorganisms and nanoparticles. In the thesis, we assume that the flow in the tangential and axial direction. The viscoelastic nanofluid with motile gyrotactic microorganisms is filled between the pair of rotating plates. The famous Differential Transform scheme is used to obtain the solution of the ordinary differential equations. Padé approximation is also applied to enhance the convergence rate of the solution obtained by the Differential Transform Method. The impact of various parameters in nanoparticle concentration, velocity, temperature, and motile microorganism function is analyzed thoroughly using graphs and tabular forms.

The current thesis has been organized into nine chapters.

Chapter 1 discusses research background, motivation, objectives, outline of the thesis and semi analytical method. Chapter 2 is concern about governing equations, literature review, important terminologies, geometry of the problem. Chapter 3 focuses on transport of motile gyrotactic microorganism in nanofluid between circular rotating plates with the effect of thermal radiation. Semi Analytic technique DTM is applied with the merger of Padé approximation. Graphical results and tables are drawn to discuss the physical outcomes of the results. Chapter 4 examines transport of motile gyrotactic microorganism in nanofluid between circular rotating plates with effect of external magnetic field. Influence of different parameters are analyzed through graphs and tables. Chapter 5 investigates the transport of motile microorganism in a Carreau fluid between circular rotating plates with effects of Arrhenius kinetics. Carreau fluid is the class of viscoelastic fluid. DTM-Padé

technique is used to solve the problem. Graphs and tables are drawn to discuss the physical outcomes of the problem. Chapter 6 focuses on transport of motile gyrotactic microorganism in a Williamsons fluid between circular rotating plates embedded in porous medium. Semi-numerical technique is applied for the solution of the governing equations. Chapter 7 investigates the transport of motile gyrotactic microorganism in a Reiner-Rivlin nanofluid flow betwixt rotating circular plates alongwith induced magnetic field and activation energy. The detail model of Sutterby fluid is explained, and flow problem is solved with the help of DTM-Padé in chapter 8. The impact of activation energy and thermal radiation parameters on nanoparticle concentration and thermal profile are shown graphically and discussed in detail. Chapter 9 provides the chapter wise conclusion of research performed and future work of this thesis.

List of Symbols

	English Symbols	Units
S_Q	Squeezing Reynolds Number	-
Re	Reynolds number	-
R_Ω	Rotational Reynolds number	-
R_d	Thermal Radiation parameter	-
D_B	Brownian coefficient	-
Pe	Péclet number	-
T_0	Lower plate temperature	(K)
C_0	Concentration at lower plate	-
T_m	Mean fluid temperature	(K)
c_p	Specific heat capacity	$(Jkg^{-1}K^{-1})$
D_T	Thermophoretic coefficient	(m^2s^{-1})
F_A	Magnetic field strength in tangential direction	-
Ec	Eckert number	-
Sh	Sherwood number	-
E	Activation energy parameter	-
We	Weissenberg number	-
q_r	Radiation heat flux	-
b	Disk radius	-
Υ_{up}	Torque at upper plate	-
t	Time	(s)
S_M	Schmidt number	-
T_t	Thermophoretic parameter	-
T_b	Brownian motion parameter	-
Q_m	Mass flux	-
P_t	Prandtl number	-
B_s	Bio convection Schmidt number	-
T_1	Upper plater temperature	(K)
C_1	Concentration at upper plate	-
T	Fluid temperature	(K)
D_B	Brownian diffusivity	(m^2s^{-1})

F_A	Magnetic field strength in axial direction	-
K^*	Porosity parameter	-
Nu	Nusselt number	-
p	Pressure	-
k	Thermal conductivity	-
D_{mo}	Microorganism diffusion coefficient	-
k	Porosity parameter	-
τ	Stress tensor	-
M_0, N_0	Dimensionless quantities	-

Greek Symbols		Units
$\tilde{\alpha}$	Thermal diffusivity	-
ρ	Fluid density	$(Kgsm^{-3})$
δ	Electrical conductivity	(Sm^{-1})
μ	Fluid viscosity	(Nsm^{-2})
Γ'	Velocity of the disk	-
σ_e	Stefan Boltzmann constant	-
β_r	Mean absorption coefficient	-
Φ	Microorganism bio convection constant	-
bW_{mo}	Chemotaxis constant	(m)
$(\rho c)_p$	Nanoparticle heat capacity	-
$(\rho c)_f$	Nano fluid heat capacity	-
H_θ, H_z	Component of magnetic field	-
Λ_1	Magnetic permeability inside the plate	-
Λ_2	Magnetic permeability outside the plate	-
ξ	Angular velocity	-
D	Representative length	-
λ	Porosity parameter	-
ϕ	Nanoparticles volume fraction	-
η	Similarity variable	-
Υ_{up}	Torque at upper plate	-
Υ_{lp}	Torque at lower plate	-

Contents

Chapter 1

Preliminary

1.1 Introduction

In this chapter, research background related to title of the thesis is discussed. Related literature review is discussed briefly. Motivation and objective of the thesis is also discussed in this chapter.

1.2 Research Background

The word "bioconvection" refers to a desirable research field that encompasses a diverse range of applications in everyday life and has the potential to lead to interesting advancements in real-world. In biology, the term "bioconvection pattern" refers to convective flow of materials on large scale caused by differences in density between two materials. Movement of microbes is responsible for the variation in the density gradient. These self-propagating microorganisms are typically examined in the upper fluid region, which is significantly denser than the lower fluid region. The instability of the system is responsible for the demarcation trend of surfaces. Biofuels, enzyme biosensors, biological tissues, micro-systems, biotechnology, transportation processes, and all incooprated this phenomenon. The bioconvection process makes use of microorganisms-enhanced oil recovery. This is used to investigate variation in permeability since it is based on combined use of microorganisms and nutrients in oil-bearing zones. Based on the movement of various microorganisms in three distinct directions, the bioconvection system may be divided into three major types which are gyrotactic, chemotaxis and geotactic microorganisms. On the other hand, nanofluid bioconvection offers a wide variety of applications, such as coolants for vehicles, architectural design, processing of nanoparticles, sterilizing in thermal sciences, colloidal stability, polymer coating, etc. Over the course of the last decades or so, number of researchers studied flow of

bioconvection nanofluids through a variety of geometries. For instance, in 1995, Dillon et al. [1] developed microscale model of bacterial swimming, which showed microorganisms as sole microbes. Another model for chemotaxis was suggested by Hopkins and Fauci [2]. Turkyilmazoglu [3] evaluated the temperature and concentration gradient properties of several nanofluid flows traveling vertically across infinite plates. Sk et al. [4] used gyrotactic motile bacteria across a vertical stretched sheet to examine the equation of motion for bioconvective nanofluid flow. Motsa and Animasaun [5] explored the movement of an unstable nanofluid flow including vertically moving gyrotactic motile microorganisms with passively managed nanofluid over convectively heated surface. Mallikarjuna et al. [6] investigated nanofluid flow in a vertical cylinder containing gyrotactic microorganisms, as well as mixed convection processes. Sudhagar et al. [7] studied the existence of gyrotactic bacteria in an isothermal cylinder fixed in porous material. They concluded the study by suggesting that gyrotactic microorganisms increase the temperature and concentration gradient while microbe thickness reduces it. Khan and Ali [8] studied the effect on transport of an unstable bio-nano-transport model with activation energy and thermal conductivity. Kotha et al. [9] studied two-dimensional bioconvective MHD flow in the vicinity of a temperature and concentration gradient in a water-based nanofluid. Basha and Sivaraj [10] looked at how MHD and gyrotactic microbe density affected hyperbolic tangent fluid flow. Awais et al. [11] used nanoparticles and gyrotactic bacteria to investigate the bioconvection phenomena of rheology.

Moreover, different authors discussed behaviour of microorganism using non-Newtonian fluid models. For instance, Raju et al. [12] studied influence of gyrotactic microorganisms on two-dimensional MHD Casson fluid flow through a wedge. They concluded the study by saying that gyrotactic bacteria increase temperature and concentration gradients. Saleem et al. [13] proposed that gyrotactic microorganisms might influence MHD in a Jeffery nanofluid. The findings showed that increasing Rayleigh number decreases magnitude of tangential velocity. The behaviour of

nanofluids in Darcy medium under the influence of MHD was explored by Kotnurkar and Giddaiah [14]. Nima et al. [15] explored mixed convective flow in porous mediums containing non-Newtonian fluids and motile gyrotactic microorganisms. The results show that mixed convection parameters affect Nusselt number, motile microbe density profiles, and Sherwood number, but only for pseudo-plastic fluid. Khan et al. [16] investigated effect of binary chemical reaction on thermal flow of thixotropic nanofluid containing gyrotactic microbe. Sohail et al. [17] investigated homogeneous-heterogeneous reactions using Maxwell fluid and motile gyrotactic microorganisms for three-dimensional entropy analysis.

Cooling down electronic equipment is one of most significant requirements in twenty-first century. Heat transfer enrichment has also been discovered in mechanical and thermal systems recently. Many commonly used fluids such as engine oil, water, kerosene oil, and ethylene glycol, had limited thermal conductivity until the discovery of nanotechnology. Choi and Eastman [18] proposed a new way to improve thermal conductivity by incorporating a sufficient number of nano size particles into the working fluid. His findings aided in the development of strategies for enhancing the thermal properties of ordinary liquids known as based fluids. The thermal suspension was improved by adding nanoparticles (size less than 100 nm) to base fluids, resulting in nanofluids. Buongiorno [19] presented significant findings that are applicable to a variety of industrial processes. He discovered Brownian motion and thermophoresis, which are important in increasing thermal conductivity of working fluids. In cooling process of machine parts, electric devices, and medicines, different fluids have distinct solicitations. Nanofluids have multitudinous applications in engineering and industry, such as smart fluids, nuclear reactors, industrial cooling, geothermal power extract, and distant energy resources, nanofluid coolant, nanofluid detergents, cooling of microchips, Brake and distant vehicular Nanofluids, and nano-drug delivery. In the light of these applications, numerical researchers discussed the nanofluids in different geometrical configurations.

Magnetohydrodynamic (MHD) has grabbed different researchers attention because of its multitudinous applications in the agricultural, physics, medicine, engineering, and petroleum industries, etc. For instance, applications of MHD involve bearing sand boundary layer control, MHD generators, rotating machines, viscometry, electronic storing components, turbomachines, lubrications, oceanographically processes, reactor chemical vapor deposition, and pumps. The magnetic field is critical and plays essential role in controlling boundary layer of momentum and heat transfer. The presence of magnetic is beneficial to control fluid movement. It's worthwhile to mention that magnetic essential modified the outcomes of heat transfer in flow by maneuvering suspended nanoparticles and reorganized the fluid concentration.

The usual models for linearly viscoelastic, isotropic and incompressible fluids for which study related with flow, heat, and mass transfer features of motile microorganisms in different geometries has not been discovered so far.

The non-Newtonian fluids have significant applications including science and engineering, such as coating of wire and blade, textile dying, papers, manufacturing of plastics, the flow of biological liquids, and food processing. In industrial applications, the flow of non-Newtonian viscoelastic Carreau-nanofluids is essential to increase energy performance. For example, it is used to release polymer sheets from the die or in plastic film drawing. Non-Newtonian fluids have drawn considerable interest among researchers and scientists because of its broad applications. Examples include apple sauce, chyme, photographic emulsion, dirt, soaps, blood, and shampoos at low-shear stress that may be noted as non-Newtonian fluids. In the chemical engineering industry, viscosity of fluid plays a significant role. Viscosity is dependent on shear-rate in case of generalized Newtonian fluids. The idea of the generalized non-Newtonian fluid was introduced by Bird et al. [20]. Fluid flow past a rigid surface has also been investigated, and literature suggests that the micro-level surface forces are essential, and that fluid layering increases viscosity. They help to increase the viscosity of fluid due to fluid coating. In the power-law model, limitation is that

when shear rate is extremely low or high, the viscosity is not adequately addressed. To tackle this problem, the model of Carreau fluid model is presented [21]. Carreau fluid model gains the attention of many researchers for several years because of their essential characteristics. The flow on the magnetized permeable shrinking sheet and radiation due to heat was examined by Yahya et al. [22]. Eid et al. [23] analyzed flow over nonlinear permeable stretching sheet due to Carreau fluid under influence of chemical reaction. Santoshi et al. [24] numerically studied Carreau nanofluids in three-dimension on a stretching sheet in addition to considering mass slip and nonlinear thermal radiation. The effects of the internal energy in the porous Von-Karman model in steady electrically Carreau fluid under ohmic heating and transverse magnetohydrodynamics were studied by Khan et al. [25]. They considered a cylindrical coordinate system, and similarity transformations are applied to obtain ordinary differential equation for proposed problem and implement a well-known shooting scheme to achieve the results. Bilal et al. [26] studied flow features of Carreau fluid by conferring the stimulating traits of thermal stratification. Appropriate use of MHD and infinite shear rate viscosity flow equation are modelled. They concluded that the thermal stratification characterizes fluid flow's thermal distribution, and Carreau fluid acts in a reverse direction for shear thickening and shear thinning liquids. Khan et al. [27] examined mass and heat transfer for convection in non-Newtonian Carreau nanofluid on a cylinder in presence of temperature-dependent thermal conductivity. They considered a well-known model, i.e., Buongiorno's model, which contains the Brownian and thermophoresis parameters.

Williamson's fluid is example of a non-Newtonian fluid that has shear thinning characteristics. This model was presented by Williamson (1929), and several scholars [28,29] used it to achieve the flow solution due to Williamson's fluid model. Khan et al. [30] investigated two-dimensional flow of Williamson's fluid with thermal radiation and effect of MHD. Amanulla et al. [31] considered magnetized Williamson's fluid flow in permeable cone with slip effect. Hamid et al. [32] investigated numerical research of Williamson fluid within chemical reactive species

using a multi-slip model. They discovered that Hartmann number had greatest impact on velocity and temperature profiles. Shamsi et al. [33] studied laminar flow in a rectangular channel filled with a non-Newtonian fluid numerically. The Jeffrey fluid model investigated by Nadeem et al. [34] over a stretching sheet. They discovered that Nusselt number decreases as Brownian parameter increases but decreased Sherwood number increases when the thermophoresis parameter decreases. In presence of magnetic thermal conductivity, Shankar et al. [35] analyzed heat transfer characteristics of Williamson fluid. They stated that increasing the index of compressed flow reduces velocity.

1.3 Research Motivation and Objectives

The current study is concerned with "Transport of Motile Gyrotactic Microorganism in viscoelastic fluids". The main focus of thesis highlights on effect of different viscoelastic fluids behaviour on bio convection of motile gyrotactic microorganisms. Only, the flow through rotating circular plates have been contemplated in present study to develop a better comparision between fluids. Further, influence of thermal radiation, viscous dissipation, porosity, thermophoresis, Brownian motion, induced magnetic field and activation energy are given due attention.

In light of the aforementioned details, the current thesis seeks to:

- Study movement of motile gyrotactic microorganisms in one-parameter viscoelastic fluid mediums.
- Examine influence of temperature for incompressible viscoelastic fluids on movement of gyrotactic microorganisms.
- Examine influence of rotation of disks on the movement of gyrotactic microorganisms.
- Compare movement of microorganisms in different viscoelastic fluids.

The current research has numerous industrial, scientific, and technical applications. Future study will use the mathematical models and results for major

flow characteristics as a standard for validating traditional and experimental studies. For the scholars in this field, this research also adds a fresh perspective to the literature.

1.4 Semi-Analytical Methods

Few numerical methods need to be developed because coupled, nonlinear higher order equations with non-linear boundary conditions (BC's) are difficult to solve analyatically. However, analytical and semi-analytical methods remains highly crucial because they serve as a benchmark. In the literature, there are many different numerical and analytical methods. Differential Transform Method (DTM), which is used in current research, is as follows:

Differential Transform Method (DTM)

The Taylor series expansion serves as the foundation for differential transform technique. This method provides analytical solution in form of polynomial. Magnetohydrodynamics and complex material flow problems can be solved by using DTM, which is reliable technique in finding solutions to nonlinear problems. To explain briefly about the DTM method, let us define the r^{th} derivative as

$$F(\eta)=\frac{1}{q!}\left[\frac{d^q f}{d\eta^q}\right]_{\eta=\eta_0}, \tag{1.1}$$

where, $f(\eta)$ and $F(\eta)$ represents the original and transformed functions. We can define differential inverse transformation of $F(\eta)$ as

$$f(\eta)=\sum_{q=0}^{\infty}F(\eta)(\eta-\eta_0)^q. \tag{1.2}$$

The aim of differential transformation is attained from the Taylor series expansion and actual application the function $f(\eta)$ can be written in terms of finite series as

$$f(\eta)\cong\sum_{q=0}^{m}F(\eta)(\eta-\eta_0)^q, \tag{1.3}$$

The convergence rate depends upon value of m. Various differential transformations used in this thesis are

$$\left.\begin{aligned}
&f'' \to (q+1)(2+q)f(2+q),\\
&f''^3 \to \left[\sum_{m=0}^{k}\left(\begin{array}{l}\sum_{q=0}^{m}(q+1)(q+2)(-q+m+1)(-m+k+1)\\ (2-m+k)f(2-m+k)f(2+q)f(-q+2+k)\end{array}\right)\right],\\
&ff'f''' \to \left[\sum_{q=0}^{k}\left(\begin{array}{l}\sum_{m=0}^{k-q}(q+1)(1+m)(2+m)(-q+k-m+1)(-q+2+k-m)\\ (-m+k-q+3)f(1+q)f(2+m)f(-q+k-m+3)\end{array}\right)\right],\\
&ff''f'^2 \to \left[\sum_{q=0}^{k}\left(\begin{array}{l}\sum_{m=0}^{k-q}(1+q)(q+2)(3+r)(m+1)(2+m)(-m+k+1-q)\\ (-m+k+2-q)(-m+k-q+3)\\ f(3+q)f(2+m)f(-m+k-q+3)\end{array}\right)\right],
\end{aligned}\right\} \quad (1.4)$$

$$\left.\begin{aligned}
&g \to g(k),\\
&\lambda g' \to \sum_{q=0}^{k}\left((-q+k+1)\varepsilon(r)g(-q+k+1)\right),
\end{aligned}\right\} \quad (1.5)$$

$$
\left.
\begin{aligned}
&gf' \to \sum_{q=0}^{k} (1-q+k)\, g(q)\, f(1-q+k), \\
&fg' \to \sum_{q=0}^{k} (-q+1+k)\, f(q)\, g(-q+1+k), \\
&g'f'g'' \to \sum_{q=0}^{k} \begin{bmatrix} (q+1)(-q+1+k)(-q+2+k)\, f(1+q)\, g(1+q) \\ g(-q+2+k) \end{bmatrix}, \\
&g'g''f''' \to \sum_{q=0}^{k} (1+q)(q+2)(-q+1+k)(-q+2+k)(-q+k+3) \\
&g(1+q)\, g(2+q)\, g(-q+k+3), \\
&f'g'f'' \to \sum_{q=0}^{k} \begin{bmatrix} (1+q)(-q+k+1)(-q+2+k)\, f(1+q)\, g(1+q) \\ f(-q+2+k) \end{bmatrix}, \\
&g'f''f''' \to \sum_{q=0}^{k} (1+q)(2+q)(-q+1+k)(-q+2+k)(-q+k+3) \\
&g(q+1)\, f(2+q)\, f(-q+3+k), \\
&f''g'^2 \to \sum_{m=0}^{k} \begin{pmatrix} \sum_{q=0}^{m} (1+q)(2+q)(1-q+m)(-m+1+k) \\ g(-m+1+k)\, f(2+q)\, g(-q+1+k) \end{pmatrix}, \\
&f''g''^2 \to \sum_{q=0}^{k} \begin{pmatrix} \sum_{m=0}^{k-q} (q+1)(2+q)(m+1)(m+2)(-m+1-q+k) \\ (-q+2+k-m)\, g(2+q)\, f(m+2)\, g(-q+2+k-m) \end{pmatrix}, \\
&f'^2g'' \to \sum_{m=0}^{k} \begin{pmatrix} \sum_{q=0}^{m} (1+q)(2+q)(-q+1+m)(-m+1+k) \\ f(-m+1+k)\, g(2+q)\, f(-q+k+1) \end{pmatrix},
\end{aligned}
\right\} \quad (1.6)
$$

$$\left.\begin{aligned}
&m'm'' \to \sum_{q=0}^{k}(q+1)(2+q)(-q+1+k)(-q+2+k)m(q+1)m(-q+2+k),\\
&\lambda m' \to \sum_{q=0}^{k}\big((-q+1+k)\varepsilon(r)m(-r+k+1)\big),\\
&mf' \to \sum_{q=0}^{k}\big((-q+k+1)m(q)f(1-q+k)\big),\\
&fm' \to \sum_{q=0}^{k}\big((-q+1+k)f(q)m(-q+1+k)\big),\\
&mg' \to \sum_{q=0}^{k}\big((-q+1+k)m(q)g(-q+1+k)\big),
\end{aligned}\right\} \quad (1.7)$$

$$\left.\begin{aligned}
&nn' \to \sum_{q=0}^{k}\big((-q+1+k)n(q)n(-q+1+k)\big),\\
&fn' \to \sum_{q=0}^{k}\big((-q+1+k)f(q)n(-q+1+k)\big),\\
&\lambda n' \to \sum_{q=0}^{k}\big((-q+1+k)\varepsilon(q)n(-q+1+k)\big),
\end{aligned}\right\} \quad (1.8)$$

$$\left.\begin{aligned}
&f\theta' \to \sum_{q=0}^{k}\big((-q+1+k)f(q)\theta(-q+1+k)\big),\\
&\theta'^{2} \to \sum_{q=0}^{k}\big((1+q)(-q+1+k)\theta(1+q)\theta(1-q+k)\big),
\end{aligned}\right\} \quad (1.9)$$

$$\left.\begin{aligned}
&\theta'\phi' \to \sum_{q=0}^{k}\big((1+q)(-q+1+k)\theta(1+q)\phi(-q+1+k)\big),\\
&f\phi' \to \sum_{q=0}^{k}\big((-q+1+k)f(q)\phi(-q+1+k)\big),
\end{aligned}\right\} \quad (1.10)$$

$$\left.\begin{aligned}
&\lambda\chi' \to \sum_{q=0}^{k}\big((-q+1+k)\varepsilon(q)\chi(-q+1+k)\big),\\
&f\chi' \to \sum_{q=0}^{k}\big((-q+1+k)f(q)\chi(-q+1+k)\big),\\
&\chi'\phi' \to \sum_{q=0}^{k}\big((1+q)(-q+1+k)\chi(q+1)\phi(-q+1+k)\big),\\
&\chi\phi'' \to \sum_{q=0}^{k}\big((-q+1+k)(-q+2+k)\chi(q)\phi(-q+2+k)\big),
\end{aligned}\right\} \quad (1.11)$$

1.5 Thesis Outlines

The current thesis comprises of nine chapters, set up from the preliminary chapter, which addresses research background, aims and motivation, and literature review. Further chapter 2, present detail about dimensionless number, governing equations, geometry of the problems and solution methodology. Different problems are investigated in subtiquent six chapters (chapter 3 to 8). Chapter 9 offers a thorough summary of all previous research and recommendations for future effort.

Chapter 2

Literature Review and Governing Equations

2.1 Introduction

In this chapter, detailed literature review is presented. Governing equation of fluid mechanics i.e., continuity, momentum, energy, nanoparticle concentration and microorganism concentration equation are defined and discussed. All non-dimensional parameters which are used in this thesis are also defined briefly in this chapter. Squeezing flow phenomena between parallel circular rotating plates is focused in this thesis. Two finite parallel rotating disks initially placed at distance D away from each other. The cylindrical polar coordinates (r,θ,z) with associated velocity field $\mathbf{U}=(v_r,v_\theta,v_z)$ is consider in this thesis. The flow problem is simplified and then solved with the help of Differential Transform Method. All differential transformations which are used in this thesis is defined in this chapter briefly. Finally, a complete layout of the thesis is given.

2.2 Literature Review

A nanofluid is substance that contains nano-sized particles suspended in base fluid. These nanoparticles are generally made of oxides, metals, carbon nanotubes, or carbides, while base fluids are often taken as water, oil, and ethylene glycol. The potential use of in many applications in industry, i.e., heat transfer, especially in pharmaceutical processes, microelectronics, engine cooling (vehicle heat management), hybrid-power engines, chiller, fuel cells, heat exchanger, grinding, and boiler flue gas temperature reduction. Gourarzi et al. [36] scrutinized impact of thermophoretic force and Brownian motion on hybrid nanofluid. They concluded with excellent point that nanoparticle formation on cold walls is more essential due to

thermophoresis migration. Ghalandari et al. [37] used CFD model silver/water nanofluid flow towards a root canal. The effects of injection height, nanofluid concentration, and rate of volumetric flow were explored and addressed. Sheikholeslami and Vajravelu [38] studied control volume-based finite element approach to determine magnetite nanofluid flow into same heat flux in whole cavity. The impact of Rayleigh number, Hartmann number and volume friction of nanofluid flow magnetite (an iron oxide) and heat transfer features were discussed. Sheikholeslami and Ganji [39] addressed hydrothermal nanofluid in existence of magnetohydrodynamics by using DTM. They discussed impact of squeezing number and nanofluid volume fraction on heat transfer and fluid flow. Biswal et al. [40] deliberated fluid flow in a semi-permeable channel with influence of transverse magnetic field. Zhang et al. [41] considered outcome of thermal diffusivity and conductivity of numerous nanofluids utilizing transient short-hot-wire technique. Fakour et al. [42] inquired laminar nanofluid flow in channel using least square approach with porous walls. This study shows that enhancing Hartman and Reynolds number, velocity of nanofluid flow in channel declines, an extreme amount of temperature is enhanced. More, enhancing Prandtl number along with Eckert number also increases temperature distribution. Zhu et al. [43] inquired second-order slip and migration of nanoparticles from a magnetically influenced annulus. They applied a well-known HAM technique for solving equations and h-curve are drawn to validate exactness of the obtained solution. Alamri et al. [44] revealed the impact of Poiseuille nanofluid flow with Stefan blowing and second-order slip. The accuracy of analytical solution is obtained by HAM and verified by h-curve and residual error norm for each case. They claim that ratio of buoyancy forces in existence of a magnetic field played a vital role in velocity distribution.

In previous decades, study of magnet fields in fluid flow grabbed substantial attention because magnetohydrodynamics (MHD) is frequently used in many areas such as crystal growth process, pumping, agriculture, and polymer industry. MHD was recently identified as very useful in biotechnology as it is used in multiple testing

processes for diseases. Recently, Lu et al. [45] studied mathematical models for axisymmetric steady magnetohydrodynamic flow of Carreau nanofluids across radially stretched surfaces under nonlinear radiation of heat and chemical reaction. The additional feature of problem, which makes it unique, is generation/absorption of heat connected with new applied zero mass flux conditions. The flow due to boundary conditions due to convection with Carreau nanofluid with a magnetic field is studied by Amanulla et al. [46-47] in addition to jump and slip conditions on a stretching cylinder. Khan et al. [48] examined flow induced by non-Newtonian Carreau fluid on stretching cylinder with magnetic field. Mustafa [49] investigated magnetohydrodynamic flow of nanofluid in presence of chemical reaction on a rotating disk under effect of buoyancy forces and partial slip. Pandey et al. [50] investigated effect of viscous dissipation in MHD nanofluid flow through a wedge in a porous media. [51-53] could be used to interpret certain additional relevant references.

Due to complicated nature of chemical reactions system, restricting to binary type alone becomes more comfortable and straightforward. A chemical reaction requires a quantity of activation energy to start. In Arrhenius equation, a reaction's activation energy is obtained by describing constant rate changes with temperature. A chemical reaction is chemical change in which reactants with varying properties may yield one or more products. Several industries need chemical reactions as essential phase in manufacturing process. Traditionally these types of responses occur in chemical reactors and are generally constrained to mass transfer. The response is sufficient when reagent volume and energy inputs enhance, and waste is reduced, then the optimum product can be obtained. Bestman [54] applied the model of binary reaction in the Arrhenius equation to produce a chemical reaction. The effects of energy of activation and binary chemical change on a two-dimensional radiative magnetohydrodynamics boundary layer flow for nanofluid on a vertical plate was discussed by Anuradha et al. [55]. They scrutinized that temperature distribution was accelerated, and nanoparticle concentration profile decelerates under effects of heat

generation, viscous dissipation, and MHD. Irfan et al. [56] discussed the Carreau nanofluid time-dependent flow for Arrhenius activation energy by using properties of binary chemical reaction with mixed convection. Khan et al. [57] explored the incompressible flow past a stretchable sheet of the Carreau-Yasuda model. Kumar et al. [58] analyzed effects of chemical binary reaction in flow of tangent hyperbolic fluid along with zero mass flux. Khan et al. [59] reported a new nanofluid relation which examines the characteristics of the energy of activation with mixed convection Carreau nanofluid. They studied radiation and magnetic field parameters on both the entropy generation and the Bejan number.

For many industrial applications such as production of glass, furnaces, space technologies, comic aircraft, space vehicles, propulsion systems, plasma physics, and aerodynamics in field of aero-structure flows, combustion processes, and other spacecraft applications, the role of thermal radiation is significant. Khan et al. [60] studied effect of multiple slips on Jeffrey fluid model in existence of Soret and radiation over a permeable sheet. Raju et al. [61] examined flow of convective magnesium oxide nanoparticles with nonlinear thermal convective over a rotating disk. Sheikholeslami et al. [62] presented the analysis of thermally radiative MHD nanofluid through the porous cavity. Muhammad et al. [63] studied characteristics of thermal radiation for Powell-Eyring nanofluid with additional effects of activation energy. Aziz et al. [64] numerically analyzed hybrid nanofluid with entropy analysis, thermal radiation, and viscous dissipation. Mahanthesh et al. [65] inquired the significance of radiation effects of the two-phase flow of nanoparticles over vertical plate. Jawad et al. [66] investigated bio-convection nanofluid flow of Darcy law through a channel (Horizontal) with magnetic field effects and thermal radiation. Majeed et al. [67] thermally analyzed magnetized bioconvection flow with additional effects of activation energy. Numerous fresh developments on this topic can be envisaged through [68-73].

Bioconvection characterizes the hydrodynamic instabilities and the forms of suspended biased swimming microorganisms. The hydrodynamics instabilities occur

due to the coupling between the cell's swimming performance and physical features of the cell, i.e., fluid flows and density. For example, a combination of gravitational and viscous torques tends to swim the cells in the direction of down welling fluid. A gyrotactic instability ensues if the fluid is less dense than the cells. Bioconvection portrays a classical structure where macroscopic mechanism occurs due to the microscopic cellular ensue in relatively dilute structures. There is the ecological impact for the bioconvection and its mechanisms, thus promising for industrial development. In the recent era, many scientists discussed the mechanism of bioconvection using nanofluid models. For instance, Makinde et al. [74] examined nanofluid flow of rotating disk and thermal radiation with titanium and aluminum nanoparticles. They showed that the base liquid thermal efficiency is remarkable when the nanoparticles of titanium alloy are introduced in contrast to the nanoparticles of aluminum alloy. Reddy et al. [75] studied the Maxwell thermally radiative nanofluid flow on double rotating disk. Waqas et al. [76] examined the effect of thermally bioconvection Sutterby nanofluid flow between two rotating disks along with microorganisms. The fluid speed with mixed convection parameters grows quicker but delays magnetic field parameter and Rayleigh number bioconvection. Some important studies on the bioconvection mechanism can be found from list of references [77-80].

Moreover, different authors discussed the behavior of microorganism using non-Newtonian fluid models. For instance, Raju et al. [81] studied the influence of gyrotactic microorganisms on two-dimensional MHD Casson fluid flow through a wedge. They concluded the study by saying that gyrotactic bacteria increase temperature and concentration gradients. Saleem et al. [82] proposed that gyrotactic microorganisms might influence MHD in a Jeffery nanofluid. The findings showed that increasing the Rayleigh number decreases the magnitude of the tangential velocity. The behavior of nanofluids in Darcy medium under the influence of MHD was explored by Kotnurkar and Giddaiah [83]. Nima et al. [84] explored mixed

convective flow in porous mediums containing non-Newtonian fluids and motile gyrotactic microorganisms. The results show that mixed convection parameters affect Nusselt number, motile microbe density profiles, and Sherwood number, but only for pseudo-plastic fluid. Khan et al. [85] investigated the effect of a binary chemical reaction on

The thermal flow of a thixotropic Nano fluid containing a gyrotactic microbe. Sohail et al. [86] investigated homogeneous-heterogeneous reactions using Maxwell fluid and motile gyrotactic microorganisms for three-dimensional entropy analysis.

The minimum amount of energy needed to begin a reaction is referred to as activation energy. Swedish physicist Svante Arrhenius coined word for the first time in 1889. The Arrhenius equation represents energy activation as well as pace of chemical reaction processing. Because of various uses in chemical engineering, geothermic reservoirs, nuclear reactor cooling and thermal oil recovery, mechanochemistry, water mechanics, and food processing, activation energy has aroused the attention of various experts. Maleque [87] looked explored how activation energy, heat sink/source, and viscous dissipation affect incompressible flow over a porous vertical plate. Awad et al. [88] solved highly nonlinear coupled PDEs for unsteady flow of incompressible rotating viscous fluid flow with influence of binary chemical reaction using the SRM approach. The influence of the second law of thermodynamics on the flow of an electrically conducting Casson Nano fluid through a wedge was explored by Zaib et al. [89]. They discovered that increasing the wedge angle parameter values increases the velocity distribution while reducing the temperature profile and nanoparticle concentration. In the presence of nanoparticles, Hamid and Khan [90] investigated the effects of a changing magnetic field on heat absorption/generation in Williamson fluid flow caused by a rotating cylinder. These findings demonstrated that raising the value of the response rate parameter lowers heat transfer across the cylinder surface. Umar et al. [91] examined the flow of non-Newtonian fluid over a stretched sheet in the presence of activation energy and slip.

They observed that when the velocity slip parameter and Hartmann number rise, the fluid velocity profile decreases while the temperature distribution and concentration profile increase. Abbas et al. [92] examined impact of EMHD on surface flow caused by porous Riga Nano fluid with a gyrotactic microbe computationally. Waqas et al. [93] used thermophoresis and Brownian motion characteristics in a cylinder containing a gyrotactic microbe to study Wu's slip, also known as the second-grade slip mechanism for the Buongiorno's relation. Usman et al. [94] examined flow of viscoelastic fluid in cylinder and influence of activation energy. References [95–104] include some existing research on the aforementioned topic.

In previous decades, the study of magnet fields in fluid flow grabbed substantial attention because magneto hydrodynamics (MHD) is frequently used in many areas such as crystal growth process, pumping, agriculture, and polymer industry. MHD was recently identified as very useful in biotechnology as it is used in multiple testing processes for diseases. Recently, Lu et al. [105] studied mathematical models for the axisymmetric steady magneto hydrodynamic flow of Carreau Nano fluids across radially stretched surfaces under nonlinear radiation of heat and chemical reaction. The additional feature of the problem, which makes it unique, is the generation/absorption of heat connected with new applied zero mass flux conditions. The flow due to boundary conditions due to convection with Carreau Nano fluid with a magnetic field is studied by Wakif et al. [106] in addition to jump and slip conditions on a stretching cylinder. Khan et al. [107, 108] examined flow induced by non-Newtonian Carreau fluid on a stretching cylinder with a magnetic field. Further, the flow on a stretching cylinder affected by homogenous and heterogeneous conditions was examined by them and applied to convective boundary conditions numerically. This study mainly aims at the direct influence of homogenous and different reactions of Carreau fluid on stretching cylinder with a magnetic field. A practical method for two-dimensional Carreau Nano fluid for a non-similar solution with magnetic field (applied) and mixed convection was analyzed by Sardar et al.

[109]. They showed that increasing the buoyancy parameter boosts both skin friction and Nusselt number. In presence of infinite shear rate viscosity, the stagnation point and the MHD flow of Carreau fluid are also detected. Salahuddin et al. [110] examined generalized slip effects of magnetic field on Carreau Nano fluid for a linear stretching cylinder with reactive species. Bhatti et al. [111] investigated peristaltic motion of small particles suspended in Carreau Nano fluid with constant density. Laminar flow in two-dimensional past a stretching cylinder covered with the porous surface was studied with the effects of the magnetic field by Bovand et al. [112]. This article presented the findings of a numerical study of the circulatory cylindrical fluid flow under the influence of magneto hydrodynamics.

From the above-mentioned literature, it is evident that no efforts are made for the flow of gyrotactic microorganism in squeezing rotating circular plates with different viscoelastic fluid models. The aim of this thesis is to study movement of motile gyrotactic microorganisms in one-parameter viscoelastic fluid medium through semi-analytical approach. In this thesis our main focus should be on one geometry i.e., pair of Circular rotating plates with different viscoelastic model because of its importance in lubrication, rotating machinery, crystal formation processes, and viscometry.

2.3 Governing Equations

The fundamental laws in fluid mechanics which expedites the flow behaviour are law of conservation of mass, energy and momentum. A brief description of mathematical formulation of these laws are presented as follows.

Continuity Equation

The continuity equation mathematically represents the law of conservation of mass. This law asserts that neither mass can be created nor destroyed, and that mass is preserved. The continuity equation for incompressible fluid is [8]

$$\nabla \cdot \mathbf{U} = 0. \tag{2.1}$$

Momentum Equation

The momentum equation can be derived from the law of conservation of momentum and is represented by the equation [8]

$$\rho\left[(\mathbf{U}\cdot\nabla)\mathbf{U}+\frac{\partial \mathbf{U}}{\partial t}\right]+\nabla p-\nabla.\tau+\rho\mathbf{b}=0, \tag{2.2}$$

where, pressure is represented by p , τ represents cauchy stress tensor , fluid density is denoted by ρ , μ is the fluid viscosity and $\mathbf{b}$ is the body force per unit mass.

Energy Equation

A relation for temperature distribution through the flow is required for the convective heat transfer problem. The energy equation for Nanofluid flow is represented by [9]

$$(\mathbf{U}\cdot\nabla)T-\frac{1}{\rho c_p}\nabla\cdot(k\nabla)T+\tau\left[D_B\nabla T\cdot\nabla C+\left(\frac{D_T}{T_m}\right)\nabla T\cdot\nabla T\right]=0, \tag{2.3}$$

where temperature denoted by T , concentration of nanoparticles is denoted by C , mean fluid temperature is denoted by T_m , specific heat at uniform temperature is denoted by c_p , D_B Brownian diffusivity, and D_T is thermophoretic diffusion coefficient.

Nanoparticle Concentration Equation

The concentration difference through the flow must be solved for the mass transfer problem. It can be expressed mathematically as follows [9]

$$(\mathbf{U}\cdot\nabla)C-D_B\nabla\cdot(\nabla\cdot C)-\frac{D_T}{T_m}\nabla\cdot(\nabla\cdot T)=0. \tag{2.4}$$

Microorganism Conservation Equation

The gyrotactic microorganism conservation equation depends on the bioconvection's model in a suspension of gyrotactic bacteria created as [8,9]

$$\frac{\partial n}{\partial t} + \nabla \cdot \mathbf{j} = 0, \tag{2.5}$$

and $\mathbf{j}$ is flux of microorganism due to fluid convection reads as

$$\mathbf{j} = n\mathbf{V} + n\psi - D_{\mathrm{mo}} \nabla \cdot n. \tag{2.6}$$

The average form of directional swimming velocity of a microorganism reads

$$\psi = \bar{b} W_{\mathrm{mo}} H(C) \nabla \cdot C, \tag{2.7}$$

Viscoelastic Fluids

Non-Newtonian fluids are fluids which do not satisfies Newton's law of viscosity, i.e., shear stress is not directly and linear propotional to strain rates. Ussally, stresses are divided into viscous and elastic components. Not every fluid has elastic nature but viscosity is the complusrily part of fluid consituivative equation such as power law fluid. If fluid shear stress processes both viscous and elastic components they are called viscoelastic fluids. In nutshell, viscoelastic fluid are a mixture of solvent and a little amount of polymer. Paints, DNA suspensions, various biological fluids, and other products from chemical industry are a few examples of these fluids. The study of viscoelastic fluids are particularly intriguing and important for industry due to a variety of characteristics, including the prevalence of polymers. For industrial applications, a thorough grasp of viscoelasticity is essential. Polymeric suspensions exhibit viscoelastic behaviour; however, it is difficult for a single model to capture the link between stress and deformation. These models are referred to as constitutive equations in rheology.

Viscoelastic fluids may behave in both linear and non-linear ways, making viscoelasticity modelling a challenging task. On the other hand, some polymeric component characteristics can be too significant to be implicitly included in these

models. Thixotropic activity in liquid crystalline dispersions and viscoelastic micellar solutions exhibits this type of behaviour.

In this thesis, we will discuss different viscoelastic fluids flow in parallel circular rotating plates and analyze the effects of different fluid model on movement of Gyrotatic microorganism in these fluids.

2.4 Dimensionless Numbers

Reynolds Number

The Reynolds number is defined as the ratio of inertial to viscous forces. Reynolds number is a dimensionless number used in fluid mechanics to determine whether a flow is laminar or turbulent. Mathematically

$$\mathrm{Re} = \frac{\text{Inertial forces}}{\text{Viscous forces}}$$

Squeezing Reynolds Number

A nondimensional number that arises in squeezing flow problems. It is the product of retardation time and square of distance between plates divided by kinematic viscosity

$$S_{\varrho} = \frac{\alpha D^2}{2\upsilon}$$

Rotational Reynolds Number

A nondimensional number emerging from rotating viscous fluid problems. It is the product of angular velocity and square of distance between plates divided by kinematic viscosity

$$R_{\Omega} = \frac{\Omega_1 D^2}{\upsilon}$$

Magnetic Reynolds Number

The magnetic Reynolds number is the magnetic analogue of the Reynolds number, a fundamental dimensionless group that occurs in magnetohydrodynamics. dimensionless quantity that estimates the relative effects of advection or induction of a magnetic field by the motion of a conducting medium to the magnetic diffusion

$$Re_M = \frac{\alpha D^2 Bt}{2v}$$

Brownian Motion Paramter

Brownian motion parameter describes the phenomena of random motion of particles suspended in a medium (a liquid or a gas).

$$T_b = \frac{\tau D_B (C_f - C_u)}{\alpha}$$

Prandtl Number

It describes the momentum-to-thermal diffusivity ratio and measures heat transfer between a moving fluid and a solid surface.

$$P_t = \frac{\upsilon}{\alpha}$$

Weissenberg Number

The Weissenberg number is the dimensionless number employed in the investigation of non-Newtonian viscoelastic fluids. It is commonly denoted with We.

$$We = \Omega_1^2 \Gamma^2$$

Activation Energy Parameter

In chemistry and physics, activation energy is minimum amount of energy that must be provided for compounds to result in a chemical reaction.

Thermal Radiation Parameter

The thermal radiation defines relative contribution of conduction heat transfer to thermal radiation transfer. Mathematically it can be written as

$$R_d = \frac{4\sigma_e T_u^3}{\beta_r k}$$

Bioconvection Schmidt Number

Schmidt number is defined as the ratio of momentum diffusivity (viscosity) to mass diffusivity. Mathematically it can be written as

$$S_M = \frac{\upsilon}{D_B}$$

2.5 Geometry of the Problem

Let us consider two finite parallel rotating disks initially placed at distance D away from each other. The distance between the disk changes with time t defined as $\Gamma(t) = (1-\alpha t)^{1/2} D$ which causes squeezing flow. The upper disc ($z = \Gamma(t)$) is rotating with an angular velocity Ω_2 and is moving towards or away with velocity $v_z = -\frac{\beta D^2}{2\Gamma(t)}$ from the fixed lower disk plate ($z = 0$) rotating with an angular velocity Ω_1. Both disks are sustained at a constant temperature T_0, T_l and nanoparticle concentration C_0, C_l respectively. Furthermore, the micro-organism density at both disks is maintained as n_l, n_u respectively. The external magnetic field on the moving plate is applied with axial and azimuthal components i.e.

$$\begin{cases} H_\theta = \dfrac{rN_0}{\Lambda_2}\sqrt{\dfrac{D}{\Gamma(t)}}, \\ H_z = \dfrac{\beta M_0 D}{\Lambda_1 \Gamma(t)}. \end{cases} \tag{2.9}$$

In which M_0, N_0 are the dimensionless quantities which make H_θ, H_z dimensionless and Λ_1, Λ_2 represents dimensionless of magnetic permeability's of squeeze film and medium external to the disks, respectively. For the liquid metals, $\Lambda_2 = \Lambda_\ell$ where Λ_ℓ denotes the permeability of free space. H_θ, H_z on the lower plate is assumed zero here. In present investigation, induced magnetic field $\mathbf{B}(r,\theta,z)$ having the component B_r, B_θ, B_z is generated by the magnetic field (applied) in a squeezed film between the plates. Also, the upper disc is under the influence of an external applied magnetic field with axial and tangential component $B_\theta = N_0 r\frac{D^2}{\Gamma^2(t)}, B_z = -\frac{\beta D M_0}{\Gamma(t)}$.

Chapter 3

Transport of Motile Gyrotactic Microorganism for Nano fluid flow between Circular Rotating Plates

3.1 Introduction

In this chapter, a mathematical model for nanofluid bioconvection axisymmetric squeezing flow between parallel rotating circular plates in presence of thermal radiation is developed. The governing equations involved continuity, momentum, energy, concentration of Nanoparticles and concentration of microorganism species for flow of Nanofluid in cylindrical polar coordinates. Problem is then simplified to non-linear coupled Ordinary Differential Equation with help of appropriate similarity transformations. Differential Transform Method (DTM) combined with Padé-approximation is applied to solve the resulting equations. Analytic results with physical interpretation are shown by drawing graphs and tables.

3.2 Mathematical Formulation

Flow Assumptions

To formulate the mathematical problem following assumptions have been taken into account. Flow of viscous Nano fluid saturating space between rotating and squeezing disks is

- Laminar, incompressible, axisymmetric flow with no-wall slip.
- A mild concentration of nanoparticles uniformly mixed with viscous base fluid.
- Radiative heat transfer is introducted with Roseland approximation.
- Viscous dissipation and forced convection are minimum therefore neglected.
- Nanoparticle concentration is governed by Brownian motion and thermophoresis.
- Motile Gyrotactic Microorganism.

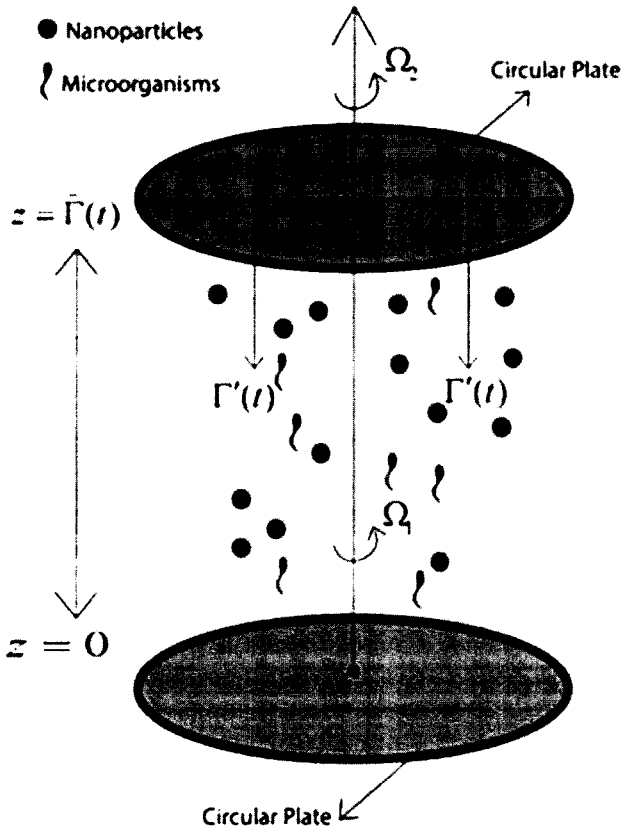

Fig. 3.1. Geometrical representation of squeezing nanofluid gyrotactic bioconvection between rotating circular disks.

Mathematical Model

The cylindrical polar coordinates (r,ψ,z) with the associated velocity field $\mathbf{V}=(v_r,v_\theta,v_z)$. In view of flow assumptions, the governing equations for mass and momentum (radial, tangential, and azimuthal) conservation for Nano fluid may be presented as

$$\frac{1}{r}\frac{\partial}{\partial\theta}(v_\theta)+\frac{1}{r}\frac{\partial}{\partial r}(rv_r)+\frac{\partial}{\partial z}(v_z)=0 \tag{3.1}$$

$$\rho\left(v_r\frac{\partial v_r}{\partial r}+\frac{\partial v_r}{\partial t}+v_z\frac{\partial v_r}{\partial z}+\frac{v_\theta}{r}\frac{\partial v_r}{\partial \theta}-\frac{v_\theta}{r}\right)=-\frac{\partial p}{\partial r}+\mu\left[\begin{array}{l}\frac{1}{r}\frac{\partial v_r}{\partial r}+\frac{1}{r^2}\frac{\partial^2 v_r}{\partial \theta^2}+\frac{\partial^2 v_r}{\partial z^2}-\frac{2}{r}\frac{\partial v_\theta}{\partial \theta}\\ -\frac{v_r}{r^2}\end{array}\right], \tag{3.2}$$

$$\rho\left(\frac{\partial v_\theta}{\partial t}+\frac{v_\theta}{r}\frac{\partial v_\theta}{\partial \theta}+v_r\frac{\partial v_\theta}{\partial r}+v_z\frac{\partial v_\theta}{\partial z}-\frac{v_r v_\theta}{r}\right)=-\frac{1}{r}\frac{\partial p}{\partial \theta}+\mu\left[\begin{array}{l}\frac{1}{r}\frac{\partial}{\partial r}\left(r\frac{\partial v_\theta}{\partial r}\right)+\frac{1}{r^2}\frac{\partial^2 v_\theta}{\partial \theta^2}\\ +\frac{\partial^2 v_\theta}{\partial z^2}+\frac{2}{r^2}\frac{\partial v_r}{\partial \theta}-\frac{v_\theta}{r^2}\end{array}\right], \tag{3.3}$$

$$\rho\left(\frac{\partial v_z}{\partial t}+\frac{v_\theta}{r}\frac{\partial v_z}{\partial \theta}+v_r\frac{\partial v_z}{\partial r}+v_z\frac{\partial v_z}{\partial z}\right)=-\frac{\partial p}{\partial z}+\mu\left[\frac{1}{r^2}\frac{\partial^2 v_z}{\partial \theta^2}+\frac{1}{r}\frac{\partial}{\partial r}\left(r\frac{\partial v_z}{\partial r}\right)+\frac{\partial^2 v_z}{\partial z^2}\right]. \tag{3.4}$$

The transport of energy with thermal radiation may be presented as

$$\begin{array}{l}\frac{\partial T}{\partial t}+v_r\frac{\partial T}{\partial r}+v_z\frac{\partial T}{\partial z}-\frac{k}{\rho c_p}\frac{\partial^2 T}{\partial z^2}\\ +\frac{(\rho c)_p}{(\rho c)_f}\left[D_B\left(\frac{\partial T}{\partial r}\frac{\partial C}{\partial r}+\frac{\partial T}{\partial z}\frac{\partial C}{\partial z}\right)+\frac{D_T}{T_u}\left[\left(\frac{\partial T}{\partial r}\right)^2+\left(\frac{\partial T}{\partial z}\right)^2\right]\right]-\frac{1}{(\rho c)_f}\left(\frac{\partial q_r}{\partial r}\right)=0,\end{array} \tag{3.5}$$

According to Rosseland approximation radiation heat flux which is uni-directional takes the form, $q_r=-\frac{4\sigma_e}{3\beta_r}\frac{\partial T^4}{\partial r}$ in which σ_e represents the Stefan–Boltzmann's constant and β_r represents the mean absorption coefficient respectively.

The nanoparticle concentration conservation equation reads as follows:

$$\frac{\partial C}{\partial t}+v_r\frac{\partial C}{\partial r}+v_z\frac{\partial C}{\partial z}=D_B\frac{\partial^2 C}{\partial z^2}+\frac{D_T}{T_u}\frac{\partial^2 T}{\partial z^2}. \tag{3.6}$$

and the microorganism species conservation equation takes the form:

$$\frac{\partial n}{\partial t}+v_r\frac{\partial n}{\partial r}+v_\theta\frac{\partial n}{\partial \theta}+v_z\frac{\partial n}{\partial z}+\frac{\bar{b}W_{mo}}{C_l-C_u}\left[\frac{\partial}{\partial z}\left(n\frac{\partial C}{\partial z}\right)\right]=D_{mo}\left(\frac{\partial^2 n}{\partial z^2}\right). \tag{3.7}$$

In Eq. (3.7), the chemotaxis constant is combined with maximal speed of cell swimming and is denoted by $\bar{b}W_{mo}$ and the diffusivity of micro-organisms is denoted by D_{mo}.

The boundary conditions prescribed at the disks which correspond to Eqs. (3.1) - (3.7) are as follows:

$$v_r = 0, v_\theta = \Omega_1 r \frac{D^2}{\Gamma^2(t)}, v_z = 0, C = C_l, T = T_l, n = n_l \quad \text{at} \quad z = 0, \tag{3.8}$$

$$\begin{cases} v_r = 0, v_\theta = \Omega_2 r \dfrac{D^2}{\Gamma^2(t)}, v_z = -\dfrac{\alpha D^2}{2\Gamma(t)}, \\ T = T_u, C = C_u, n = n_u. \end{cases} \quad \text{at} \quad z = \Gamma(t) \tag{3.9}$$

3.3 Similarity Transformations

The nonlinear partial differential equation defined by Eqs. (3.1)-(3.7), with the boundary conditions Eqs. (3.8)-(3.9) are reduced to ordinary differential equations by introducing following set of similarity transformations

$$\begin{cases} v_r = r\dfrac{\partial F}{\partial z} = \dfrac{\beta r}{2}\dfrac{D^2}{\Gamma^2(t)} f'(\eta), \theta = \dfrac{T - T_u}{T_l - T_u}, v_\theta = rG(z,t) = r\Omega_1 \dfrac{D^2}{\Gamma^2(t)} g(\eta), \\ v_z = -2F(z,t) = -\dfrac{\alpha D^2 f(\eta)}{\Gamma(t)}, \phi(\eta) = \dfrac{C - C_u}{C_l - C_u}, \chi(\eta) = \dfrac{n - n_u}{n_l - n_u}, \eta = \dfrac{z}{\Gamma(t)}. \end{cases} \tag{3.10}$$

Using the Eq. (3.10) in Eqs. (3.1)-(3.7), the following nonlinear coupled ordinary differential equations with independent variable η are obtained as

$$f^{(iv)} = S_Q \left[3f'' - 2\left(\frac{R_\Omega}{S_Q}\right)^2 gg' - (2f - \eta) f''' \right], \tag{3.11}$$

$$g'' = S_Q \left[2g + \eta g' + 2gf' - fg' \right], \tag{3.12}$$

$$\theta''\left(1 + \frac{4}{3}R_d\right) + S_Q P_l f\theta' + T_l \theta'^2 + T_b \theta'\phi' = 0, \tag{3.13}$$

$$\phi'' + \frac{T_l}{T_b}\theta'' + S_Q S_M f\phi' = 0, \tag{3.14}$$

$$\chi'' - S_Q B_s\left(\frac{\eta}{2}\right)\chi' + B_s S_Q f\chi' - P_l\left[\chi'\phi' + (\chi+\varphi)\phi''\right] = 0. \tag{3.15}$$

In Eqs. (3.11)-(3.15) the Squeezing Reynolds number is represented by $S_Q = \frac{\alpha D^2}{2\upsilon}$, Rotational Reynolds number is denoted by $R_\Omega = \frac{\Omega_1 D^2}{\upsilon}$, Brownian motion parameter is represented by $T_b = \frac{\tau D_B (C_l - C_u)}{\tilde{\alpha}}$, thermophoresis parameter is designated by $T_l = \frac{\tau D_T (T_l - T_u)}{\tilde{\alpha}}$, Prandtl number is $P_l = \frac{\upsilon}{\tilde{\alpha}}$, Schmidt number is $S_M = \frac{\upsilon}{D_B}$, bioconvection Schmidt number is $B_s = \frac{\upsilon}{D_n}$, and bioconvection Péclet number is $Pe = \frac{\bar{b}W_{\mathrm{mo}}}{D_{\mathrm{mo}}}$, $R_d = \frac{4\sigma_e T_u^3}{\beta_r k}$ represents the radiation parameter and $\varphi = \frac{n_u}{n_l - n_u}$ is a micro-organism bioconvection constant.

The corresponding boundary conditions in Eqs. (3.8)- (3.9) are reduced to:

$$\begin{cases} f(0) = f'(0) = 0, g(0) = 1, \theta(0) = 1, \phi(0) = 1, \chi(0) = 1, \\ f(1) = \frac{1}{2}, g(1) = \dot{\xi},\ \theta(1) = 0, \phi(1) = 0, \chi(1) = 0, \end{cases} \tag{3.16}$$

where, f represents axial velocity, g represents the tangential velocity, θ represents temperature, ϕ represents nanoparticle concentration, χ is motile microorganism density number. Also, $\dot{\xi}\left(=\Omega_2/\Omega_1\right)$ denotes the angular velocity and the spin velocity range for the dual disk system i.e., for the rotating disks is $-1 \le \dot{\xi} \le 1$.

The dimensionless torque on the upper moving disk is defined as:

$$\Upsilon_{\mathrm{up}} = 2\pi\rho\int_0^b \left(\frac{\partial v}{\partial z}\right)_{z=\Gamma(t)} \mathrm{d}r. \tag{3.17}$$

Here disk radius is denoted by b. Using Eq. (3.10) in Eq. (3.17), yields:

$$\Upsilon_{\mathrm{up}} = \frac{dg(1)}{d\eta}. \tag{3.18}$$

This provides an expression for the non-dimensional torque on the upper moving disk by the swirling nanofluid Υ_{up} and furthermore the gradient of the tangential velocity on the moving disk is $dg(1)/d\eta$. Similarly, the torque in dimensionless form on the lower (fixed) disk is obtained by the same calculation at $\eta = 0$, gives

$$\Upsilon_{lp} = \frac{dg(0)}{d\eta}. \tag{3.19}$$

3.4 Solution Methodology

The non-linear dimensionless ordinary differential Eqs. (3.11)-(3.15) with boundary conditions mentioned in Eq. (2.16) is solved using the Differential Transform Method (DTM). Applying differential transforms mentioned in Eqs. (1.1)- (1.11) to Eqs. (3.11)-(3.15), we get:

$$\begin{aligned} F(q+4) = {} & \frac{S_Q}{(3+q)(q+2)(4+q)(1+q)}\Big[3(2+q)(q+1)F(2+q) \\ & + \sum_{i=0}^{q}\big[(-i+q+1)(-i+2+q)(q+3-i)F(3+q-i)\varepsilon(i)\big] \\ & - \sum_{i=0}^{q}\big[2(1-i+q)(q-i+2)(q-i+3)F(i)F(-i+q+3)\big] \\ & - 2\frac{R_\Omega^2}{S_Q^2}\sum_{i=0}^{q}\big[(q-i+1)G(i)G(-i+q+1)\big], \end{aligned} \tag{3.20}$$

$$\begin{aligned} G(q+2) = {} & \frac{S_Q}{(q+2)(1+q)}\Big[2G(q) + \sum_{i=0}^{q}\big[(1-i+q)+\varepsilon(i)G(-i+1+q)\big] \\ & + \sum_{i=0}^{q}\big[2(-i+1+q)G(i)F(1-i+q) - (1+q-i)G(q-i+1)F(i)\big], \end{aligned} \tag{3.21}$$

$$\begin{aligned} \Theta(q+2) = {} & \frac{1}{(q+1)\left(1+\frac{4}{3}R_d\right)(q+2)}\Big[-P_t S_Q\sum_{i=0}^{q}(1+q-i)F(i)\Theta(q+1-i) \\ & - \sum_{i=0}^{q}T_t(1+i)(1-i+q)\Theta(i+1)\Theta(q-i+1) \\ & - \sum_{i=0}^{p}T_b(1+i)(1+q-i)\Phi(1-i+q)\theta(i+1)\Big], \end{aligned} \tag{3.22}$$

$$\Phi(q+2)=\frac{1}{(2+q)(1+q)}\left[\begin{array}{l}-S_Q S_M\sum_{i=0}^{q}(q-i+1)\Phi(1-i+q)F(i)-\\ \left(\frac{T_t}{T_b}\right)\Theta(2+q)(2+q)(q+1)\end{array}\right], \tag{3.23}$$

$$\begin{aligned}\mathrm{X}(q+2)=\frac{1}{(2+q)(1+q)}\Bigg[&S_Q S_M\sum_{i=0}^{q}\frac{\varepsilon(i)}{2}(q-i+1)\mathrm{X}(-i+1+q)\\ &-S_Q S_M\sum_{i=0}^{q}(-i+1+q)F(i)\mathrm{X}(-i+1+q)\\ &+P_l\Bigg[\sum_{i=0}^{q}(1+i)(-r+1+q)\mathrm{X}(i+1)\Phi(q-i+1)\\ &+\sum_{i=0}^{q}(q-i+1)(2-i+q)\mathrm{X}(i)\Phi(2+q+i)\\ &+\big(\mathrm{X}(i)+\varphi\big)(2+q)(1+q)\Phi(2+q)\Bigg]\Bigg].\end{aligned} \tag{3.24}$$

Here, the transformed functions of $f(\eta), g(\eta), \theta(\eta), \phi(\eta)$ and $\chi(\eta)$ are $F(q), G(q), \Theta(q), \Phi(q)$ and $\mathrm{X}(q)$ respectively and are expressed as follows:

$$f(\eta)=\sum_{q=0}^{\infty}F(q)\eta^q, \tag{3.25}$$

$$g(\eta)=\sum_{q=0}^{\infty}G(q)\eta^q, \tag{3.26}$$

$$\theta(\eta)=\sum_{q=0}^{\infty}\Theta(q)\eta^q, \tag{3.27}$$

$$\phi(\eta)=\sum_{q=0}^{\infty}\Phi(q)\eta^q, \tag{3.28}$$

$$\chi(\eta)=\sum_{q=0}^{\infty}\mathrm{X}(q)\eta^q. \tag{3.29}$$

The associated boundary conditions are:

Need For Scanning

$$\left.\begin{array}{lllll} F(0)=0, & F(1)=\frac{1}{2}, & G(0)=1, & \Theta(0)=1, & \Phi(0)=1, \\ \mathrm{X}(0)=1, & F(2)=\Pi_1, & F(3)=\Pi_2, & G(1)=\Pi_3, & \Theta(1)=\Pi_4, \\ \Phi(1)=\Pi_5, & \mathrm{X}(1)=\Pi_6 & & & \end{array}\right\} \quad (3.30)$$

Solving Eqs. (3.20)-(3.24) with help of boundary conditions given in Eq. (3.30), we obtain the following series solutions:

$$F(\eta)=f_1\eta^2+f_2\eta^3+f_3\eta^4+f_4\eta^5+..., \quad (3.31)$$

$$G(\eta)=1-g_1\eta+g_2\eta^2+g_3\eta^3+g_4\eta^4+..., \quad (3.32)$$

$$\Theta(\eta)=1+\theta_1\eta+\theta_2\eta^2+\theta_3\eta^3+\theta_4\eta^4+..., \quad (3.33)$$

$$\Phi(\eta)=1+\phi_1\eta+\phi_2\eta^2+\phi_3\eta^3+\phi_4\eta^4+..., \quad (3.34)$$

$$\mathrm{X}(\eta)=1+\chi_1\eta+\chi_2\eta^2+\chi_3\eta^3+\chi_4\eta^4+..., \quad (3.35)$$

Here $f_i, g_i, m_i, n_i, \theta_i, \phi_i\ \chi_i\ ; (i=1,2,3,...)$ are constants. With the aid of computational software "MATHEMATICA", the above equations are solved up to 30 iterations. However, the desired rate of convergence is not obtained. Therefore, by deploying DTM-Padé simulation, the analytic solution obtained by DTM is combined with the Padé approximation, which gives a reasonable convergence rate at $\eta=1$. So, appling the Padé approximation of order [5×5] to solution obtained in Eqs. (3.31)-(3.35), the Padé approximants are as follows.

$$f(\eta)=\frac{1.70053\eta^2-1.44890\eta^3+0.31487\eta^4-0.06248\eta^5}{1+0.01261\eta-0.00403\eta^2-0.00040\eta^3-0.00020\eta^4+0.000063\eta^5}, \quad (3.36)$$

$$g(\eta)=\frac{1-1.35929\eta-0.14544\eta^2+0.36560\eta^3+0.12128\eta^4+0.01785\eta^5}{1-0.35119\eta-0.50948\eta^2-0.14511\eta^3-0.01605\eta^4+0.00075\eta^5}, \quad (3.37)$$

$$\theta(\eta)=\frac{1-0.80195\eta-0.20532\eta^2+0.00583\eta^3-0.00169\eta^4+0.00325\eta^5}{1+0.07466\eta-0.02210\eta^2+0.00570\eta^3-0.00616\eta^4+0.00017\eta^5}, \quad (3.38)$$

$$\phi(\eta)=\frac{1-0.71280\eta-0.58592\eta^2+0.33874\eta^3-0.056254\eta^4+0.02364\eta^5}{1+0.66107\eta-0.03568\eta^2+0.02127\lambda^3-0.02173\eta^4-0.00312\eta^5}, \quad (3.39)$$

$$\chi(\eta)=\frac{1-0.36377\eta-0.71281\eta^2+0.16843\eta^3-0.128773\eta^4+0.03811\eta^5}{1+1.07139\eta+0.15110\eta^2-0.02106\eta^3-0.02634\eta^4-0.01361\eta^5}. \quad (3.40)$$

3.5 Graphical and Tabular Results

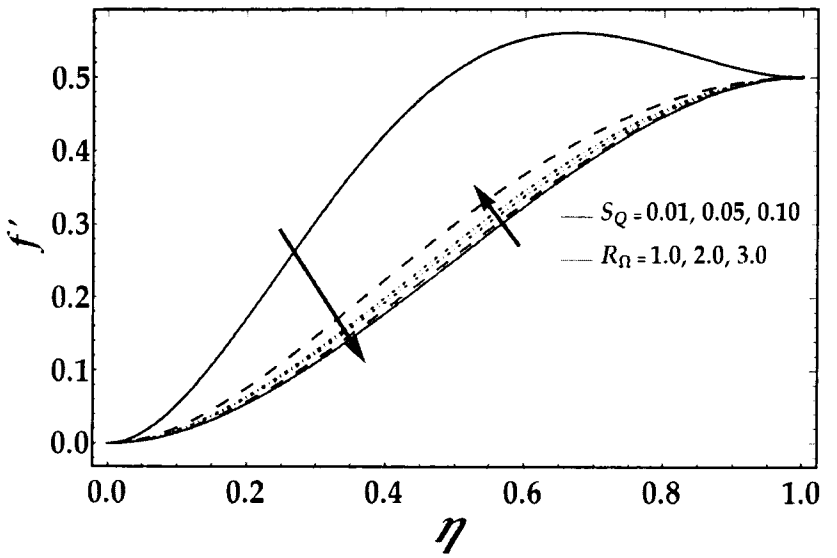

Figure 3.2: Impact of various values of squeezing Reynolds number S_Q and rotational Reynolds number R_Ω on axial velocity distribution $f'(\eta)$.

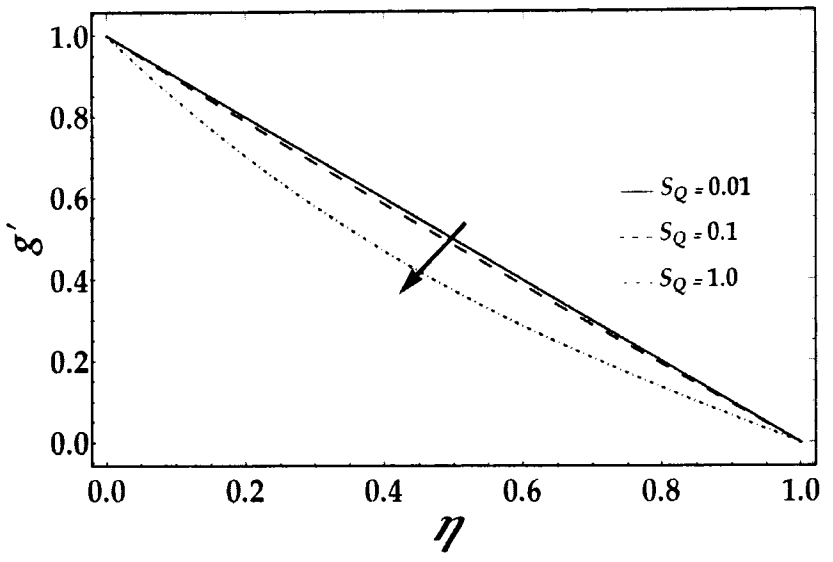

Figure 3.3: Impact of various values of squeezing Reynolds number S_Q on tangential velocity distribution $g'(\eta)$.

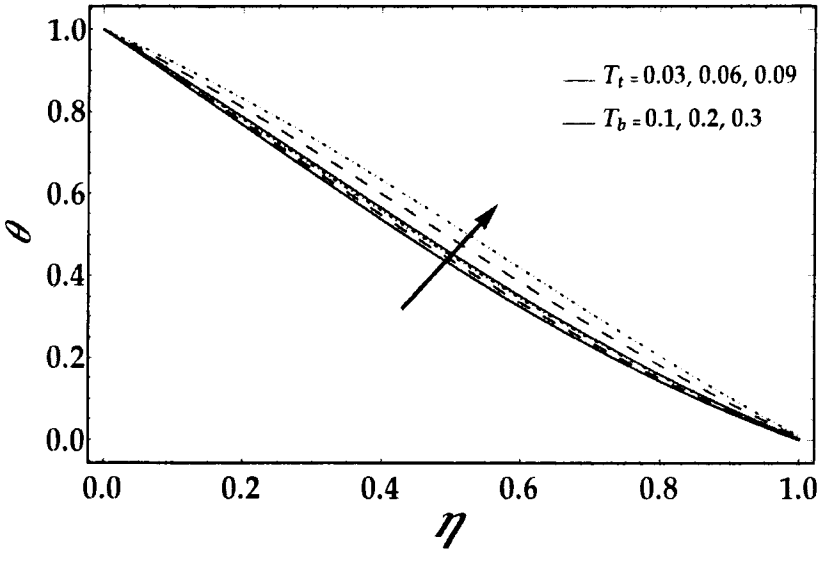

Figure 3.4: Impact of various values of thermophoresis parameter T_t and Brownian motion parameter T_b on temperature distribution $\theta(\eta)$.

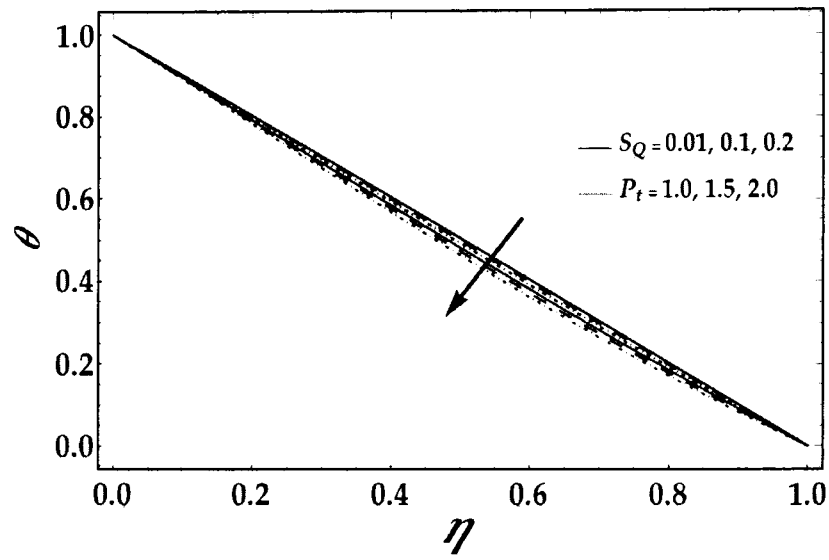

Figure 3.5: Impact of various values of squeezing Reynolds number S_Q, Prandtl number P_t on temperature distribution $\theta(\eta)$.

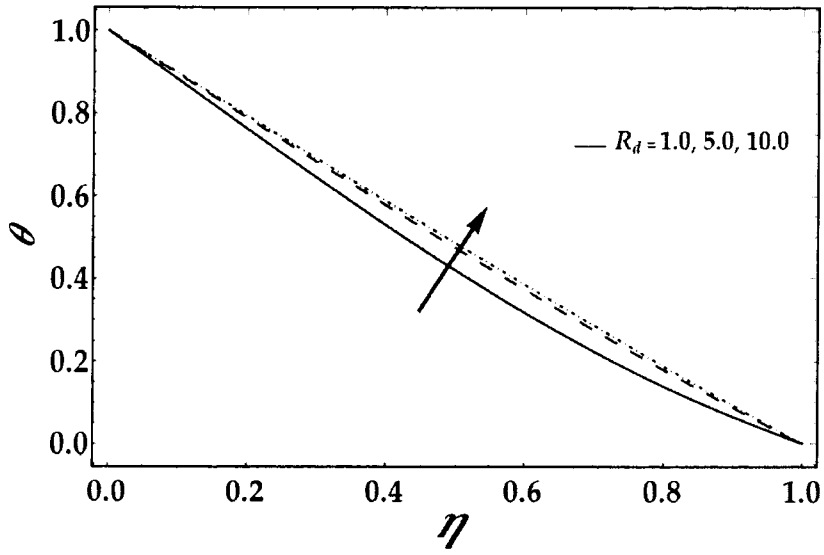

Figure 3.6: Impact of different values of radiation parameter R_d on temperature distribution $\theta(\eta)$.

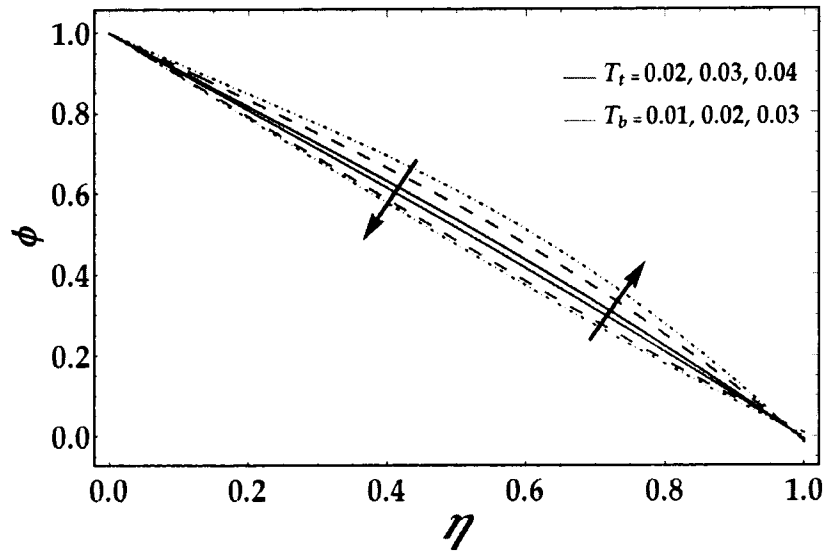

Figure 3.7: Impact of various values of thermophoresis parameter T_t and Brownian motion parameter T_b on nanoparticle volume fraction $\phi(\eta)$.

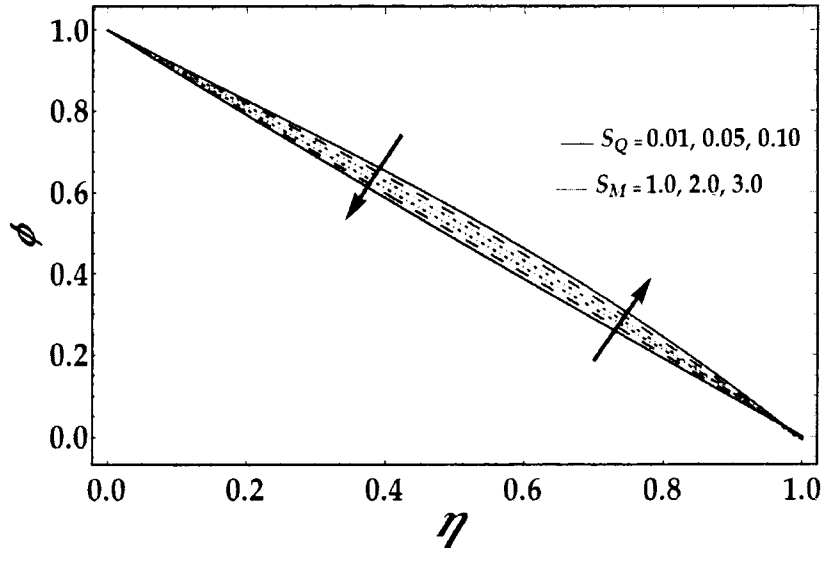

Figure 3.8: Impact of various values of squeezing Reynolds number S_Q, Schmidt number S_M on nanoparticle volume fraction $\phi(\eta)$.

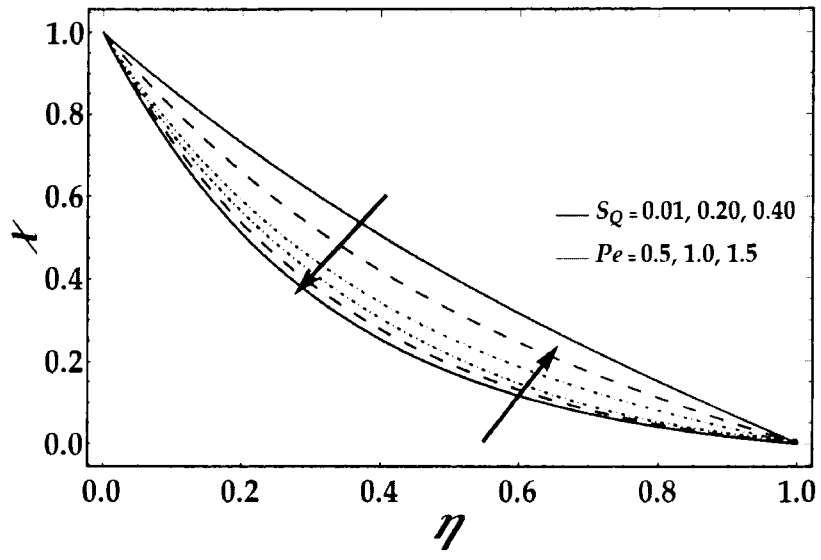

Figure 3.9: Impact of various values of squeezing Reynolds number S_Q, Péclet number Pe on motile microorganism density function $\chi(\eta)$.

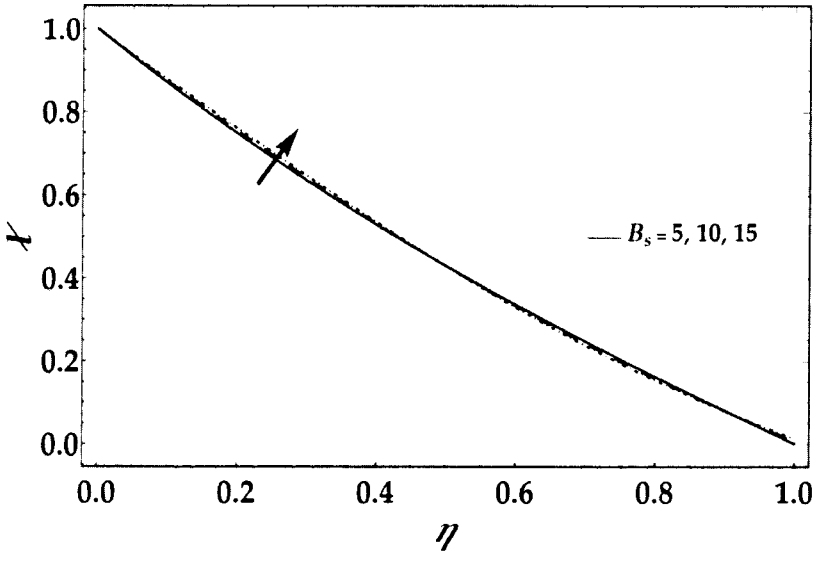

Figure 3.10: Impact of various values of Bio convection Schmidt Number B_s on motile microorganism density function $\chi(\eta)$.

Table 3.1: Comparison of $\theta'(0), \phi'(0), \chi'(0)$ for various values $T_t, T_b, P_t, S_Q, S_M, P_l$ by DTM-Padé$[5\times5]$ and the numerical Shooting Method.

						$\theta'(0)$		$\phi'(0)$		$\chi'(0)$	
T_t	T_b	P_t	S_Q	S_M	P_l	**Shooting Method**	**DTM-Padé**	**Shooting Method**	**DTM-Padé**	**Shooting Method**	**DTM-Padé**
0.03	0.01	6.8	0.01	5	0.5	-0.876624	-0.876624	-1.373875	-1.373875	-1.435174	-1.435174
0.06						-0.788046	-0.788046	-2.275155	-2.275155	-1.831637	-1.831637
0.09						-0.706065	-0.706065	-3.648415	-3.648415	-2.438629	-2.438629
0.05	0.1					-0.583239	-0.583239	-1.212212	-1.212212	-1.361695	-1.361695
	0.3					-0.249589	-0.249589	-1.128954	-1.128954	-1.323609	-1.323609
	0.5					-0.095107	-0.095107	-1.094404	-1.094404	-1.307756	-1.307756
	0.1	4				-0.735315	-0.735315	-1.136189	-1.136189	-1.329559	-1.329559
		7				-0.573375	-0.573375	-1.217143	-1.217143	-1.363747	-1.363747
		10				-0.440450	-0.440450	-1.283606	-1.283606	-1.390905	-1.390905
		6.8	0.01			-0.583239	-0.583239	-1.212212	-1.212212	-1.361695	-1.361695
			0.05			-0.596730	-0.596730	-1.220156	-1.220156	-1.363114	-1.363114
			0.10			-0.613646	-0.613646	-1.229987	-1.229987	-1.364822	-1.364822
			0.01	5		-0.583239	-0.583239	-1.212212	-1.212212	-1.361695	-1.361695
				10		-0.582837	-0.582837	-1.216244	-1.216244	-1.363346	-1.363346
				15		-0.582435	-0.582435	-1.220274	-1.220274	-1.364997	-1.364997
				5	0.5	-0.583239	-0.583239	-1.212212	-1.212212	-1.361695	-1.361695
					1.0	-0.583239	-0.583239	-1.212212	-1.212212	-1.772446	-1.772446
					1.5	-0.583239	-0.583239	-1.212212	-1.212212	-2.226726	-2.226726

Table 3.2: Values of torque at the lower (fixed) and upper (moving) disks for different values of S_Q.

	$\frac{dg(0)}{d\eta}$		$\frac{dg(1)}{d\eta}$	
S_Q	**Shooting Method**	**DTM-Padé**	**Shooting Method**	**DTM-Padé**
0.01	-1.008097	-1.008097	-0.991545	-0.991545
0.05	-1.039719	-1.039719	-0.977810	-0.977810
0.10	-1.078561	-1.078561	-0.956358	-0.956358

3.6 Discussion

Extensive DTM-Padé computations have been performed with computational software MATHEMATICA to investigate the impact of various parameters on the transport characteristics for the dual disk squeezing regime is considered. To verify the exactness of the results, solutions with the shooting method are compared with the DTM-Padé. The influence of squeezing Reynolds number S_Q, rotational Reynolds number R_Ω, Prandtl number P_t, thermophoresis parameter T_t, Brownian motion T_b, thermal radiation parameter R_d, Schmidt number S_M, bio convection number B_s, and Péclet number Pe on velocity distribution, temperature profile, nanoparticle concentration, and motile microorganism function are visualized in figures (3.2)-(3.10).

In all graphs strong data is extracted for numerous parameters. This provides a realistic range for squeezing rotating bio-Nano fluid radiative systems. The physical description of the figures are as follows.

Velocity Distribution

Figure (3.2) shows the collective impact of squeezing Reynolds number S_Q and rotational Reynolds number R_Ω on axial velocity distribution. It is observed that when values of squeezing Reynolds number S_Q are enhanced, the axial velocity distribution decreases. Momentum in squeezing regime is suppressed clearly as upper disk approaches the lower disk. This inhibits axial flow and produces axial flow retardation. It is also noteworthy that for very low squeezing Reynolds number $S_Q = 0.01$, a velocity overshoot is computed closer to the upper disk $\eta = 1.0$. This feature vanishes with higher S_Q values owing to the damping effect induced on the axial flow with more intense squeezing. However, with increasing the values of rotational Reynolds number R_Ω axial velocity increased, since the rotational inertial force is amplified with greater R_Ω values, relative to the viscous hydrodynamic force. $R_\Omega = \frac{\Omega_1 D^2}{\upsilon}$ Expresses the ratio of these two forces, both velocity components are either directly or indirectly influenced by Reynolds number. The dominant effect is however an acceleration in axial flow.

Figure (3.3) shows the impact of squeezing Reynolds S_Q number on tangential velocity distribution. It is evident that by enhancing value of squeezing Reynolds number, tangential velocity distribution also decreases. Large estimates of S_Q disrupt mass diffusivity that eventually lowers tangential velocity profile.

Temperature Distribution

Figure (3.4) displays the influence of thermophoresis parameter T_t and Brownian motion parameter T_b on temperature profile. The graph illustrates that enhancing values of thermophoresis parameter and Brownian motion parameter considerably elevate temperature magnitudes. The ballistic collisions of nanoparticles

produce an enhancement in conversion of kinetic energy of nanoparticles to thermal energy. This is dissipated as heat and temperatures are rises. The presence of rotational body force would also appear to amplify this effect. In all cases approximately linear decays in temperature are computed from the lower disk (maximum) to the upper disk (minimum). The influence of Brownian dynamics is also more pronounced than for thermophoretic body force which encourages the migration of the nanoparticles under a temperature gradient to cooler zones in the regime.

Figure (3.5) illustrates evolution in temperature, with a variation in squeezing Reynolds number, S_Q and Prandtl number P_t. It is observed that increment in Prandtl number P_t, leads to depletion in temperature magnitudes. This is attributable to depletion in thermal conductivity with larger Prandtl number since it is inversely proportional to thermal conductivity for fixed values of dynamic viscosity and specific heat capacity of nanofluid which cools the regime i.e., produces a resulting temperature decline. It is also noted that the temperature profile declines with enhancing value of squeezing Reynolds number S_Q. The destruction in axial momentum with greater squeezing also inhibits thermal diffusion in the regime which a produces cooling effect. This is clearly beneficial in lubrication applications and also assists in improved thermal control of the regime in rotating bioreactor design.

Figure (3.6) depicts effects of thermal radiation parameter, R_d on temperature distribution between two disks. It is seen that an increment in value of thermal radiation parameter considerably accentuates the temperature magnitudes. The thermal radiation parameter simulates relative role of radiative heat transfer to thermal conduction heat transfer. This is because, increase of radiation property causes reduction in absorptivity, consequently increases rate of heat transfer for fluid.

Nanoparticle Concentration Distribution

Figure (3.7) visualizes influence of thermophoresis parameter T_t and Brownian motion T_b for nanoparticle concentration $\phi(\eta)$. It observed that concentration of nanoparticles falls with an increment in Brownian motion parameter T_b since ballistic collisions are exacerbated and this inhibits transport of nanoparticles in fluent medium. Conversely, the concentration of nanoparticle increases when values of the thermophoresis parameter T_t are elevated. Thermal gradient driving the thermophoretic migration is therefore beneficial to the diffusion of nanoparticles whereas the haphazard motion associated with Brownian dynamics impedes nanoparticle migration.

Figure (3.8) shows impact of squeezing Reynolds number S_Q and Schmidt number S_M. By increasing values of squeezing Reynolds number S_Q, nanoparticle concentration is boosted, while opposite behavior is observed with increment in value of Schmidt number S_M. Clearly the suppressive effect of enhanced squeezing decreases volume of Nano fluid film intercalated between the disks. This increases concentration of nanoparticles since same quantity of nanoparticles is squeezed into a smaller overall volume. However, with increasing Schmidt number, as defined by $S_M = \frac{\upsilon}{D_B}$ for fixed dynamic viscosity, there must be a reduction in nanoparticle mass diffusivity. This manifests in a depletion in the nanoparticle concentration magnitudes as the nanoparticle diffusion rate is reduced.

Motile Gyrotactic Microorganism Distribution

Figure (3.9) portrays influence of squeezing Reynolds number S_Q and bioconvection Péclet number Pe on gyrotactic microorganism density number function. It is apparent that there is substantial increment in microorganism density number with rise in squeezing Reynolds number S_Q which may be attributed to

significant decrease in volume of nanofluid due to enhanced squeezing. This constrains the same number of micro-organisms in a smaller overall nanofluid film volume and naturally elevates their concentrations. On contrary, elevation in bioconvection Péclet number Pe induces opposite effect there is significant reduction in microorganism density number. As defined bioconvection Péclet number and is inversely proportional to species diffusivity of the microorganisms. Larger Péclet values will inevitably result in a reduction in micro-organism diffusivity. This will counteract the propulsion of the gyrotactic micro-organisms and result in a significant suppression in microorganism density number magnitudes. Figure (3.10) is displayed to get the physical behaviour of the Bio convection Schmidt number. It is shown that when the values of the Bio convection Schmidt number increase, the microorganism density increases, but the effects are minimal.

Physical Quantities

In Table 3.1, numerical results for local Nusselt number, local nanoparticle Sherwood number, and motile density number wall gradient are Shown. From this table, it is evident that very good agreement is achieved between DTM-Padé simulation and numerical shooting method. Eqs. (3.18)-(3.19) are used to calculate the effects of torque on the upper fixed and lower moving disk, and the DTM-Padé computations are displayed in Table 3.2. Finally it is noteworthy from inspection of Table 3.2, that the torque at the lower (fixed) disk $\frac{dg(0)}{d\eta}$ i.e., tangential velocity gradient, and the torque at the upper (moving) disk, $\frac{dg(1)}{d\eta}$ are respectively decreased and increased with an increase in the squeezing Reynolds number, S_Q. Therefore, while axial momentum is reduced in the squeezing regime it has a different impact on the torque at the lower and upper disks. The amplification in squeezing effect reduces torque at the lower disk whereas it enhances torque at the upper disk.

Chapter 4

Transport of Motile Gyrotactic Microorganism for Magnetized Nano fluid Flow between Circular Rotating Plates

4.1 Introduction

In this chapter, a mathematical model for magnetized Nano fluid flow between rotating circular plates filled with nanoparticles and gyrotactic microorganisms is developed. A generalized form of induced magnetic field is used for mathematical modelling of nanofluid flow. The governing equations involves continuity, momentum, energy, nanoparticle concentration and concentration of microorganism species for the flow of Nano fluid in cylindrical polar coordinates. Problem then simplified to non-linear coupled ordinary differential equations by using suitable similarity transformations. DTM combined with Padé-approximation is applied to solve resulting equations. Analytic results with physical interpretation are shown by drawing graphs and tables.

4.2 Mathematical Formulation

Flow Assumptions

The mathematical model for the flow of Motile Gyrotactic Microorganism for Magnetized Nano fluid Flow between Circular Rotating Plates following assumptions have been accounted. Along with the flow assumptions from chapter two, Viscous Nano fluid saturating space between rotating and squeezing disks with

- Induced magnetic field.

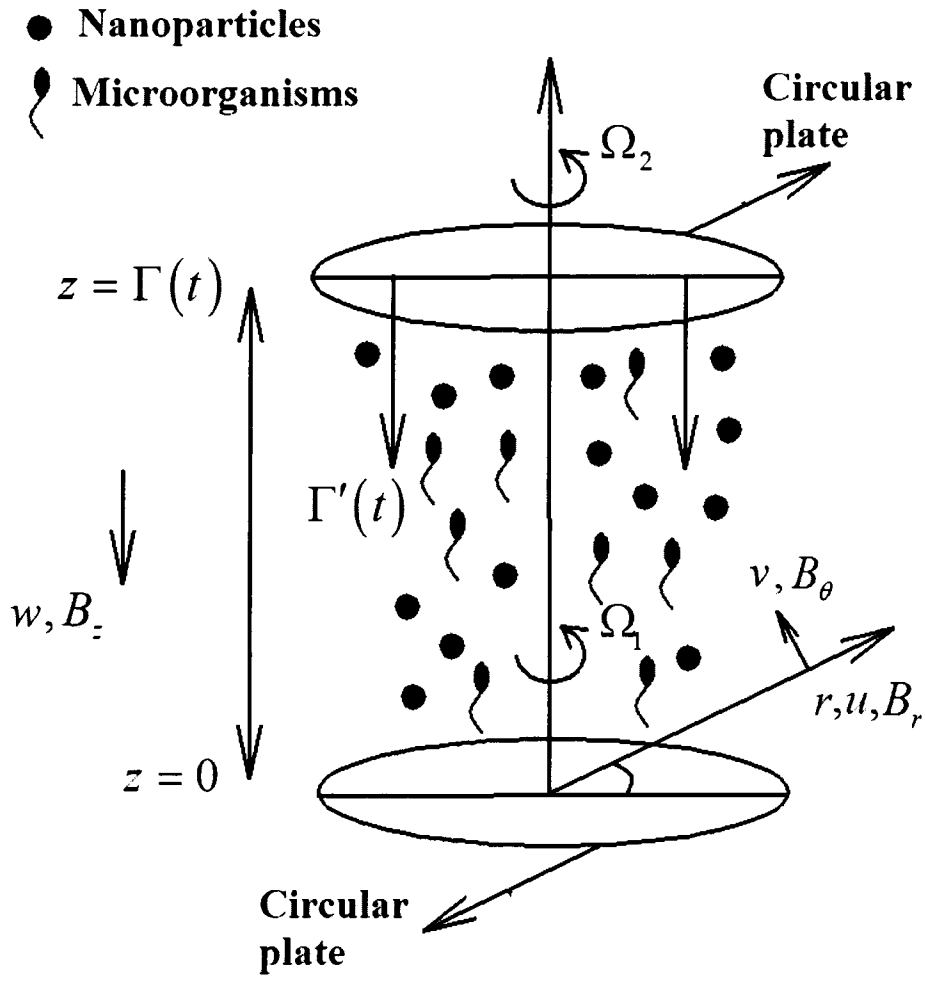

Figure 4.1: The schematic diagram of nanoparticles between parallel finite plates in presence of Microorganisms.

Mathematical Model

The governing equations by taking the above assumptions, the hydro-magnetic squeeze film regime for the equation of continuity and momentum read as

$$\frac{1}{r}\frac{\partial}{\partial\theta}(v_\theta)\frac{1}{r}\frac{\partial}{\partial r}(rv_r)+\frac{\partial}{\partial z}(v_z)=0 \tag{4.1}$$

$$\rho\left(v_r\frac{\partial v_r}{\partial r}+\frac{\partial v_r}{\partial t}+v_z\frac{\partial v_r}{\partial z}+\frac{v_\theta}{r}\frac{\partial v_r}{\partial\theta}-\frac{v_\theta}{r}\right)=-\frac{\partial p}{\partial r}+ \mu\left[\frac{1}{r}\frac{\partial v_r}{\partial r}+\frac{1}{r^2}\frac{\partial^2 v_r}{\partial\theta^2}+\frac{\partial^2 v_r}{\partial z^2}-\frac{2}{r}\frac{\partial v_\theta}{\partial\theta}-\frac{v_r}{r^2}\right]-\frac{\partial B_r}{\partial z}B_z-\frac{\partial B_\theta}{\partial z}B_\theta, \tag{4.2}$$

$$\rho\left(\frac{\partial v_\theta}{\partial t}+\frac{v_\theta}{r}\frac{\partial v_\theta}{\partial\theta}+v_r\frac{\partial v_\theta}{\partial r}+v_z\frac{\partial v_\theta}{\partial z}-\frac{v_r v_\theta}{r}\right)=-\frac{1}{r}\frac{\partial p}{\partial\theta}+ \mu\left[\frac{1}{r^2}\frac{\partial^2 v_\theta}{\partial\theta^2}+\frac{1}{r}\frac{\partial}{\partial r}\left(r\frac{\partial v_\theta}{\partial r}\right)+\frac{\partial^2 v_\theta}{\partial z^2}+\frac{2}{r^2}\frac{\partial v_r}{\partial\theta}-\frac{v_\theta}{r^2}\right]-\frac{\partial B_\theta}{\partial z}B_z-\frac{\partial B_\theta}{\partial r}B_r, \tag{4.3}$$

$$\rho\left(\frac{\partial v_z}{\partial t}+\frac{v_\theta}{r}\frac{\partial v_z}{\partial\theta}+v_r\frac{\partial v_z}{\partial r}+v_z\frac{\partial v_z}{\partial z}\right)=-\frac{\partial p}{\partial z}+ \mu\left[\frac{1}{r^2}\frac{\partial^2 v_z}{\partial\theta^2}+\frac{1}{r}\frac{\partial}{\partial r}\left(r\frac{\partial v_z}{\partial r}\right)+\frac{\partial^2 v_z}{\partial z^2}\right]-\frac{\partial B_\theta}{\partial z}B_\theta+\frac{\partial B_r}{\partial z}B_r, \tag{4.4}$$

The magnetic field equations read as

$$\frac{1}{r}\frac{\partial}{\partial r}(rB_r)+\frac{1}{r}\frac{\partial B_\theta}{\partial\theta}+\frac{\partial B_z}{\partial z}=0, \tag{4.5}$$

$$\frac{\partial B_r}{\partial t}+u\frac{\partial B_r}{\partial r}+v\frac{\partial B_r}{\partial\theta}+w\frac{\partial B_r}{\partial z}=-\frac{\partial}{\partial z}(v_rB_z-v_zB_r)+\frac{1}{\delta\mu_2}\left(\frac{\partial^2 B_r}{\partial z^2}\right), \tag{4.6}$$

$$\frac{\partial B_\theta}{\partial t}+u\frac{\partial B_\theta}{\partial r}+v\frac{\partial B_\theta}{\partial\theta}+w\frac{\partial B_\theta}{\partial z}=\frac{\partial}{\partial r}(v_rB_\theta-v_\theta B_r)-\frac{\partial}{\partial z}(v_\theta B_z-B_\theta v_z)+\frac{1}{\delta\mu_2}\left(\frac{\partial^2 B_\theta}{\partial z^2}\right), \tag{4.7}$$

$$\frac{\partial B_z}{\partial t}+u\frac{\partial B_z}{\partial r}+v\frac{\partial B_z}{\partial\theta}+w\frac{\partial B_z}{\partial z}=\frac{\partial}{\partial r}(v_rB_z-v_zB_r)+\frac{1}{\delta\mu_2}\left(\frac{\partial^2 B_z}{\partial z^2}\right), \tag{4.8}$$

where, δ the electrical conductivity.

The energy equation reads as

$$\frac{\partial T}{\partial t}+v_r\frac{\partial T}{\partial r}+v_z\frac{\partial T}{\partial z}-\frac{k}{\rho c_p}\frac{\partial^2 T}{\partial z^2}+\frac{(\rho c)_p}{(\rho c)_f}\left[D_B\left(\frac{\partial T}{\partial z}\frac{\partial C}{\partial z}+\frac{\partial T}{\partial r}\frac{\partial C}{\partial r}\right)+\frac{D_T}{T_u}\left[\left(\frac{\partial T}{\partial r}\right)^2+\left(\frac{\partial T}{\partial z}\right)^2\right]\right] \tag{4.9}$$

where the temperature is denoted by T, concentration is denoted by C, mean fluid temperature is denoted by T_m, specific heat at uniform temperature is denoted by c_p, D_B is Brownian diffusivity, and D_T is thermophoretic diffusion coefficient.

The nanoparticle concentration equation reads as

$$\frac{\partial C}{\partial t}+v_r\frac{\partial C}{\partial r}+v_z\frac{\partial C}{\partial z}=D_B\frac{\partial^2 C}{\partial z^2}+\frac{D_T}{T_u}\frac{\partial^2 T}{\partial z^2}. \tag{4.10}$$

The equation for conservation of microorganism reads as

$$\frac{\partial n}{\partial t}+v_r\frac{\partial n}{\partial r}+v_\theta\frac{\partial n}{\partial \theta}+v_z\frac{\partial n}{\partial z}+\frac{\bar{b}W_{mo}}{C_l-C_u}\left[\frac{\partial}{\partial z}\left(n\frac{\partial C}{\partial z}\right)\right]=D_{mo}\left(\frac{\partial^2 n}{\partial z^2}\right). \tag{4.11}$$

The corresponding boundary conditions are

$$u=0, v=\Omega_1 r\frac{D^2}{\Gamma^2(t)}, w=0, B_z=B_\theta=0, C=C_l, T=T_l, n=n_l \quad \text{at} \quad z=0, \tag{4.12}$$

$$\begin{cases} u=0, v=\Omega_2 r\dfrac{D^2}{\Gamma^2(t)}, B_\theta=N_0 r\dfrac{D^2}{\Gamma^2(t)}, B_z=-\dfrac{\beta D M_0}{\Gamma(t)}, w=-\dfrac{\beta D^2}{2\Gamma(t)}, & \text{at} \quad z=\Gamma(t). \\ T=T_u, C=C_u, n=n_u, \end{cases} \tag{4.13}$$

4.3 Similarity Transformation

Along with the similarity transformation from chapter two, Introducing following similarity transformations

$$\begin{cases} B_r=r\dfrac{\partial M}{\partial z}=\dfrac{\beta r D M_0}{2\Gamma^2(t)}\dfrac{dm}{d\eta}, B_\theta=rN(z,t)=rN_0\dfrac{D^2}{\Gamma^2(t)}n(\eta), \\ B_z=-2M(z,t)=-\dfrac{\beta D M_0 m(\eta)}{\Gamma(t)}. \end{cases} \tag{4.14}$$

Substituting the above similarity transformations to Eq. (4.1)-(4.11), we obtain set of following coupled ordinary differential equations with dimensioanless variable η, we have

$$f^{(iv)} = S_Q\left[3f'' - 2\left(\frac{R_\Omega}{S_Q}\right)^2 gg' + 2F_A^2\left(mm''' + m'm''\right) - \left(2f - \eta\right)f''' + 2F_T^2\left(\frac{R_\Omega}{S_Q}\right)^2 nn'\right], \tag{4.15}$$

$$g'' = S_Q\left[2g + \eta g' + 2gf' - fg' + 2N_T M_T\left(mn' + nm'\right)\right], \tag{4.16}$$

$$m'' = \mathrm{Re}_M\left[\eta m' + m - 2fm' + 2mf'\right], \tag{4.17}$$

$$n'' = \mathrm{Re}_M\left[\eta n' + 2n + 2\left(\frac{F_A}{F_T}\right)mg' - fn'\right], \tag{4.18}$$

$$\theta'' + T_b\theta'\phi' + T_t\theta'^2 + S_Q P_t f\theta' = 0, \tag{4.19}$$

$$\phi'' + \frac{T_t}{T_b}\theta'' + S_Q S_M f\phi' = 0, \tag{4.20}$$

$$\chi'' - S_Q B_s\left(\frac{\eta}{2}\right)\chi' + B_s S_Q f\chi' - P_l\left[\chi'\phi' + (\chi + \varphi)\phi''\right] = 0. \tag{4.21}$$

The corresponding boundary conditions read as

$$\begin{cases} f(0) = 0,\ f'(0) = 0, g(0) = 1, m(0) = 0, n(0) = 1, \theta(0) = 1, \chi(0) = 1, \phi(0) = 1, \\ f(1) = \dfrac{1}{2}, g(1) = \xi, m(1) = 1, n(1) = 1, \theta(1) = 0, \phi(1) = 0, \chi(1) = 0, \end{cases} \tag{4.22}$$

where f and g are the axial and tangential velocity, m and n are the axial and tangential induced magnetic field component, θ the temperature profile of nanoparticles, ϕ is concentration of nanoparticles volume fraction, χ is motile density microorganism profile, and $\xi\left(=\Omega_2/\Omega_1\right)$ represents the corresponding angular velocity between the plates having range $-1 \le \xi \le 1$, which is beneficial to examine different flow features associated to the plates that rotates in opposite and same directions. Torque on both disk is also calculated using Eqs. (3.17) - (3.19).

4.4 Solution Methodolgy

Applying the differential transformations mentioned in Eq. (2.12) -(2.19) to Eqs. (4.15) -(4.21), we get

$$
\begin{aligned}
F(q+4) = \frac{S_Q}{(q+4)(q+3)(q+2)(q+1)}\Big[&3(1+q)(2+q)F(2+q) \\
&+\sum_{i=0}^{q}\big[(1-i+q)(2-i+q)(3-i+q)\varepsilon(i)F(3-i+q)\big] \\
&-\sum_{i=0}^{q}\big[2(1-i+q)(2-i+q)(3-i+q)F(i)F(3-i+q)\big] \\
&-2\frac{R_\Omega^2}{S_Q^2}\sum_{i=0}^{q}\big[(1-i+q)G(i)G(1-i+q)\big] \\
&+2F_T^2\sum_{i=0}^{q}\begin{bmatrix}(1-i+q)(2-i+q)(3-i+q+)M(i)M(3-i+q)\\ +(1+i)(i+2)(1-i+q)(2-i+q)M(i+1)M(2-i+q)\end{bmatrix} \\
&+2F_A^2\left(\frac{R_\Omega^2}{S_Q^2}\right)^2\sum_{i=0}^{q}\big[(q-i+1)N(q+1-i)N(i)\big],
\end{aligned}
\tag{4.23}
$$

$$
\begin{aligned}
G(q+2) = \frac{S_Q}{(q+2)(q+1)}\Big[&2G(q)+\sum_{i=0}^{q}\big[(1-i+q)+\varepsilon(i)G(1-i+q)\big] \\
&+\sum_{i=0}^{q}\big[2(1-i+q)G(i)F(1-i+q)-2(1-i+q)F(i)G(1-i+q)\big] \\
&+2F_AF_T\sum_{i=0}^{q}\big[(1-i+q)M(i)N(1-i+q)-(1-i+q)N(i)M(1-i+q)\big]\Big],
\end{aligned}
\tag{4.24}
$$

$$
\begin{aligned}
M(q+2) = \frac{\mathrm{Re}_M}{(q+1)(q+2)}\Big[&M(q)+\sum_{i=0}^{p}(1-i+q)\varepsilon(i)M(1-i+q) \\
&-\sum_{i=0}^{q}\big[2(1-i+q)f(i)M(1-i+q)-2(1-i+q)M(i)F(1-i+q)\big]\Big],
\end{aligned}
\tag{4.25}
$$

$$
\begin{aligned}
N(q+2) = \frac{\mathrm{Re}_M}{(q+1)(q+2)}\Big[&2N(q)+\sum_{i=0}^{p}(1-i+q)\varepsilon(i)N(1-i+q) \\
&-\sum_{i=0}^{p}\left[2(1-i+q)F(i)N(1-i+q)-2\left(\frac{F_A}{F_T}\right)(1-i+q)G(1-i+q)M(i)\right]\Big],
\end{aligned}
\tag{4.26}
$$

$$
\begin{aligned}
\Theta(q+2) = \frac{P_t}{(q+1)(q+2)}\Big[&-S_Q\sum_{i=0}^{q}(1-i+q)F(i)\Theta(1-i+q) \\
&-\sum_{i=0}^{q}T_l(1+i)(1-i+q)\Theta(1+i)\Theta(1-i+q) \\
&-\sum_{i=0}^{p}T_h(1+i)(1-i+q)\Phi(1-i+q)\Theta(i+1)\Big],
\end{aligned}
\tag{4.27}
$$

$$\Phi(q+2)=\frac{1}{(q+1)(q+2)}\left[-S_Q S_M\sum_{i=0}^{q}(1-i+q)F(i)\Phi(1-i+q)-\left(\frac{T_t}{T_b}\right)\Theta(q+2)(2+q)(1+q)\right], \tag{3.28}$$

$$\begin{aligned}\mathrm{X}(q+2)=\frac{1}{(2+q)(1+q)}\Bigg[&S_Q S_M\sum_{i=0}^{q}\frac{\varepsilon(i)}{2}(q+1-i)\mathrm{X}(1-i+q)\\&-S_Q S_M\sum_{i=0}^{q}(1-i+q)F(i)\mathrm{X}(1-i+q)\\&+P_t\Bigg[\sum_{i=0}^{q}(i+1)(1-r+q)\mathrm{X}(1+i)\Phi(q+1-i)\\&+\sum_{i=0}^{q}(1-i+q)(2-i+q)\mathrm{X}(i)\Phi(2-i+q)\\&+\big(\mathrm{X}(i)+\varphi\big)(1+q)(2+q)\Phi(2+q)\Bigg]\Bigg],\end{aligned} \tag{4.29}$$

Where $F(q), G(q), m(q), n(q)\Theta(q), \Phi(q)$ and $\mathrm{X}(q)$ are the differential transformations of $f(\eta), g(\eta), m(\eta), n(\eta), \theta(\eta), \phi(\eta)$ and $\chi(\eta)$ are shown as

$$f(\eta)=\sum_{q=0}^{\infty}F(q)\eta^q, \tag{4.30}$$

$$g(\eta)=\sum_{q=0}^{\infty}G(q)\eta^q, \tag{4.31}$$

$$m(\eta)=\sum_{q=0}^{\infty}M(q)\eta^q, \tag{4.32}$$

$$n(\eta)=\sum_{q=0}^{\infty}N(q)\eta^q, \tag{4.33}$$

$$\theta(\eta)=\sum_{q=0}^{\infty}\Theta(q)\eta^q, \tag{4.34}$$

$$\phi(\eta)=\sum_{q=0}^{\infty}\Phi(q)\eta^q, \tag{4.35}$$

$$\chi(\eta)=\sum_{q=0}^{\infty}\mathrm{X}(q)\eta^q, \tag{4.36}$$

and the BC's take the form

$$\begin{cases} F(0)=0, F(1)=\dfrac{1}{2}, G(0)=1, M(0)=0, N(0)=0, \Theta(0)=1,\ \Phi(0)=0, \mathrm{X}(0)=0, \\ F(2)=\alpha_1, F(3)=\alpha_2, G(1)=\alpha_3, M(1)=\alpha_4, N(1)=\alpha_5, \Theta(1)=\alpha_6, \Phi(1)=\alpha_7, \mathrm{X}(1)=\alpha_8. \end{cases} \tag{4.37}$$

Where $\alpha_i \ (i=1,2,3\ldots 8)$ are the constants. Solving Eq. (4.30)-(4.36) with the help of the boundary conditions given in Eq. (4.41), we obtain the following series solutions:

$$F(\eta)=f_1\eta^2+f_2\eta^3+f_3\eta^4+f_4\eta^5+\ldots, \tag{4.38}$$

$$G(\eta)=1-g_1\eta+g_2\eta^2+g_3\eta^3+g_4\eta^4+\ldots, \tag{4.39}$$

$$M(\eta)=m_1\eta+m_2\eta^3+m_3\eta^4+m_4\eta^5+\ldots, \tag{4.40}$$

$$N(\eta)=n_1\eta+n_2\eta^3+n_3\eta^4+n_4\eta^5+\ldots, \tag{4.41}$$

$$\Theta(\lambda)=1+\theta_1\eta+\theta_2\eta^2+\theta_3\eta^3+\theta_4\eta^4+\ldots, \tag{4.42}$$

$$\Phi(\eta)=1+\phi_1\eta+\phi_2\eta^2+\phi_3\eta^3+\phi_4\eta^4+\ldots, \tag{4.43}$$

$$\mathrm{X}(\eta)=1+\chi_1\eta+\chi_2\eta^2+\chi_3\eta^3+\chi_4\eta^4+\ldots, \tag{4.44}$$

Where $f_i, g_i, m_i, n_i, \theta_i, \phi_i, \chi_i; (i=1,2,3,\ldots)$ are the constants which are difficult to express here because of their long and complex values. Solving these equations by using MATHEMATICA software with 30 iterations, but the convergence rate is prolonged. For more and accurate convergence radius, the Padé approximation is used because without employing the Padé approximation; the DTM is not able to fulfill the conditions. So, after appling the Padé approximation of order $[5\times 5]$ to Eqs. (4.38) - (4.44), the Padé approximants are as follows.

$$f(\eta)=\frac{-1.50366\eta^2-0.53347\eta^3+0.34357\eta^4+0.00947\eta^5+\cdots}{1-0.32573\eta-0.02657\eta^2+0.00339\eta^3-0.00045\eta^4+0.00034\eta^5+\cdots}, \tag{4.45}$$

$$g(\eta)=\frac{1-1.32274\eta+0.23691\eta^2-0.01472\eta^3+0.03806\eta^4+0.06019\eta^5+\ldots}{1-0.37540\eta-0.21872\eta^2-0.03677\eta^3-0.00622\eta^4+0.00231\eta^5+\ldots}, \tag{4.46}$$

$$m(\eta)=\frac{1.73369\eta+4.65046\eta^2-1.76021\eta^3+0.72791\eta^4-4.19317\eta^5+\ldots}{1+\ 2.68240\eta-1.51530\eta^2-0.54542\eta^3-0.49565\eta^4+0.15187\eta^5+\ldots}, \quad (4.47)$$

$$n(\eta)=\frac{1.12735\eta+0.35672\eta^2+0.17081\eta^3-0.04666\eta^4-0.47583\eta^5+\ldots}{1+0.31642\eta+0.12994\eta^2-0.50103\eta^3-0.51832\eta^4-0.23613\eta^5+\ldots}, \quad (4.48)$$

$$\theta(\eta)=\frac{1-3.34504\eta+3.00336\eta^2-1.45387\eta^3+0.59371\eta^4-0.23645\eta^5+\ldots}{1-1.70091\eta+1.29240\eta^2-0.69759\eta^3+0.33483\eta^4-0.08123\eta^5+\ldots}, \quad (4.49)$$

$$\phi(\eta)=\frac{1-1.13657\eta+1.56823\eta^2-0.69396\eta^3+0.26938\eta^4-0.00714\eta^5+\ldots}{1-0.83875\eta+0.23289\eta^2-0.19192\eta^3+0.08102\eta^4+0.02318\eta^5+\ldots}, \quad (4.50)$$

$$\chi(\eta)=\frac{1-1.28783\eta+1.03347\eta^2-0.654857\eta^3+0.39785\eta^4-0.01894\eta^5+\ldots}{1-0.7717\eta-0.53805\eta^2+0.00179\eta^3+0.25526\eta^4+0.10999\eta^5+\ldots}. \quad (4.51)$$

4.5 Graphical and Tabular Results

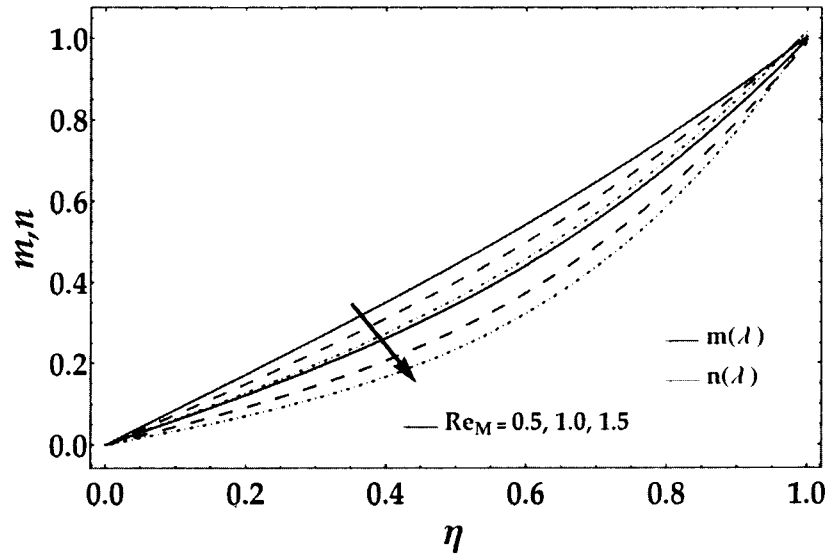

Figure 4.2: Effect of different values of magnetic Reynolds number Re_M on the axial and tangential induced magnetic field distribution $m(\eta), n(\eta)$.

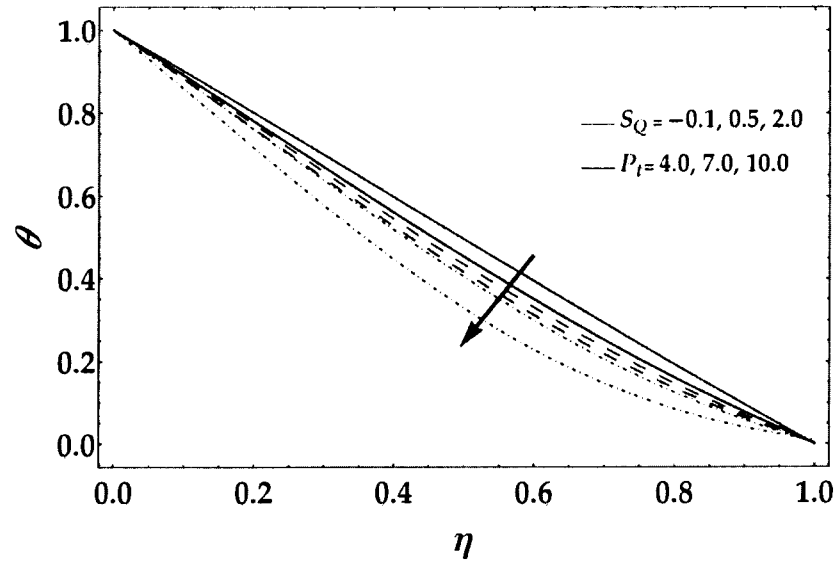

Figure 4.3: Effect of different values of Squeezing Reynolds number S_Q and Prandtl number P_t on the temperature distribution $\theta(\eta)$.

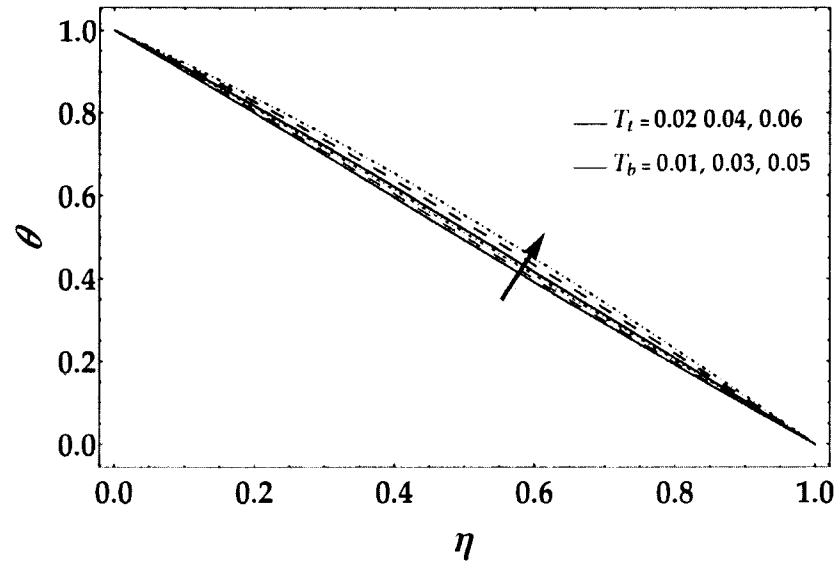

Figure 4.4: Effect of different values of thermophoresis parameter T_t and Brownian motion parameter T_b on the Temperature distribution $\theta(\eta)$.

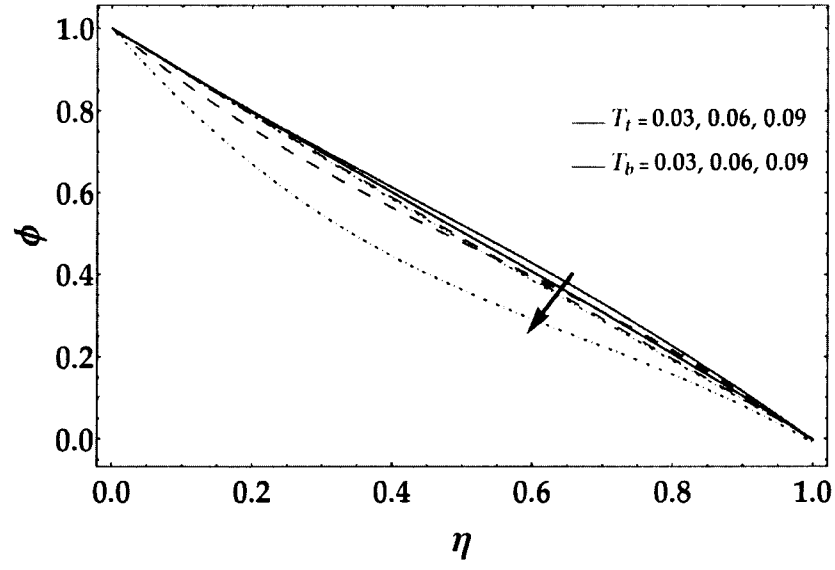

Figure 4.5: Effect of different values of thermophoresis parameter T_t and Brownian motion parameter T_b on the nanoparticle concentration distribution $\phi(\eta)$.

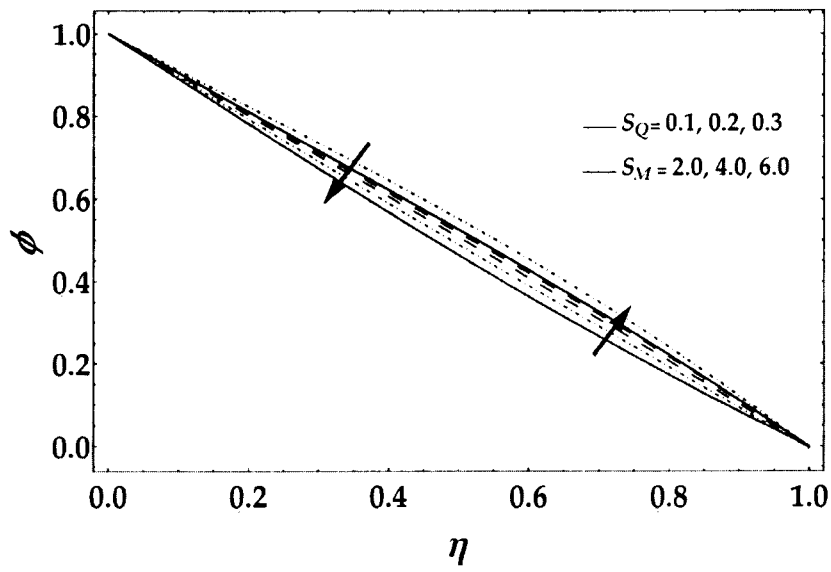

Figure 4.6: Effect of different values of squeezing Reynolds number S_Q and Schmidt number S_M on the nanoparticle concentration distribution $\phi(\eta)$.

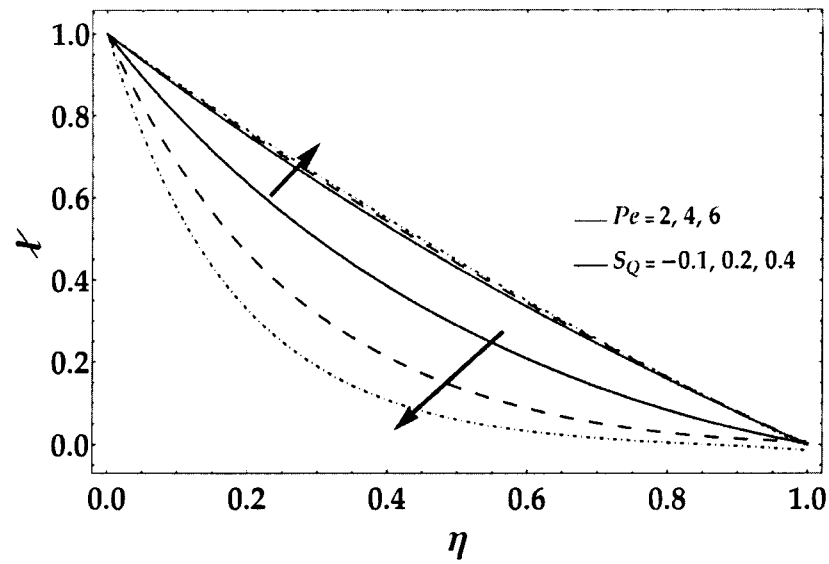

Figure 4.7: Effect of different values of Péclet number Pe and squeezing Reynolds number S_Q on the motile density function $\chi(\eta)$.

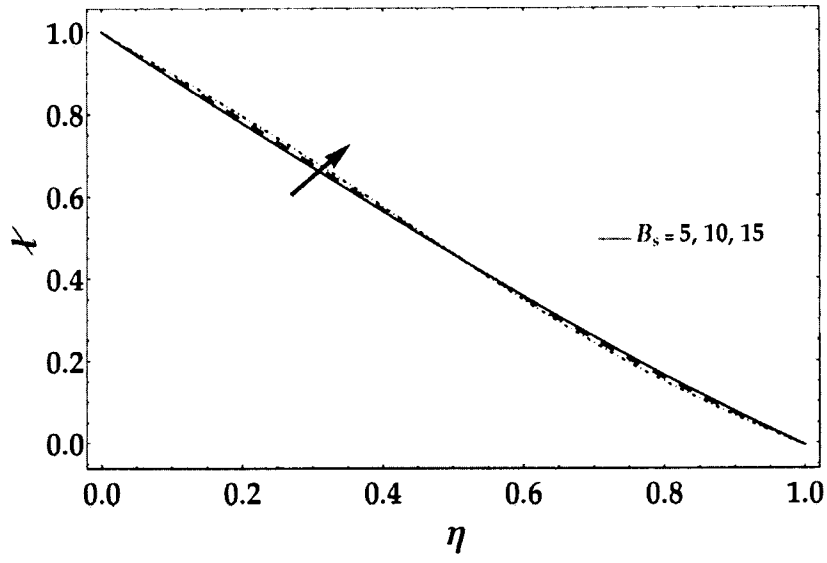

Figure 4.8: Effect of different values of bio convection Schmidt number B_s on the motile density function $\chi(\eta)$.

Table 4.1: Values of $\theta'(0), \phi'(0), \chi'(0)$ obtained by DTM-Padé [5×5].

		$\theta'(0)$		$\phi'(0)$		$\chi'(0)$	
		Shooting Method	**DTM-Padé**	**Shooting Method**	**DTM-Padé**	**Shooting Method**	**DTM-Padé**
T_t	0.10	-0.619650	-0.619650	-1.922555	-1.922555	-1.613755	-1.613755
	0.20	-0.413998	-0.413998	-3.168139	-3.168139	-1.987593	-1.987593
T_b	0.10	-0.955216	-0.955216	-1.769984	-1.769984	-1.568817	-1.568817
	0.20	-0.680870	-0.680870	-1.800588	-1.800588	-1.580640	-1.580640
P_t	5.0	-0.863804	-0.863804	-1.511531	-1.511531	-1.633151	-1.633151
	10.0	-0.733705	-0.733705	-1.647605	-1.647605	-1.710388	-1.710388
S_Q	-2.0	-0.009741	-0.009741	-0.909232	-0.909232	-1.050186	-1.050186
	1.0	-0.733705	-0.733705	-1.512289	-1.512289	-1.510372	-1.510372
B_s	5.0	-0.737106	-0.737106	-1.511531	-1.511531	-1.380064	-1.380064
	10.0	-0.736283	-0.736283	-1.512289	-1.512289	-1.324426	-1.324426
S_M	5.0	-0.683897	-0.683897	-1.511531	-1.511531	-1.424089	-1.424089
	10.0	-0.635811	-0.635811	-1.844023	-1.844023	-1.561973	-1.561973

Table 4.2: Error analysis between DTM-Padé and shooting method [5×5]

	Shooting Method	DTM-Padé [5x5]	Error
$f''(1)$	-2.9974946291988984	-2.9974946291988984	0
$f'''(1)$	-6.069084589598415	-6.069084589598414	-1×10^{-15}
$g'(1)$	-0.9472655092972202	-0.9472655092972202	0
$m'(1)$	1.5231212819375095	1.5231212819375095	0
$n'(1)$	1.0688314914593107	1.0688314914593107	0
$\theta'(1)$	-1.084379592223696	-1.084379592223696	0
$\phi'(1)$	-0.8990243846144889	-0.8990243846144887	-2×10^{-16}
$\chi'(1)$	-0.763298959655151	-0.763298959655151	0

Table 4.3: Torque values at the lower and upper plate when $R_\Omega = 0.3, F_T = 0.5, Bt = 0.6$ for various values of S_Q.

	$\frac{dg(0)}{d\eta}$		$\frac{dg(1)}{d\eta}$	
S_Q	**DTM-Padé Result**	**Numerical Result (Shooting Method)**	**DTM-Padé Result**	**Numerical Result (Shooting Method)**
0.1	-1.0929372214309236	-1.0929372214309236	-0.948663684660318	-0.948663684660318
0.2	-1.180889912821983	-1.180889912821983	-0.9013607839508947	-0.9013607839508948

Table 4.4: Torque values at the lower and upper plate when $S_Q = 0.3$, $F_T = 0.5$, $Bt = 0.6$ for various values of R_Ω.

	$\frac{dg(0)}{d\eta}$		$\frac{dg(1)}{d\eta}$	
R_Ω	**DTM-Padé Result**	**Numerical Result (Shooting Method)**	**DTM-Padé Result**	**Numerical Result (Shooting Method)**
0.1	-1.265492575299778	-1.2654925752997779	-0.8533000683642988	-0.8533000683642988
0.2	-1.2652748717875888	-1.2652748717875888	-0.8549052425970227	-0.8549052425970226

4.6 Discussion

In this section, we discuss the Analytical and numerical results obtained with DTM-Padé method by a computational software *MATHEMATICA*. DTM is applied successfully to find the analytical solution of coupled non-linear differential equations for governing flow. Therefore, the physical and graphical significance of different parameters on heat transfer, induced MHD, temperature distribution, nanoparticle concentration, and gyrotactic microorganism distribution are discussed. Mainly, the effects of magnetic Reynolds number Re_M on the axial and tangential induced magnetic field distribution $m(\eta), n(\eta)$, the effects of Prandtl number P_t, Brownian motion parameter T_b, thermophoresis parameter T_t, Schmidt number S_M, bioconvection B_s, Péclet number P_l are also considered for temperature distribution, nanoparticle concentration distribution, and motile microorganism density profile. To explore the physical more, figure (4.2-4.8) have been plotted.

To authenticate the exactness of our current results, a comparison with the shooting method is given. Padé approximation is used to validate the convergence of the series solutions. The describe outcomes is associated with shooting method for multiple values of leading parameters, as shown in Table 4.1. One can observe from

this table that the results perfectly match with numerical shooting method. It can be also seen from Table 4.2 that the error between both schemes is minimal and almost negligible, which shows that the present technique used is an efficient tool to examine the highly nonlinear equations. Table 4.3 and Table 4.4 reveals the Torque effects on the upper and lower circular plate, which is calculated with the help of Eqs. (3.17-3.19). The physical description of the figure are as follows.

Induced Magnetic Field

From figure (4.2), magnetic Reynolds number Re_M effect on the axial and tangential induced magnetic field distribution is observed. From this figure, it is keenly observed that increasing values of Re_M causes a significant decrement in the axial and tangential induced magnetic field distribution.

Temperature Distribution

The impact of Prandtl number P_t and squeeze Reynolds number S_Q on the dimensionless temperature profile $\theta(\eta)$ can be seen in figure (4.3). It is understood that for superior values of Prandtl number P_t, the temperature distribution decreases over the whole region η, because increasing the Prandtl number enhances the momentum diffusivity, which in results temperature profile declines. It also perceived that temperature profile significantly falls with rise of squeeze Reynolds number S_Q. Figure (4.4) displays effect of thermophoresis parameter T_t and Brownian motion parameter T_b for fixed values of other parameters on the temperature distribution $\theta(\eta)$. Results reveal that rise in thermophoresis parameter results in an increase in temperature profile. A similar phenomenon is also noticed against Brownian motion parameter for temperature profile $\theta(\eta)$.

Concentration Distribution

The significance of thermophoresis parameter T_t and Brownian motion parameter T_b on nanoparticle concentration are shown in figure (4.5). It reveals that a notable declines in the nanoparticle concentration, when the values of T_b increases. Moreover, quite opposite phenomena occur while increasing the values of T_t. Effect of squeezing Reynolds Number S_Q and Schmidt number S_M on the nanoparticle concentration field ϕ is shown in figure (4.6). Nanoparticle concentration profile rises with the increase in the values of squeezing Reynolds parameter S_Q. While the nanoparticle concentration field $\phi(\eta)$ declines with the rise in Schmidt number S_M.

Motile Gyrotactic Microorganism Distribution

Effect of squeezed Reynolds number S_Q and Péclet number P_l on the microorganism density function $\chi(\eta)$ sketched in figure (4.7). It is perceived that by increasing the value of squeezing Reynolds number S_Q the behaviour of microorganism density function $\chi(\eta)$ increases and increasing the value of Péclet number P_l, the behaviour of the microorganism density function $\chi(\eta)$ is decreasing. Therefore, for higher values of P_l the speed of microorganisms is reduced, and the diffusivity of microorganisms is reduced. Figure (4.8) is displayed to get the physical behaviour of the Schmidt number S_M. It is established that by increasing the value of Schmidt number S_M the microorganism density function increases, but the effects are minimal.

Physical Quantities

In Table 4.1, the numerical findings for the motile density number wall gradient, local nanoparticle Sherwood number, and local Nusselt number are reported.

This table clearly shows that the DTM-Padé simulation and the numerical shooting technique have extremely excellent agreement. Table 4.2 shows the Error analysis between shooting method and DTM-Padé [5×5]. It also shows that the results obtained with DTM- Padé is accurate and in good agreement with shooting method. Eqs. (3.18) -(3.19) are used to calculate the effects of torque on the upper fixed and lower moving disk, and the DTM-Padé computations are displayed in Table (4.3-4.4). Finally, it is noteworthy from inspection, that the torque at the lower disk i.e., tangential velocity gradient, and the torque at the upper disk are decreased and increased with an increase in the squeezing Reynolds number respectively. Therefore, while axial momentum is decreased in the squeezing regime it has a different impact on torque at the lower and upper disks. The amplification in squeezing effect reduces torque at the lower disk whereas it enhances torque at the upper disk.

Chapter 5

Transport of Motile Gyrotactic Microorganism in a Carreau Fluid between a Pair of Rotating Circular Plates

5.1 Introduction

In this chapter, the flow behaviour between a parallel rotating plate filled with Carreau fluid with suspended nanoparticles and motile gyrotactic microorganisms in presence of generalized magnetic Reynolds number. The activation energy is also contemplated with nanoparticle concentration equation. The appropriate similarity transformations are used to formulate proposed mathematical modelling in three-dimension. The impact of Carreau fluid velocity for shear thinning, Newtonian case, and thickening cases on velocity field $f'(\eta)$ discussed in tabular form and graphical figures.

5.2 Mathematical Formulation

Flow Assumptions

The assumption along with thoses discussed in previous chapters, for mathematical formulation of flow problem of Carreau viscoelastic Nano fluid saturating space between rotating and squeezing disks is

- Careau base fluid
- Arrhenius equation is used to analyze chemical kinetics.

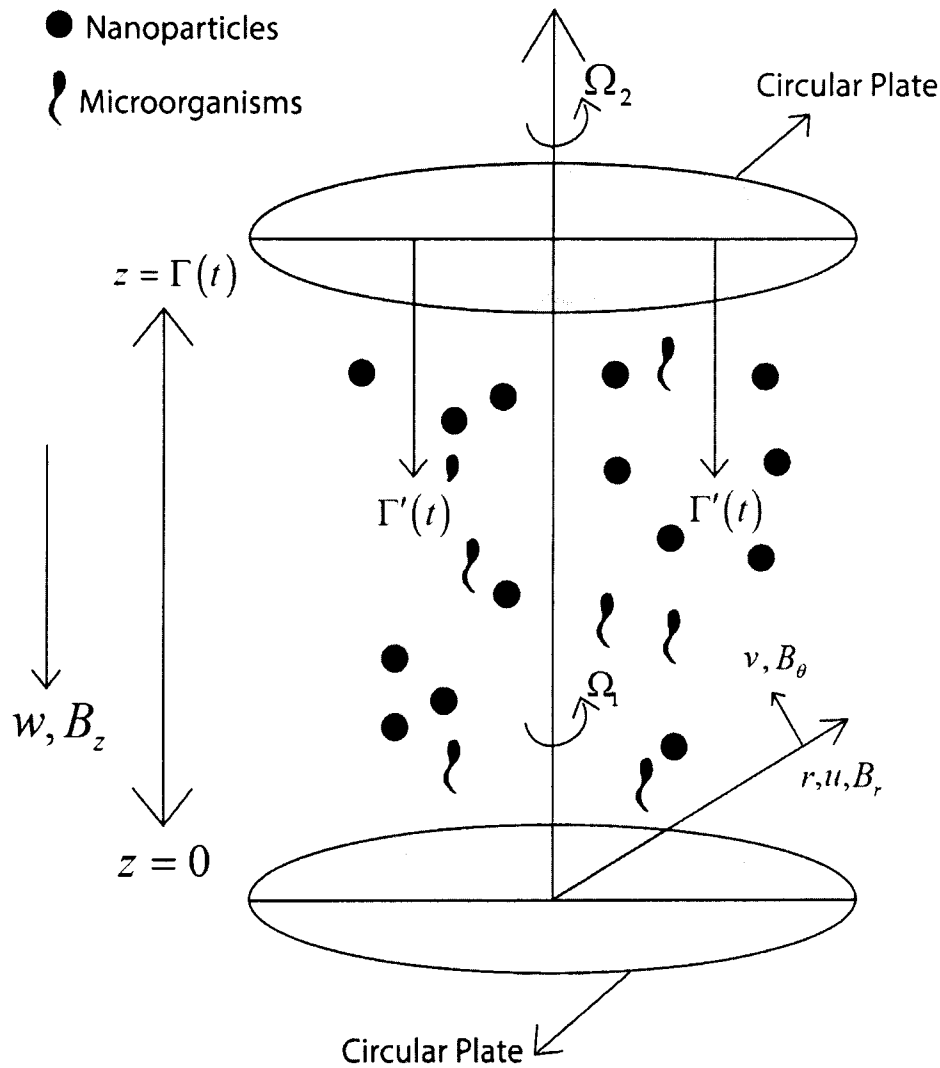

Figure 5.1: The schematic diagram of nanoparticles between parallel finite plates in the presence of Microorganisms.

Rheological Model for Carreau fluid

The Carreau fluid model is defined as [105]

$$\tau_{ij} = \left[\mu_\infty + (\mu_0 - \mu_\infty)\left(1 + (\Gamma\dot{\gamma})^2\right)^{\frac{n-1}{2}}\right] A_1, \tag{5.1}$$

In which, τ_{ij} represents the stress tensor, μ_0 represents the zero shear rate viscosity μ_∞ represents the limiting constant viscosity at infinite shear rate viscosity, Γ represents the constant of time, n represents the power law index, A_1 represents the first Rivlin-

Erickson tensor and $\dot{\gamma}$ represents the second invariant rate of strain tensor which is defined as

$$\dot{\gamma} = \sqrt{\frac{1}{2}\mathrm{tr}(A_1)}, \tag{5.2}$$

$$A_1 = (L + L^T) = \left[(\nabla V + \nabla V^T)\right], \tag{5.3}$$

Assume that μ_∞ is zero, and by using binomial series approximation of first order of Eq. (5.1) becomes

$$\tau_{ij} = \left[\mu_0\left(1 + \frac{n-1}{2}(\Gamma\dot{\gamma})^2\right)\right]A_1. \tag{5.4}$$

Mathematical Model

The governing flow equations by taking the above assumptions, the MHD squeezed film regime for Carreau fluid model the equation of continuity and momentum in (r,θ,z) direction read as

$$\frac{1}{r}\frac{\partial}{\partial r}(rv_r) + \frac{1}{r}\frac{\partial}{\partial \theta}(v_\theta) + \frac{\partial}{\partial z}(v_z) = 0 \tag{5.5}$$

$$\begin{aligned}\rho\left(\frac{\partial v_r}{\partial t} + v_r\frac{\partial v_r}{\partial r} + \frac{v_\theta}{r}\frac{\partial v_r}{\partial \theta} + v_z\frac{\partial v_r}{\partial z} - \frac{v_\theta}{r}\right) &= -\frac{\partial p}{\partial r} \\ + \frac{1}{r}\frac{\partial}{\partial r}(r\tau_{rr}) + \frac{1}{r}\frac{\partial \tau_{r\theta}}{\partial \theta} - \frac{\tau_{\theta\theta}}{r} + \frac{\partial \tau_{rz}}{\partial z} - \frac{\partial B_r}{\partial z}B_z - \frac{\partial B_\theta}{\partial z}B_\theta,\end{aligned} \tag{5.6}$$

$$\begin{aligned}\rho\left(\frac{\partial v_\theta}{\partial t} + v_r\frac{\partial v_\theta}{\partial r} + \frac{v_\theta}{r}\frac{\partial v_\theta}{\partial \theta} + v_z\frac{\partial v_\theta}{\partial z} - \frac{v_r v_\theta}{r}\right) &= -\frac{1}{r}\frac{\partial p}{\partial \theta} \\ + \frac{1}{r}\frac{\partial \tau_{\theta\theta}}{\partial \theta} + \frac{1}{r^2}\frac{\partial(r^2\tau_{r\theta})}{\partial r} + \frac{\partial \tau_{\theta z}}{\partial z} - \frac{\partial B_\theta}{\partial z}B_z - \frac{\partial B_\theta}{\partial r}B_r,\end{aligned} \tag{5.7}$$

$$\begin{aligned}\rho\left(\frac{\partial v_z}{\partial t} + v_r\frac{\partial v_z}{\partial r} + \frac{v_\theta}{r}\frac{\partial v_z}{\partial \theta} + v_z\frac{\partial v_z}{\partial z}\right) &= -\frac{\partial p}{\partial z} \\ + \frac{1}{r}\frac{\partial}{\partial r}(r\tau_{rz}) + \frac{1}{r}\frac{\partial \tau_{\theta z}}{\partial \theta} + \frac{\partial \tau_{zz}}{\partial z} - \frac{\partial B_\theta}{\partial z}B_\theta + \frac{\partial B_r}{\partial z}B_r,\end{aligned} \tag{5.8}$$

where,

$$\tau_{rr} = -p + \mu_0 \left[1 + \frac{(n-1)}{2} \Gamma^2 \left(2\left(\frac{\partial v_r}{\partial r}\right)^2 + \left(\frac{\partial v_r}{\partial z}\right)^2 + \left(\frac{\partial v_\theta}{\partial z}\right)^2 + \left(\frac{\partial v_\theta}{\partial r} - \frac{v_\theta}{r}\right)^2 + 2\left(\frac{v_r}{r}\right)^2 \right) \right] 2\frac{\partial v_r}{\partial r},$$

$$\tau_{r\theta} = \mu_0 \left[1 + \frac{(n-1)}{2} \Gamma^2 \left(2\left(\frac{\partial v_r}{\partial r}\right)^2 + \left(\frac{\partial v_r}{\partial z}\right)^2 + \left(\frac{\partial v_\theta}{\partial z}\right)^2 + \left(\frac{\partial v_\theta}{\partial r} - \frac{v_\theta}{r}\right)^2 + 2\left(\frac{v_r}{r}\right)^2 \right) \right] \left(\frac{\partial v_\theta}{\partial r} - \frac{v_\theta}{r} \right),$$

$$\tau_{rz} = \mu_0 \left[1 + \frac{(n-1)}{2} \Gamma^2 \left(2\left(\frac{\partial v_r}{\partial r}\right)^2 + \left(\frac{\partial v_r}{\partial z}\right)^2 + \left(\frac{\partial v_\theta}{\partial z}\right)^2 + \left(\frac{\partial v_\theta}{\partial r} - \frac{v_\theta}{r}\right)^2 + 2\left(\frac{v_r}{r}\right)^2 \right) \right] \frac{\partial v_r}{\partial z},$$

$$\tau_{\theta r} = \mu_0 \left[1 + \frac{(n-1)}{2} \Gamma^2 \left(2\left(\frac{\partial v_r}{\partial r}\right)^2 + \left(\frac{\partial v_r}{\partial z}\right)^2 + \left(\frac{\partial v_\theta}{\partial z}\right)^2 + \left(\frac{\partial v_\theta}{\partial r} - \frac{v_\theta}{r}\right)^2 + 2\left(\frac{v_r}{r}\right)^2 \right) \right] \left(\frac{\partial v_\theta}{\partial r} - \frac{v_\theta}{r} \right),$$

$$\tau_{\theta\theta} = -p + \mu_0 \left[1 + \frac{(n-1)}{2} \Gamma^2 \left(2\left(\frac{\partial v_r}{\partial r}\right)^2 + \left(\frac{\partial v_r}{\partial z}\right)^2 + \left(\frac{\partial v_\theta}{\partial z}\right)^2 + \left(\frac{\partial v_\theta}{\partial r} - \frac{v_\theta}{r}\right)^2 + 2\left(\frac{v_r}{r}\right)^2 \right) \right] 2\left(\frac{v_r}{r} \right),$$

$$\tau_{\theta z} = \mu_0 \left[1 + \frac{(n-1)}{2} \Gamma^2 \left(2\left(\frac{\partial v_r}{\partial r}\right)^2 + \left(\frac{\partial v_r}{\partial z}\right)^2 + \left(\frac{\partial v_\theta}{\partial z}\right)^2 + \left(\frac{\partial v_\theta}{\partial r} - \frac{v_\theta}{r}\right)^2 + 2\left(\frac{v_r}{r}\right)^2 \right) \right] \frac{\partial v_\theta}{\partial z},$$

$$\tau_{zr} = \mu_0 \left[1 + \frac{(n-1)}{2} \Gamma^2 \left(2\left(\frac{\partial v_r}{\partial r}\right)^2 + \left(\frac{\partial v_r}{\partial z}\right)^2 + \left(\frac{\partial v_\theta}{\partial z}\right)^2 + \left(\frac{\partial v_\theta}{\partial r} - \frac{v_\theta}{r}\right)^2 + 2\left(\frac{v_r}{r}\right)^2 \right) \right] \frac{\partial v_r}{\partial z},$$

$$\tau_{z\theta} = \mu_0 \left[1 + \frac{(n-1)}{2} \Gamma^2 \left(2\left(\frac{\partial v_r}{\partial r}\right)^2 + \left(\frac{\partial v_r}{\partial z}\right)^2 + \left(\frac{\partial v_\theta}{\partial z}\right)^2 + \left(\frac{\partial v_\theta}{\partial r} - \frac{v_\theta}{r}\right)^2 + 2\left(\frac{v_r}{r}\right)^2 \right) \right] \frac{\partial v_\theta}{\partial z},$$

$$\tau_{zz} = 0.$$

The equation of magnetic field read as

$$\frac{1}{r}\frac{\partial}{\partial r}(rB_r) + \frac{1}{r}\frac{\partial B_\theta}{\partial \theta} + \frac{\partial B_z}{\partial z} = 0, \tag{5.9}$$

$$\frac{\partial B_r}{\partial t} + u\frac{\partial B_r}{\partial r} + v\frac{\partial B_r}{\partial \theta} + w\frac{\partial B_r}{\partial z} = -\frac{\partial}{\partial z}(v_r B_z - v_z B_r) + \frac{1}{\delta \mu_2}\left(\frac{\partial^2 B_r}{\partial z^2}\right), \tag{5.10}$$

$$\frac{\partial B_\theta}{\partial t}+u\frac{\partial B_\theta}{\partial r}+v\frac{\partial B_\theta}{\partial \theta}+w\frac{\partial B_\theta}{\partial z}=\frac{\partial}{\partial r}(v_r B_\theta - v_\theta B_r)-\frac{\partial}{\partial z}(v_\theta B_z - B_\theta v_z)+\frac{1}{\delta\mu_2}\left(\frac{\partial^2 B_\theta}{\partial z^2}\right),$$

(5.11)

$$\frac{\partial B_z}{\partial t}+u\frac{\partial B_z}{\partial r}+v\frac{\partial B_z}{\partial \theta}+w\frac{\partial B_z}{\partial z}=\frac{\partial}{\partial r}(v_r B_z - v_z B_r)+\frac{1}{\delta\mu_2}\left(\frac{\partial^2 B_z}{\partial z^2}\right). \tag{5.12}$$

The energy equation for the proposed problem reads as

$$\frac{\partial T}{\partial t}+v_r\frac{\partial T}{\partial r}+v_z\frac{\partial T}{\partial z}=\tilde{\alpha}\frac{\partial^2 T}{\partial z^2}+\tau\left[D_B\left(\frac{\partial T}{\partial r}\frac{\partial C}{\partial r}+\frac{\partial T}{\partial z}\frac{\partial C}{\partial z}\right)+\frac{D_T}{T_u}\left[\left(\frac{\partial T}{\partial r}\right)^2+\left(\frac{\partial T}{\partial z}\right)^2\right]\right],$$

(5.13)

The concentration of nanoparticle equation with activation energy reads as

$$\frac{\partial C}{\partial t}+v_r\frac{\partial C}{\partial r}+v_z\frac{\partial C}{\partial z}=D_B\frac{\partial^2 C}{\partial z^2}+\frac{D_T}{T_u}\frac{\partial^2 T}{\partial z^2}-k_r^{\,2}(C-C_\infty)\left(\frac{T}{T_\infty}\right)^{\bar{n}}\exp\left(-\frac{E_a}{1+\kappa T}\right), \tag{5.14}$$

where, κ $k_r^{\,2}$ $\bar{n}$ and E_a represent the Boltzmann constant, reaction rate, rate constant, activation energy respectively.

The conservation of microorganism reads as

$$\frac{\partial n}{\partial t}+v_r\frac{\partial n}{\partial r}+v_\theta\frac{\partial n}{\partial \theta}+v_z\frac{\partial n}{\partial z}+\frac{\bar{b}W_{mo}}{(C_l-C_u)}\left[\frac{\partial}{\partial z}\left(n\frac{\partial C}{\partial z}\right)\right]=D_{mo}\left(\frac{\partial^2 n}{\partial z^2}\right). \tag{5.15}$$

The initial and boundary conditions for the Eqs. (4.5)-(4.14) with our assumptions are

$$v_r=0, v_\theta=\Omega_1 r\frac{D^2}{\Gamma^2(t)}, v_z=0, B_z=B_\theta=0, C=C_l, T=T_l, n=n_l \quad \text{at} \quad z=0, \tag{5.16}$$

$$\begin{cases} v_r=0, v_\theta=\Omega_2 r\dfrac{D^2}{\Gamma^2(t)}, B_\theta=N_0 r\dfrac{D^2}{\Gamma^2(t)}, B_z=-\dfrac{\alpha D M_0}{\Gamma(t)}, v_z=-\dfrac{\alpha D^2}{2\Gamma(t)}, \\ T=T_u, C=C_u, n=n_u. \end{cases} \quad \text{at} \quad z=\Gamma(t). \tag{5.17}$$

5.3 Similarity Transformations

By using the similarity transformation of chapter two and three, substituting similarity transformation and component form of Carreau fluid model in Eqs. (5.5)-(5.13), the following highly coupled, nonlinear ordinary differential equations (ODE's) with unit-spaced variable η are obtained as

$$f^{(iv)} = 8S_Q\left[3f''-2\left(\frac{R_\Omega}{S_Q}\right)^2 gg'+2F_T^2\left(mm'''+m'm''\right)-\left(2f-\eta\right)f'''+2F_A^2\left(\frac{R_\Omega}{S_Q}\right)^2 nn'\right]$$
$$-4(n-1)We\left[\begin{array}{l}\frac{1}{S_Q}\left(2f'g'g''+f''g'^2\right)+\frac{S_Q}{R_\Omega^2}\left[7ff''f'''+3f''^3+\frac{1}{2}f'^2f^{iv}-\frac{3\mathrm{Re}}{4R_\Omega}\left(2f''f'''^2+f''^2f^{iv}\right)\right]\\ -\frac{\mathrm{Re}}{2R_\Omega S_Q}\left[\left(gf''g'''+gf'''g''+f''g''^2\right)-\frac{1}{4}\left(g'^2f^{iv}+2g'g''f'''\right)\right]\end{array}\right], \tag{5.18}$$

$$g''(\eta) = 2S_Q^{\,2}\left[2g+\eta g'+2gf'-fg'+2F_AF_T\left(mn'+nm'\right)\right]$$
$$-(n-1)WeS_Q\left[\frac{2S_Q}{R_\Omega^{\,2}}\left(f'^2g''+2ff''g'\right)-\frac{3\mathrm{Re}}{2S_QR_\Omega}g'^2g''-\frac{\mathrm{Re}\,S_Q}{R_\Omega^{\,3}}\left(\frac{3f''^2g''}{4}+gf''f'''\right)\right], \tag{5.19}$$

$$m'' = \mathrm{Re}_M\left[m+\eta m'+2mf'-2fm'\right], \tag{5.20}$$

$$n'' = \mathrm{Re}_M\left[2n-fn'+\eta n'+2\left(\frac{F_A}{F_T}\right)mg'\right], \tag{5.21}$$

$$\theta''+S_QP_rf\theta'+T_l\theta'^2+T_b\theta'\phi' = 0, \tag{5.22}$$

$$\phi''+\frac{T_l}{T_b}\theta''+S_QS_Mf\phi'-S_M\sigma(1+\tilde{\delta}\theta)^{\bar{n}}\exp\left(-\frac{E}{1+\tilde{\delta}\theta}\right)\phi = 0, \tag{5.23}$$

$$\chi''-S_QB_s\left(\frac{\eta}{2}\right)\chi'+B_sS_Qf\chi'-P_l\left[\chi'\phi'+(\chi+\Phi)\phi''\right] = 0. \tag{5.24}$$

Weissenberg number represented by $We=\Omega_1^{\,2}\Gamma^2$, chemical reaction parameter is represented by $\sigma=\frac{k_r^{\,2}\Gamma(t)^2}{\upsilon}$, temperature difference represented by $\tilde{\delta}=\frac{T_l-T_u}{T_u}$ and energy Parameter represented by $E=\frac{E_a}{\kappa T_u}$.

The corresponding boundary mentioned in Eqs. (5.16)- (5.17) reduced as

$$\begin{cases} f(0)=0=f'(0), g(0)=1, m(0)=0, n(0)=1, \theta(0)=1, \chi(0)=1, \phi(0)=1, \\ f(1)=\frac{1}{2}, g(1)=\xi, m(1)=1, n(1)=1, \theta(1)=0, \phi(1)=0, \chi(1)=0, \end{cases} \tag{5.25}$$

5.4 Solution Methodolgy

The non-linear dimensionless ordinary differential Eqs. (5.18)-(5.24) with boundary conditions (5.26) is elucidated with DTM. Substituting differential transformation mentioned in Eq. (1.1)-(1.11) into Eqs. (5.18)-(5.24), and solving with the help of boundary conditions given in Eqs. (5.25), The obtained series solutions are

$$F(\eta) = f_1\eta^2 + f_2\eta^3 + f_3\eta^4 + f_4\eta^5 + ..., \tag{5.26}$$

$$G(\eta) = 1 - g_1\eta + g_2\eta^2 + g_3\eta^3 + g_4\eta^4 + ..., \tag{5.27}$$

$$M(\eta) = m_1\eta + m_2\eta^3 + m_3\eta^4 + m_4\eta^5 + ..., \tag{5.28}$$

$$N(\eta) = n_1\eta + n_2\eta^3 + n_3\eta^4 + n_4\eta^5 + ..., \tag{5.29}$$

$$\Theta(\lambda) = 1 + \theta_1\eta + \theta_2\eta^2 + \theta_3\eta^3 + \theta_4\eta^4 + ..., \tag{5.30}$$

$$\Phi(\eta) = 1 + \phi_1\eta + \phi_2\eta^2 + \phi_3\eta^3 + \phi_4\eta^4 + ..., \tag{5.31}$$

$$\mathrm{X}(\eta) = 1 + \chi_1\eta + \chi_2\eta^2 + \chi_3\eta^3 + \chi_4\eta^4 + ..., \tag{5.32}$$

where, $f_i, g_i, m_i, n_i, \theta_i, \phi_i \chi_i; (i = 1,2,3,...)$ are constants but difficult to represent here. With the aid of *Mathematica (12v)* software, the above equations are solved with 30 iterations. However, the rate of convergence is not obtained. Some schemes are available to increase the rate of convergence. One of the easiest ways to enhance the rate of convergence of the truncated series is Padé approximation, which is utilized into the form of rational fraction (ratio of two polynomials). Without the use of Padé approximation, the results attained by DTM not satisfy the boundary condition at infinity because of the nonlinearity in the governing equations. So, it is compulsory to combine the analytic solution obtained by DTM with the Padé approximation which

gives good convergence rate at infinity. As a result of numerical values to a desired exactness, the number of terms required is determined by the higher approximation of the order. The Padé approximation of order $[5\times5]$ is applied to Eqs. (5.26)-(5.32), the Padé approximants are as follows.

$$f(\eta)=\frac{1.90345\eta^2-1.46791\eta^3+0.30574\eta^4-0.09613\eta^5+\ldots}{1+0.25421\eta+0.05445\eta^2-0.00576\eta^3-0.01063\eta^4-0.00369\eta^5+\ldots} \tag{5.33}$$

$$g(\eta)=\frac{1-2.53210\eta+0.14630\eta^2+0.82149\eta^3+0.44129\eta^4+0.130549\eta^5+\ldots}{1-1.53185\eta-1.38353\eta^2-0.56653\eta^3-0.12647\eta^4-0.00042\eta^5+\ldots} \tag{5.34}$$

$$m(\eta)=\frac{0.70958\eta+0.08891\eta^2-0.01376\eta^3+0.30161\eta^4-0.32837\eta^5+\ldots}{1+0.12530\eta-0.35273\eta^2+0.06605\eta^3-0.06125\eta^4-0.01978\eta^5+\ldots} \tag{5.35}$$

$$n(\eta)=\frac{0.93923\eta+1.48352\eta^2+0.90448\eta^3+0.46249\eta^4+0.19181\eta^5+\ldots}{1+1.57950\eta+0.71489\eta^2+0.41838\eta^3+0.29677\eta^4-0.02225\eta^5+\ldots} \tag{5.36}$$

$$\theta(\eta)=\frac{1-0.80937\eta-0.21526\eta^2+0.01351\eta^3+0.00412\eta^4+0.0070\eta^5+\ldots}{1+0.12854\eta-0.02712\eta^2-0.00391\eta^3-0.01074\eta^4+0.00056\eta^5+\ldots} \tag{5.36}$$

$$\phi(\eta)=\frac{1-0.12123\eta-0.34409\eta^2-0.48574\eta^3-0.00010\eta^4-0.04746\eta^5+\ldots}{1+1.05982\eta+0.65555\eta^2+0.09425\eta^3+0.02288\eta^4+0.00115\eta^5+\ldots} \tag{5.37}$$

$$\chi(\eta)=\frac{1-0.14732\eta-0.62596\eta^2-0.16040\eta^3-0.05519\eta^4-0.01107\eta^5+\ldots}{1+0.91928\eta+0.26633\eta^2+0.07215\eta^3+0.01584\eta^4+0.00046\eta^5+\ldots} \tag{5.38}$$

5.5 Graphical and Tabular Results

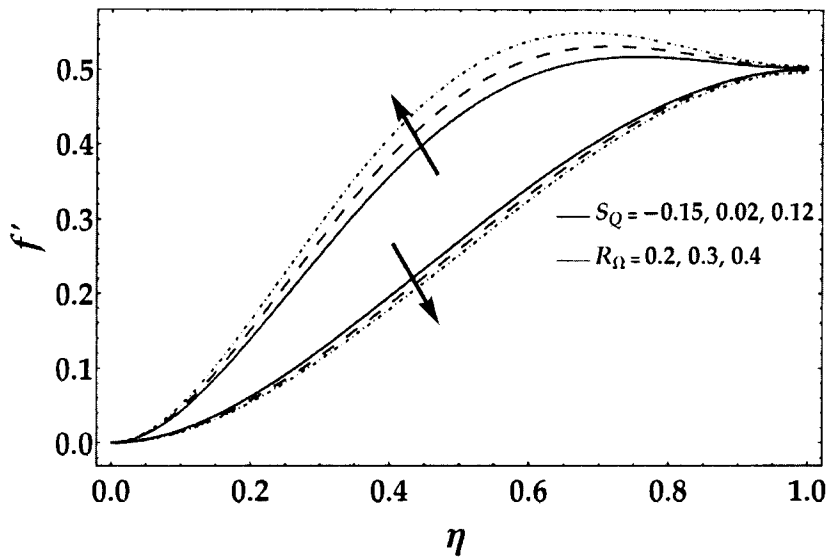

Figure 5.2: Effect of various values of squeeze Reynolds number S_Q, rotational Reynolds number R_Ω on axial velocity distribution $f'(\eta)$

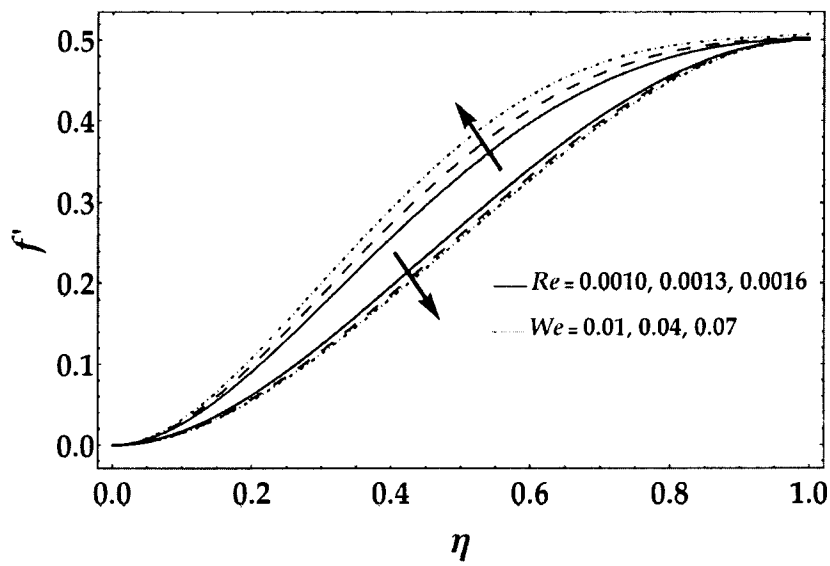

Figure 5.3: Effect of various values of Reynolds number Re, Weissenberg number We on axial velocity distribution $f'(\eta)$.

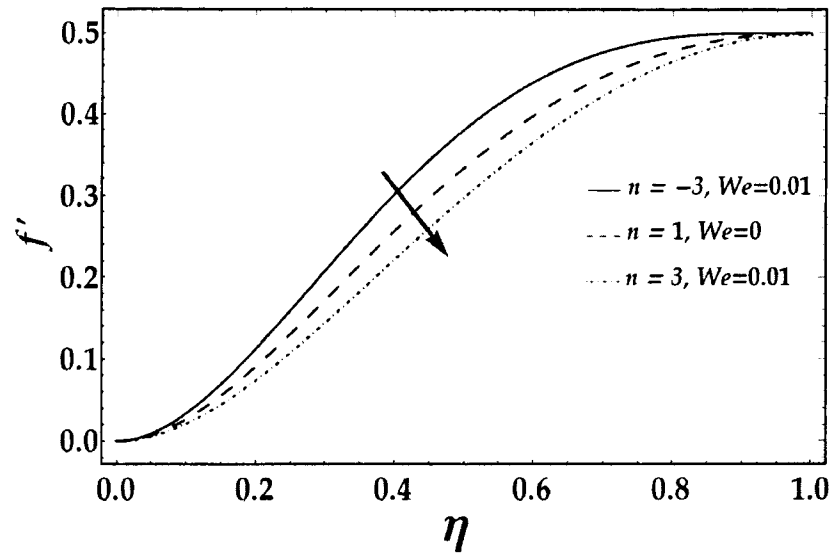

Figure 5.4: Effect of different values of Power law index n, Weissenberg number We on axial velocity distribution $f'(\eta)$.

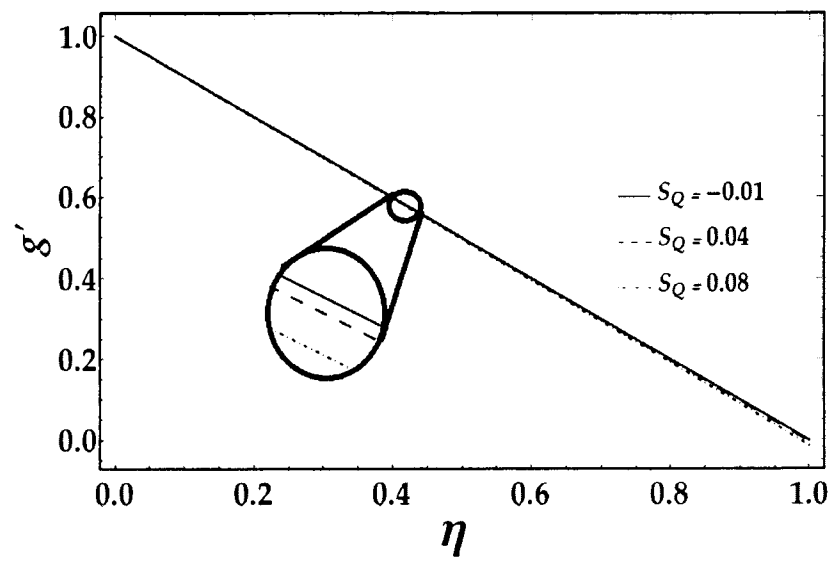

Figure 5.5: Effect of various values of squeeze Reynolds number S_Q on the tangential velocity distribution $g'(\eta)$.

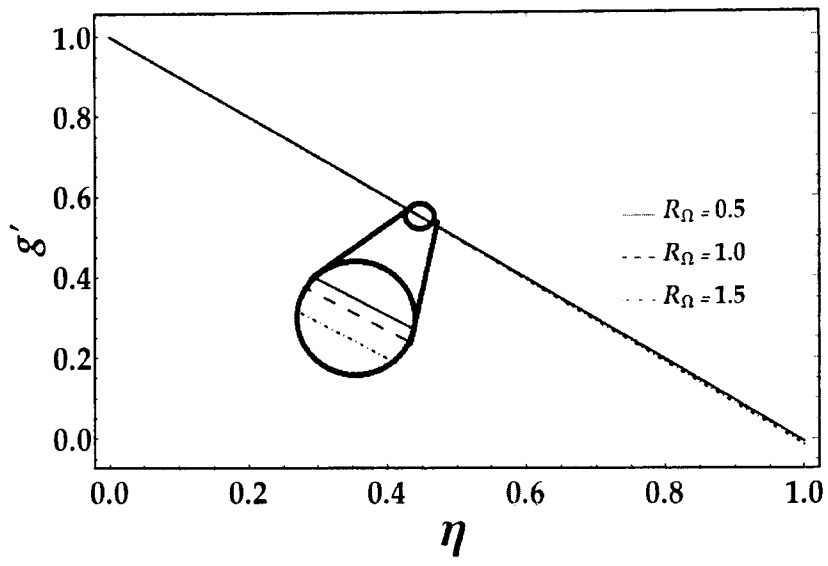

Figure 5.6: Effect of various values of rotational Reynolds number R_Ω on the tangential velocity distribution $g'(\eta)$.

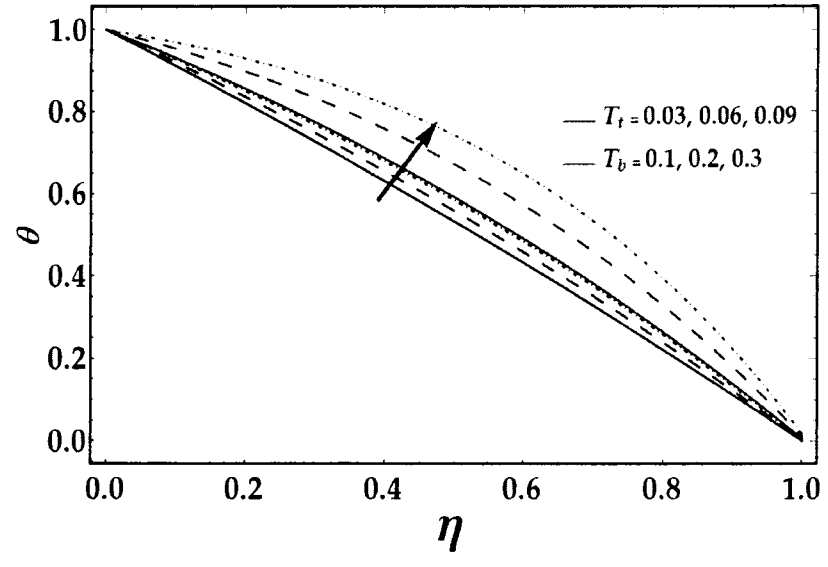

Figure 5.7: Effect of different values of thermophoresis parameter T_f and Brownian motion parameter T_b on temperature distribution $\theta(\eta)$.

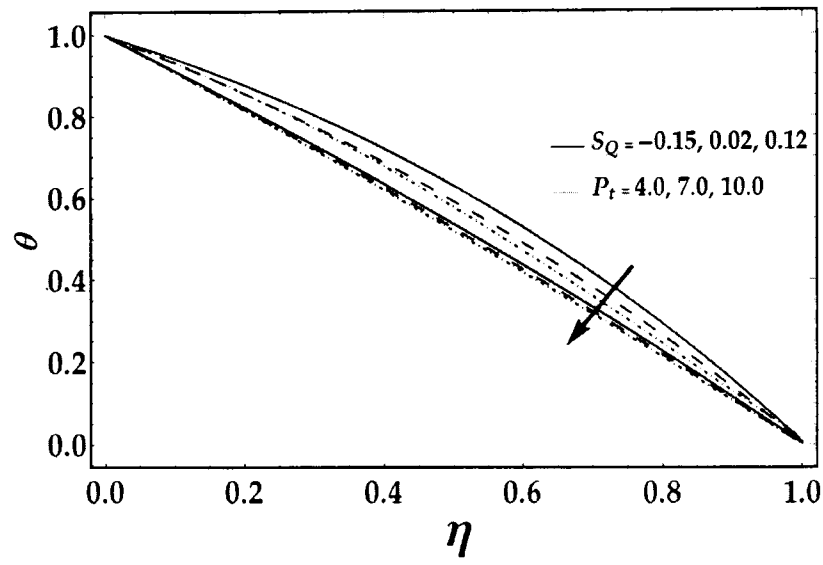

Figure 5.8: Effect of various values of squeeze Reynolds number S_Q, Prandtl number P_t on the temperature distribution $\theta(\eta)$.

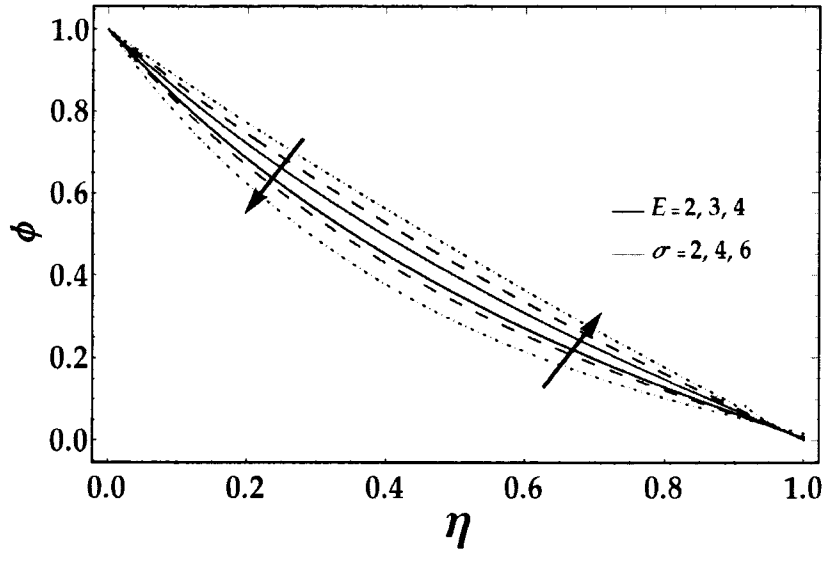

Figure 5.9: Effect of different values of activation energy E and reaction rate σ on nanoparticle volume fraction $\phi(\eta)$.

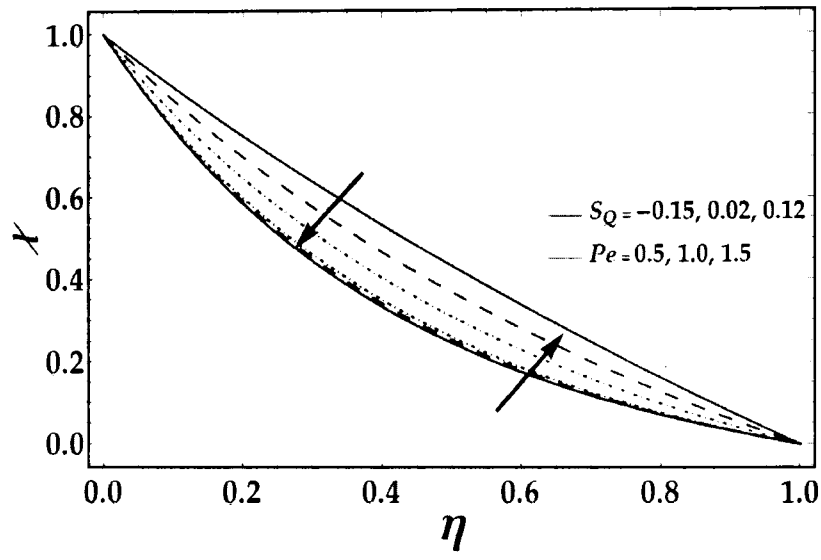

Figure 5.10: Effect of various values of squeeze Reynolds number S_Q, Péclet number Pe on the motile microorganism density function $\chi(\eta)$.

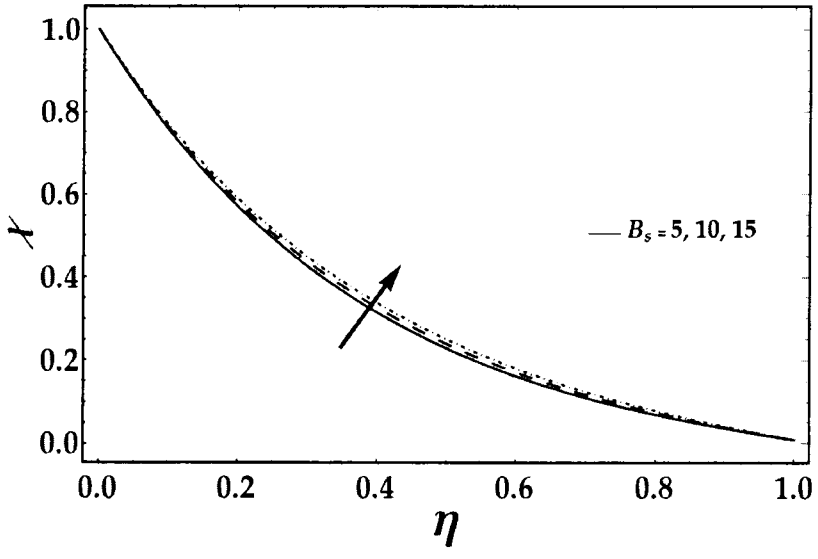

Figure 5.11: Effect of various values of bio-convection number B_s on motile microorganism density function $\chi(\eta)$.

Table 5.1: Comparison of Nusselt number $-\theta'(0)$ for various values T_t, T_b, P_t, S_Q by Shooting Method and DTM-Padé $[5\times5]$.

				$n=-3, We=0.01$		$n=1, We=0$		$n=3, We=0.01$	
T_t	T_b	P_t	S_Q	**Shooting Method**	**DTM-Padé**	**Shooting Method**	**DTM-Padé**	**Shooting Method**	**DTM-Padé**
0.03	0.01	6.8	0.05	0.89308203	0.89308203	0.89309699	0.89309699	0.89310474	0.89310474
0.06				0.80302479	0.80302479	0.80303833	0.80303833	0.80304535	0.80304535
0.09				0.71985201	0.71985201	0.71986417	0.71986417	0.71987048	0.71987048
0.05	0.1			0.58574689	0.58574689	0.58575671	0.58575671	0.58576180	0.58576180
	0.3			0.24295587	0.25072139	0.24295986	0.24295986	0.24296193	0.24296193
	0.5			0.08998096	0.08998096	0.08998239	0.08998239	0.08998315	0.08998315
	0.01	4		0.89845222	0.89845222	0.89846105	0.89846105	0.89846562	0.89846562
		7		0.82769241	0.82769241	0.82770676	0.82770676	0.82771419	0.82771419
		10		0.76139836	0.76139836	0.76141735	0.76141735	0.76142719	0.76142719
		6.8	-0.05	0.78688575	0.78688575	0.78688221	0.78688221	0.78688033	0.78688033
			0.02	0.81862905	0.81862905	0.81863007	0.81863007	0.81863059	0.81863059
			0.12	0.97452857	0.97452857	0.86421817	0.86421817	0.85056260	0.85056260

Table 5.2: Comparison of $\chi'(0)$ for various values of $T_t, T_b, S_Q, S_M, E, \sigma$ by Shooting Method and DTM-Padé

						$n=-3, We=0.01$		$n=1, We=0$		$n=3, We=0.01$	
T_t	T_b	S_Q	S_M	E	σ	**Shooting Method**	**DTM-Padé**	**Shooting Method**	**DTM-Padé**	**Shooting Method**	**DTM-Padé**
0.03	0.01	0.05	5	3	2	-1.48750051	-1.48750051	-1.48747228	-1.48747228	-1.48745764	-1.48745764
0.06						-2.31230089	-2.31230089	-2.31224459	-2.31224459	-2.31221539	-2.31221539
0.09						-3.59230155	-3.59230155	-3.59222994	-3.59222994	-3.59219276	-3.59219276
0.05	0.1					-1.37683310	-1.37683310	-1.37684321	-1.37684321	-1.60791008	-1.60791008
	0.3					-1.29862771	-1.29862771	-1.29864147	-1.29864147	-1.40562686	-1.40562686
	0.5					-1.26476393	-1.26476393	-1.26477795	-1.26477795	-1.33606822	-1.33606822
	0.01	-0.05				-2.16407621	-2.16407621	-2.16408297	-2.16408297	-3.91679239	-3.91679239
		0.02				-2.03817454	-2.03817454	-2.03817048	-2.03817048	-3.69044429	-3.69044429
		0.12				-1.96569720	-1.96569720	-1.85623506	-1.85623506	-3.49325834	-3.49325834
		0.01	5			-2.05625050	-2.05625050	-2.05624885	-2.05624885	-3.72303640	-3.72303640
			10			-2.17949478	-2.17949478	-2.17949321	-2.17949321	-3.77225894	-3.77225894
			15			-2.29665895	-2.29665895	-2.29665738	-2.29665738	-3.82221775	-3.82221775
			5	2		-1.99640130	-1.99640130	-2.81393318	-2.81393318	-3.69971651	-3.69971651
				3		-1.95271335	-1.95271335	-2.29665738	-2.29665738	-3.68433831	-3.68433831
				4		-1.93641884	-1.93641884	-2.07634697	-2.07634697	-3.67871779	-3.67871779
				2	2	-1.99640130	-1.99640130	-2.81393318	-2.81393318	-3.69971651	-3.69971651
					4	-2.06392299	-2.06392299	-3.48018830	-3.48018830	-3.72438933	-3.72438933
					6	-2.12957297	-2.12957297	-4.03630116	-4.03630116	-3.74942313	-3.74942313

Table 5.3: Comparison of $\chi'(0)$ for various values S_Q, S_M, B_s by Shooting Method and DTM-Padé$[5\times5]$.

			$n=-3, We=0.01$		$n=1, We=0$		$n=3, We=0.01$	
S_Q	S_M	P_l	**Shooting Method**	**DTM-Padé**	**Shooting Method**	**DTM-Padé**	**Shooting Method**	**DTM-Padé**
-0.05		0.5	-3.68071264	-3.68071264	-3.68070328	-3.68070328	-3.68069877	-3.68069877
0.02			-3.40398671	-3.40398671	-3.40397880	-3.40397880	-3.40397480	-3.40397480
0.12			-3.24595020	-3.24595020	-3.20633134	-3.20633134	-3.20623463	-3.20623463
0.01	5		-3.44353509	-3.44353509	-3.44353113	-3.44353113	-3.44352914	-3.44352914
	10		-3.44262691	-3.44262691	-3.44262260	-3.44262260	-3.44262046	-3.44262046
	15		-3.44171898	-3.44171898	-3.44171434	-3.44171434	-3.44171203	-3.44171203
	1	0.5	-3.23321118	-3.23321118	-3.23320693	-3.23320693	-3.23320481	-3.23320481
		1.0	-5.75926435	-5.75926435	-5.75925402	-5.75925402	-5.75924883	-5.75924883
		1.5	-8.53042052	-8.53042052	-8.53040286	-8.53040286	-8.53039401	-8.53039401

Table 5.4: Values of Torque at the lower (fix) and upper (moving) plates.

				$\frac{dg(0)}{d\eta}$		$\frac{dg(1)}{d\eta}$	
S_Q	R_Ω	We	Re	**DTM-Padé**	**Shooting Method**	**DTM-Padé**	**Shooting Method**
0.01	0.1	0.01	0.01	-1.05591667	-1.05591667	-1.00586254	-0.99994831
0.03				-1.00101432	-1.00101432	-1.00688815	-0.99954622
0.05				-1.03595883	-1.03595883	-1.01803750	-0.99874826
0.01	0.1			-1.00101432	-1.00101432	-1.00586254	-0.99994831
	0.2			-1.00087495	-1.00087495	-1.00030989	-0.99989969
	0.3			-1.00091052	-1.00091052	-1.00062003	-0.99988534
	0.1	0.01		-1.00101432	-1.00101432	-1.00586254	-0.99994831
		0.04		-1.00174207	-1.00174207	-1.02341830	-1.00012927
		0.07		-1.00247679	-1.00247679	-1.04340432	-1.00031195
		0.01	0.0013	-1.00101290	-1.00101290	-1.00054533	-0.99994839
			0.0016	-1.00101295	-1.00101295	-1.00053459	-0.99994839
			0.0019	-1.00101299	-1.00101299	1.00051846	-0.99994839

5.6 Discussion

The numerical results of DTM-Padé, which is employed to solve nonlinear coupled ordinary differential equations for the governing flow, are discussed in this chapter. Computational software *Mathematica (12v)* is used to obtain solutions of system of equations. Results are compared with the shooting method to verify the accuracy of the present method. The primary purpose is to analyze the physical significance of various parameters involved in the energy equation, induced MHD equation, nanoparticle concentration equation, momentum equation, and motile microorganism function. Multiple parameters are discussed, i.e., squeezing Reynolds number S_Q, rotational Reynolds number R_Ω, Weissenberg number We, Reynolds number Re, magnetic Reynolds number Re_M on velocity profiles and induced magnetic field. Furthermore, the influence of squeezing Reynolds number S_Q, Prandtl number P_r, thermophoresis parameter T_t, Brownian motion T_b, activation energy E, activation

rate σ, Schmidt number S_M, Bio convection number B_s, and Péclet number are also discussed. The numerical results for local Nusselt number, local Sherwood number, and motile density number are presented in Tables (5.1)-(5.3). From these tables, it is observed that our outcomes are in good agreement with the numerical shooting method. Eqs. (2.19)-(2.20) is used to calculate the effects of torque on the fixed and moving plate, which is displayed in Table (5.4) For the graphical outcomes, we have selected the following parametric values against each parameter $S_M = 0.2, Pe = 0.5, B_s = 5, S_Q = 0.02, R_\Omega = 0.2, We = 0.01, \mathrm{Re} = 0.001, \mathrm{Re}_M = 0.5,$ $T_t = 0.03, T_b = 0.1, P_t = 6.8, E = 2, \sigma = 2.$

Velocity Profile

Figure (5.2) shows the impact on the velocity field in the axial direction due to squeezed Reynolds number, and rotational Reynolds number. It is seen that when values of squeezed Reynolds number enhance, the axial velocity distribution decreases. However, increasing the values of the axial velocity increases. This is because the rotation of the plates accelerates the velocity of the fluid. Furthermore, in figure (5.3), it is seen that the increasing value of the velocity of the fluid decline and the Weissenberg number increases the axial velocity profile. Physically, when the values of the Weissenberg number is increased, the relaxation time increases for the particles of Carreau fluid, so these particles and velocity decreases the resistance. This is because that the Weissenberg number is the ratio of relaxation time of fluid and particular process time. In figure (5.4), it is seen that the impact of Weissenberg number on Carreau fluid velocity for shear thinning$(n < 1)$, Newtonian case$(n = 1)$, and thickening $(n > 1)$ cases on velocity field. This is because, in shear-thinning case, the fluid viscosity is lower with shear strain, and the velocity is high compared to the Newtonian and shear-thickening case. Figures (5.5-5.6) represent the influence of squeezed Reynolds number and rotational Reynolds number on tangential velocity distribution. It is notice that by enhancing value of squeezed Reynolds number and

rotational Reynolds number, the tangential velocity distribution decreases, but the effects are negligible.

Temperature Distribution

Figure (5.7) shows the influence of the thermophoresis parameter T_t and the Brownian motion parameter T_b on temperature profile by keeping rest of parameters unaltered. The effect indicates that increasing the values of both parameters raises the temperature profile. The impact of S_Q and Prandtl number P_t is portrayed in figure (5.8). It is seen that by upgrading the Prandtl number P_t, the temperature profile decline. The reason behind this is that when increasing the value of the Prandtl number P_t, the thermal conductivity reduces, and due to this reason, the temperature profile declines. It is also seen that temperature distribution decreases with increase in values of squeezed Reynolds number S_Q.

Concentration Distribution

Figure (5.9) depicts the influence of Activation energy and reaction rate on nanoparticle concentration. It can be seen that by enhancing the dimensionless activation energy, the concentration of nanoparticle increases. That is because low temperatures and high energy activation contribute to a constant reaction rate, and thus, the chemical reaction slows down. As a result, the concentration of solute increases. Besides that, higher values of reaction rate σ the nanoparticle concentration declines.

Motile Gyrotactic Microorganism Distribution

Figure (5.10) depicts the influence of squeezed Reynolds number and Péclet number on microorganism density function. It is perceived that increase in the value of squeezed Reynolds number the microorganism density function increases and increases in the value of Péclet number; the behaviour of the microorganism density function shows the opposite phenomenon. The reason behind that the speed of microorganisms is decreased when a rise in the value of Péclet number, and therefore diffusivity of the microorganism decreases. Figure (5.11) demonstrates the physical

behaviour of the Schmidt number. It is seen that the density of motile microorganism function increases by enhancing the value of the bioconvection Schmidt number, but the influence is nominal.

Physical Quantities

In Table (5.1-5.3), the numerical findings for the motile density number wall gradient, local nanoparticle Sherwood number, and local Nusselt number are reported. It is seen that by increasing the value of thermophoresis parameter the Nusselt number decrease but opposite phenomena is observed for Sherwood number. Also, by increasing the value of Brownian motion parameter the value of Nusselt number decrease and reverse is observed for Sherwood number. This table clearly shows that the DTM-Padé simulation and the numerical shooting technique have extremely excellent agreement. Eqs. (3.18) -(3.19) are used to calculate the effects of torque on the upper fixed and lower moving disk, and the DTM-Padé computations are displayed in Table (5.4). Finally, it is noteworthy from inspection, that the torque at the lower disk is increasing the torque at the upper disk are decreased with an increase in the squeezing Reynolds number respectively.

Chapter 6

Transport of Motile Gyrotactic Microorganism in a Williamson Fluid between a Pair of Rotating Circular Plates

6.1 Introduction

In this chapter, the unsteady flow confined by parallel rotating circular plates in a porous media filled with Williamson Nano fluid is studied. Nanoparticles, magnetic field and motile gyrotactic microorganisms are included in the Williamson fluid model. A numerical methodology known as the differential transform method is used to solve nonlinear differential equations. The Padé approximation is also employed with the suggested technique to improve the convergence rate. The tabular and graphical approaches are used to discuss the physical impact of various characteristics.

6.2 Mathematical Formulation

Flow Assumptions

To formulate the mathematical problem, following assumptions along with assumption of chapter 3 and 4 have been considered. Flow of magnetized viscoelastic Nano fluid saturating space between rotating and squeezing disks is modelled with

- Willamson fluid as base fluid.
- Porous media satisfies Darcy's law.

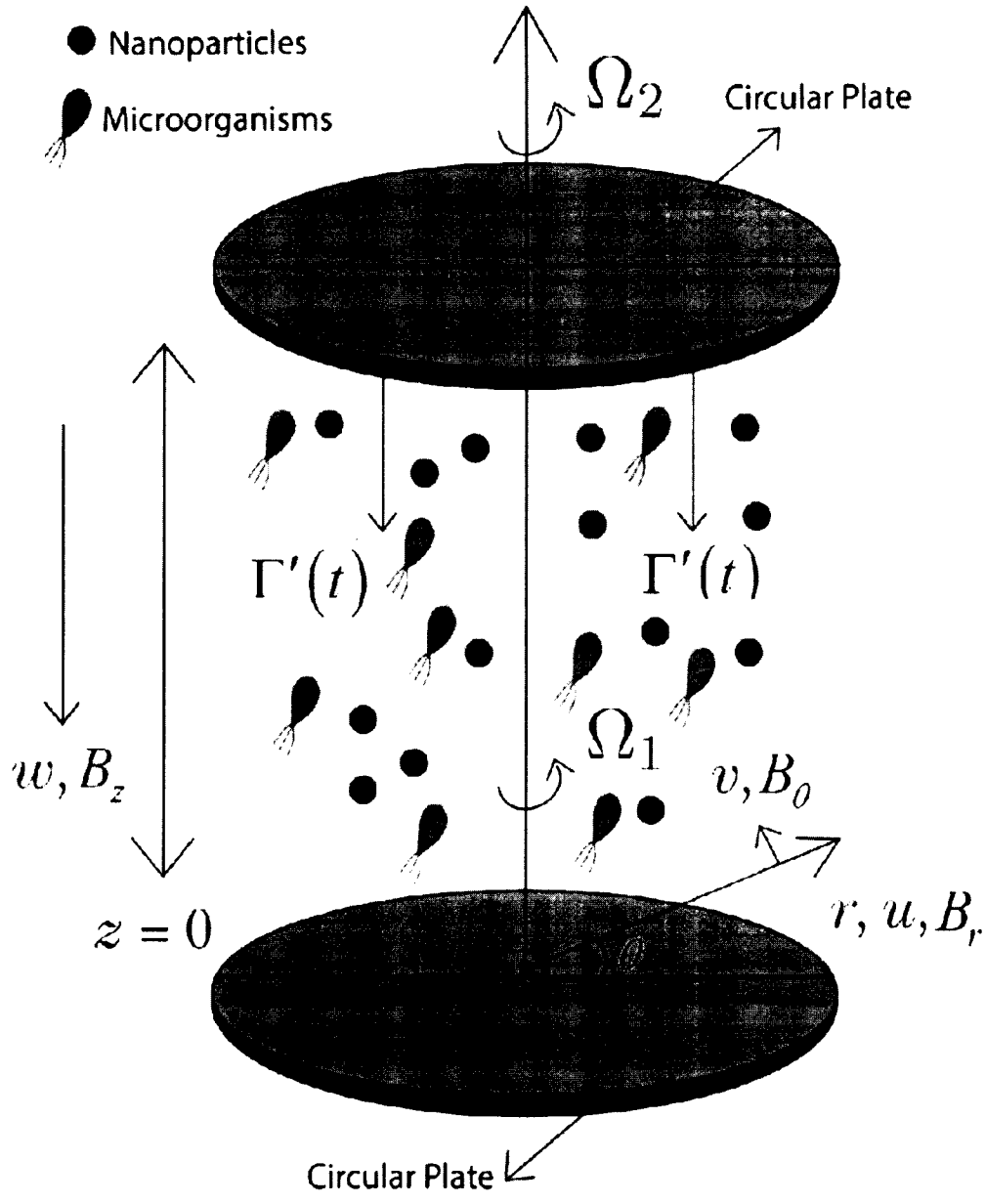

Figure 6.1: A physical structure for magnetized Nano fluid flow between finite parallel disks in the existence of motile gyrotactic microorganisms.

Rheological Model for Williamson Fluid

The constitutive equation of Williamson fluid flow is defined as [115]

$$\tau_{ij} = \left[\mu_\infty + (\mu_0 - \mu_\infty)\left(1-(\Gamma\gamma)^{-1}\right)\right] A_1, \tag{6.1}$$

Where τ_{ij} denotes stress tensor, μ_0 denotes shear rate viscosity (zero) μ_∞ denotes infinity shear rate viscosity, Γ denotes constant of time, A_1 denotes the first Rivlin-Erickson rate tensor and γ denotes rate of strain tensor and it is defined as

$$\gamma = \sqrt{\frac{1}{2}\mathrm{tr}(A_1)}, \tag{6.2}$$

$$A_1 = (L + L^T) = \left[(\nabla V + \nabla V^T)\right], \tag{6.3}$$

Using the Taylor series approximation of first order as $(1-\Gamma\gamma)^{-1} \cong (1+\Gamma\gamma)$ with $\Gamma^2 \ll 1$, Eq. (6.1) takes the form

$$\tau_{ij} = \left[\mu_\infty + (\mu_0 - \mu_\infty)\Gamma\gamma\right] A_1. \tag{6.4}$$

Mathematical Model

Assuming Williamson fluid flow in the MHD squeezed film, the continuity and momentum equation in the direction of r, θ, z read as follows:

$$\frac{1}{r}\frac{\partial}{\partial r}(rv_r) + \frac{1}{r}\frac{\partial}{\partial \theta}(v_\theta) + \frac{\partial}{\partial z}(v_z) = 0, \tag{6.5}$$

$$\begin{aligned}\rho\left(\frac{\partial v_r}{\partial t} + v_r\frac{\partial v_r}{\partial r} + \frac{v_\theta}{r}\frac{\partial v_r}{\partial \theta} + v_z\frac{\partial v_r}{\partial z} - \frac{v_\theta}{r}\right) &= -\frac{\partial p}{\partial r} \\ + \frac{1}{r}\frac{\partial}{\partial r}(r\tau_{rr}) + \frac{1}{r}\frac{\partial \tau_{r\theta}}{\partial \theta} - \frac{\tau_{\theta\theta}}{r} + \frac{\partial \tau_{rz}}{\partial z} - \frac{\partial B_r}{\partial z}B_z - \frac{\partial B_\theta}{\partial z}B_\theta - \frac{\upsilon}{K}v_r,\end{aligned} \tag{6.6}$$

$$\begin{aligned}\rho\left(\frac{\partial v_\theta}{\partial t} + v_r\frac{\partial v_\theta}{\partial r} + \frac{v_\theta}{r}\frac{\partial v_\theta}{\partial \theta} + v_z\frac{\partial v_\theta}{\partial z} - \frac{v_r v_\theta}{r}\right) &= -\frac{1}{r}\frac{\partial p}{\partial \theta} \\ + \frac{1}{r}\frac{\partial \tau_{\theta\theta}}{\partial \theta} + \frac{1}{r^2}\frac{\partial (r^2\tau_{r\theta})}{\partial r} + \frac{\partial \tau_{\theta z}}{\partial z} - \frac{\partial B_\theta}{\partial z}B_z - \frac{\partial B_\theta}{\partial r}B_r - \frac{\upsilon}{K}v_\theta,\end{aligned} \tag{6.7}$$

$$\rho\left(\frac{\partial v_z}{\partial t}+v_r\frac{\partial v_z}{\partial r}+\frac{v_\theta}{r}\frac{\partial v_z}{\partial \theta}+v_z\frac{\partial v_z}{\partial z}\right)=-\frac{\partial p}{\partial z}$$
$$+\frac{1}{r}\frac{\partial}{\partial r}(r\tau_{rz})+\frac{1}{r}\frac{\partial \tau_{\theta z}}{\partial \theta}+\frac{\partial \tau_{zz}}{\partial z}-\frac{\partial B_\theta}{\partial z}B_\theta+\frac{\partial B_r}{\partial z}B_r-\frac{\upsilon}{K}v_z, \tag{6.8}$$

where

$$\tau_{rr}=\left[\left(\mu_0+(\mu_0-\mu_\infty)\Gamma\left(2\left(\frac{\partial v_r}{\partial r}\right)^2+\left(\frac{\partial v_r}{\partial z}\right)^2+\left(\frac{\partial v_\theta}{\partial z}\right)^2+\left(\frac{\partial v_\theta}{\partial r}-\frac{v_\theta}{r}\right)^2+2\left(\frac{v_r}{r}\right)^2\right)^{\frac{1}{2}}\right)\right]2\frac{\partial v_r}{\partial r},$$

$$\tau_{r\theta}=\left[\left(\mu_0+(\mu_0-\mu_\infty)\Gamma\left(2\left(\frac{\partial v_r}{\partial r}\right)^2+\left(\frac{\partial v_r}{\partial z}\right)^2+\left(\frac{\partial v_\theta}{\partial z}\right)^2+\left(\frac{\partial v_\theta}{\partial r}-\frac{v_\theta}{r}\right)^2+2\left(\frac{v_r}{r}\right)^2\right)^{\frac{1}{2}}\right)\right]\left(\frac{\partial v_\theta}{\partial r}-\frac{v_\theta}{r}\right),$$

$$\tau_{rz}=\left[\left(\mu_0+(\mu_0-\mu_\infty)\Gamma\left(2\left(\frac{\partial v_r}{\partial r}\right)^2+\left(\frac{\partial v_r}{\partial z}\right)^2+\left(\frac{\partial v_\theta}{\partial z}\right)^2+\left(\frac{\partial v_\theta}{\partial r}-\frac{v_\theta}{r}\right)^2+2\left(\frac{v_r}{r}\right)^2\right)^{\frac{1}{2}}\right)\right]\frac{\partial v_r}{\partial z},$$

$$\tau_{\theta r}=\left[\left(\mu_0+(\mu_0-\mu_\infty)\Gamma\left(2\left(\frac{\partial v_r}{\partial r}\right)^2+\left(\frac{\partial v_r}{\partial z}\right)^2+\left(\frac{\partial v_\theta}{\partial z}\right)^2+\left(\frac{\partial v_\theta}{\partial r}-\frac{v_\theta}{r}\right)^2+2\left(\frac{v_r}{r}\right)^2\right)^{\frac{1}{2}}\right)\right]\left(\frac{\partial v_\theta}{\partial r}-\frac{v_\theta}{r}\right),$$

$$\tau_{\theta\theta}=\left[\left(\mu_0+(\mu_0-\mu_\infty)\Gamma\left(2\left(\frac{\partial v_r}{\partial r}\right)^2+\left(\frac{\partial v_r}{\partial z}\right)^2+\left(\frac{\partial v_\theta}{\partial z}\right)^2+\left(\frac{\partial v_\theta}{\partial r}-\frac{v_\theta}{r}\right)^2+2\left(\frac{v_r}{r}\right)^2\right)^{\frac{1}{2}}\right)\right]2\left(\frac{v_r}{r}\right),$$

$$\tau_{\theta z}=\left[\left(\mu_0+(\mu_0-\mu_\infty)\Gamma\left(2\left(\frac{\partial v_r}{\partial r}\right)^2+\left(\frac{\partial v_r}{\partial z}\right)^2+\left(\frac{\partial v_\theta}{\partial z}\right)^2+\left(\frac{\partial v_\theta}{\partial r}-\frac{v_\theta}{r}\right)^2+2\left(\frac{v_r}{r}\right)^2\right)^{\frac{1}{2}}\right)\right]\frac{\partial v_\theta}{\partial z},$$

$$\tau_{zr}=\left[\left(\mu_0+(\mu_0-\mu_\infty)\Gamma\left(2\left(\frac{\partial v_r}{\partial r}\right)^2+\left(\frac{\partial v_r}{\partial z}\right)^2+\left(\frac{\partial v_\theta}{\partial z}\right)^2+\left(\frac{\partial v_\theta}{\partial r}-\frac{v_\theta}{r}\right)^2+2\left(\frac{v_r}{r}\right)^2\right)^{\frac{1}{2}}\right)\right]\frac{\partial v_r}{\partial z},$$

$$\tau_{z\theta}=\left[\left(\mu_0+(\mu_0-\mu_\infty)\Gamma\left(2\left(\frac{\partial v_r}{\partial r}\right)^2+\left(\frac{\partial v_r}{\partial z}\right)^2+\left(\frac{\partial v_\theta}{\partial z}\right)^2+\left(\frac{\partial v_\theta}{\partial r}-\frac{v_\theta}{r}\right)^2+2\left(\frac{v_r}{r}\right)^2\right)^{\frac{1}{2}}\right)\right]\frac{\partial v_\theta}{\partial z},$$

$\tau_{zz} = 0.$

The magnetic field equation read as

$$\frac{1}{r}\frac{\partial}{\partial r}(rB_r)+\frac{1}{r}\frac{\partial B_\theta}{\partial \theta}+\frac{\partial B_z}{\partial z}=0, \tag{6.9}$$

$$\frac{\partial B_r}{\partial t}+v_r\frac{\partial B_r}{\partial r}+v_\theta\frac{\partial B_r}{\partial \theta}+v_z\frac{\partial B_r}{\partial z}=-\frac{\partial}{\partial z}(v_rB_z-v_zB_r)+\frac{1}{\delta\mu_2}\left(\frac{\partial^2 B_r}{\partial z^2}\right), \tag{6.10}$$

$$\frac{\partial B_\theta}{\partial t}+v_r\frac{\partial B_\theta}{\partial r}+v_\theta\frac{\partial B_\theta}{\partial \theta}+v_z\frac{\partial B_\theta}{\partial z}=\frac{\partial}{\partial r}(v_rB_\theta-v_\theta B_r)-\frac{\partial}{\partial z}(v_\theta B_z-B_\theta v_z)+\frac{1}{\delta\mu_2}\left(\frac{\partial^2 B_\theta}{\partial z^2}\right), \tag{5.11}$$

$$\frac{\partial B_z}{\partial t}+v_r\frac{\partial B_r}{\partial r}+v_\theta\frac{\partial B_r}{\partial \theta}+v_z\frac{\partial B_r}{\partial z}=\frac{\partial}{\partial r}(v_rB_z-v_zB_r)+\frac{1}{\delta\mu_2}\left(\frac{\partial^2 B_z}{\partial z^2}\right). \tag{6.12}$$

The energy equation reads as

$$\frac{\partial T}{\partial t}+v_r\frac{\partial T}{\partial r}+v_\theta\frac{\partial T}{\partial \theta}+v_z\frac{\partial T}{\partial z}=\tilde{\alpha}\frac{\partial^2 T}{\partial z^2}+\tau\left[D_B\left(\frac{\partial T}{\partial r}\frac{\partial C}{\partial r}+\frac{\partial T}{\partial z}\frac{\partial C}{\partial z}\right)+\frac{D_T}{T_u}\left[\left(\frac{\partial T}{\partial r}\right)^2+\left(\frac{\partial T}{\partial z}\right)^2\right]\right]. \tag{6.13}$$

The concentration of nanoparticle equation reads as

$$\frac{\partial C}{\partial t}+v_r\frac{\partial C}{\partial r}+v_\theta\frac{\partial C}{\partial \theta}+v_z\frac{\partial C}{\partial z}=D_B\frac{\partial^2 C}{\partial z^2}+\frac{D_T}{T_u}\frac{\partial^2 T}{\partial z^2}. \tag{6.14}$$

The conservation of microorganism reads as

$$\frac{\partial n}{\partial t}+v_r\frac{\partial n}{\partial r}+v_\theta\frac{\partial n}{\partial \theta}+v_z\frac{\partial n}{\partial z}+\frac{\bar{b}W_{mo}}{C_l-C_u}\left[\frac{\partial}{\partial z}\left(n\frac{\partial C}{\partial z}\right)\right]=D_{mo}\left(\frac{\partial^2 n}{\partial z^2}\right). \tag{6.15}$$

The Initial Conditions and Boundary Conditions for the Eqs. (6.5)-(6.15) with our assumptions are

$$v_r=0, v_\theta=\Omega_1 r\frac{D^2}{\Gamma^2(t)}, v_z=0, B_z=B_\theta=0, C=C_l, T=T_l, n=n_l \quad \text{at} \quad z=0, \tag{6.16}$$

$$\left.\begin{aligned} &v_r = 0, v_\theta = \Omega_2 r\frac{D^2}{\Gamma^2(t)}, B_\theta = N_0 r\frac{D^2}{\Gamma^2(t)}, B_z = -\frac{\alpha D M_0}{\Gamma(t)}, v_z = -\frac{\alpha D^2}{2\Gamma(t)}, \\ &T = T_u, C = C_u, n = n_u. \end{aligned}\right] \quad \text{at} \quad z = \Gamma(t). \tag{6.17}$$

6.3 Similarity Transformations

Substituting similarity transformation of chapter five, and using component form of Willaimasons fluid model in above mentioned governing equations, the following nonlinear, coupled ordinary differential equations (ODE's) with independent variable are generated

$$\left[\begin{aligned} &f^{iv} = 4S_Q\left[3f'' - 2\left(\frac{R_\Omega}{S_Q}\right)^2 gg' + 2F_T^2\left(mm''' + m'm''\right) - \left(2f - \eta\right)f''' + 2F_A^2\left(\frac{R_\Omega}{S_Q}\right)^2 nn'\right] \\ &-\frac{We}{\ddot{\gamma}}\left(\begin{aligned} &\frac{1}{S_Q}\left(\mathrm{Re}\left(f''g'''g' + f''g''^2 - g''g'f''' - f^{iv}g'^2\right) - 2R_\Omega\left(f''g'^2 + 2g'f'g''\right)\right) \\ &-\frac{S_Q}{R_\Omega}\left(\left(4f'^2f^{iv} - 6f''^3 - 4f''f'f'''\right) + \frac{2\,\mathrm{Re}}{R_\Omega}\left(f'''^2 + f''f^{iv}\right)\right) \end{aligned}\right) - \frac{\lambda}{2}f'(\eta), \end{aligned}\right. \tag{6.18}$$

$$\left[\begin{aligned} &\left(\frac{R_\Omega}{S_Q} + We\ddot{\gamma}\right)g'' = S_Q\left[2g + \eta g' + 2\left(gf' - fg'\right) + 2N_T M_T\left(mn' + nm'\right)\right] \\ &\qquad -4We\left(\frac{S_Q}{\ddot{\gamma}R_\Omega}g'f'f'' + \mathrm{Re}\left(\frac{R_\Omega}{4\ddot{\gamma}S_Q^{\,2}}g''g'^2 + \frac{1}{R_\Omega\ddot{\gamma}}f''g'f'''\right)\right) - 2\lambda S_Q g(\eta), \end{aligned}\right. \tag{6.19}$$

$$m'' = \mathrm{Re}_M\left[m + \eta m' + 2mf' - 2fm'\right], \tag{6.20}$$

$$n'' = \mathrm{Re}_M\left[2n - fn' + \eta n' + 2\left(\frac{F_A}{F_T}\right)mg'\right], \tag{6.21}$$

$$\theta'' + S_Q P_t f\theta' + T_t\theta'^2 + T_b\theta'\phi' = 0, \tag{6.22}$$

$$\phi'' + \frac{T_t}{T_b}\theta'' + S_Q S_M f\phi' = 0, \tag{6.23}$$

$$\chi'' - S_Q B_s\left(\frac{\eta}{2}\right)\chi' + B_s S_Q f\chi' - P_t\left[\chi'\phi' + (\chi + \varphi)\phi''\right] = 0. \tag{6.24}$$

Where $We=\frac{\Omega_1\Gamma(\mu_0-\mu_\infty)}{\mu_0}$ Weissenberg number and $\lambda=\frac{\upsilon(1-\alpha t)}{\alpha K}$ represents porosity parameter.

The boundary conditions in Eqs. (6.16)- (6.17) assume the following form after utilizing the similarity variables:

$$\begin{bmatrix} f(0)=0=f'(0),g(0)=1,m(0)=0,n(0)=1,\theta(0)=1,\chi(0)=1,\phi(0)=1, \\ f(1)=\frac{1}{2},g(1)=\dot{\xi},m(1)=1,n(1)=1,\theta(1)=0,\phi(1)=0,\chi(1)=0. \end{bmatrix} \tag{6.25}$$

6.4 Solution Methodolgy

The dimensionless Eqs. (6.18)-(6.24) generated using the similarity transformation mentioned in chapter five and then solved using DTM with the help of boundary conditions mentioned in Eq. (6.25). Substituting Differential transformations given in Eqs. (1.1)-(1.11),in which $F(q),G(q),M(q),N(q),\Theta(q),\Phi(q)$ and $\mathrm{X}(q)$ are transformed function of $f(\eta),g(\eta),m(\eta),n(\eta),\theta(\eta),\phi(\eta)$ and $\chi(\eta)$ respectively and are expressed as

$$f(\eta)=\sum_{q=0}^{\infty}F(q)\eta^q, \tag{6.26}$$

$$g(\eta)=\sum_{q=0}^{\infty}G(q)\eta^q, \tag{6.27}$$

$$m(\eta)=\sum_{q=0}^{\infty}M(q)\eta^q, \tag{6.28}$$

$$n(\eta)=\sum_{q=0}^{\infty}N(q)\eta^q, \tag{6.29}$$

$$\theta(\eta)=\sum_{q=0}^{\infty}\Theta(q)\eta^q, \tag{6.30}$$

$$\phi(\eta)=\sum_{q=0}^{\infty}\Phi(q)\eta^q, \tag{6.31}$$

$$\chi(\eta)=\sum_{q=0}^{\infty}\mathrm{X}(q)\eta^{q}. \tag{6.32}$$

The differential transform of the corresponding boundary conditions (BC's) is:

$$\left.\begin{array}{lllll} F(0)=0, & F(1)=\frac{1}{2}, & G(0)=1, & M(0)=0, & N(0)=0, \\ \Theta(0)=1, & \Phi(0)=0, & \mathrm{X}(0)=0, & F(2)=\Pi_1, & F(3)=\Pi_2, \\ G(1)=\Pi_3, & M(1)=\Pi_4, & N(1)=\Pi_5, & \Theta(1)=\Pi_6, & \Phi(1)=\Pi_6, \\ \mathrm{X}(1)=\Pi_8, & & & & \end{array}\right] \tag{6.33}$$

Where Π_k $(k=1,2,3,...8)$ are the constant values. By substituting the transformations given in Eqs. (1.1)-(1.11) into Eqs. (6.18)-(6.24) and using the associated boundary conditions given in Eq. (6.33). The following are the series solutions:

$$F(\eta)=f_1\eta^2+f_2\eta^3+f_3\eta^4+f_4\eta^5+..., \tag{6.34}$$

$$G(\eta)=1-g_1\eta+g_2\eta^2+g_3\eta^3+g_4\eta^4+..., \tag{6.35}$$

$$M(\eta)=m_1\eta+m_2\eta^3+m_3\eta^4+m_4\eta^5+..., \tag{6.36}$$

$$N(\eta)=n_1\eta+n_2\eta^3+n_3\eta^4+n_4\eta^5+..., \tag{6.37}$$

$$\Theta(\eta)=1+\theta_1\eta+\theta_2\eta^2+\theta_3\eta^3+\theta_4\eta^4+..., \tag{6.38}$$

$$\Phi(\eta)=1+\phi_1\eta+\phi_2\eta^2+\phi_3\eta^3+\phi_4\eta^4+..., \tag{6.39}$$

$$\chi(\eta)=1+\chi_1\eta+\chi_2\eta^2+\chi_3\eta^3+\chi_4\eta^4+..., \tag{6.40}$$

where, $f_i, g_i, m_i, n_i, \theta_i, \phi_i\ \chi_i$; $i(=1,2,3,...)$ all are fixed values but difficult to provide here. The previously given equations are solved with 30 iterations using *Mathematica* software. However, because we were unable to achieve an excellent convergence rate, the Padé approximation was used. The ratio of two polynomials, i.e., rational fractional form, is defined as the Padé approximation. Because of the nonlinearity of

the governing equations, the results obtained by DTM do not meet the boundary requirements at the end point without using the Padé approximation. The DTM solutions must then be combined with the Padé approximation, which has a significant rate of convergence at infinity. A higher order of approximation is necessary depending on the desired accurateness. Here, $[5\times5]$ order approximation is applied to Eqs. (6.34)-(6.40), the Padé approximants are as follows:

$$f(\eta)=\frac{1.90345\eta^2-1.46791\eta^3+0.30574\eta^4-0.09613\eta^5}{1+0.25421\eta+0.05445\eta^2-0.00576\eta^3-0.01063\eta^4-0.00369\eta^5} \tag{6.41}$$

$$g(\eta)=\frac{1-2.5321\eta+0.14630\eta^2+0.82149\eta^3+0.44129\eta^4+0.13054\eta^5}{1-1.53185\eta-1.38353\eta^2-0.56653\eta^3-0.12647\eta^4-0.00042\eta^5} \tag{6.42}$$

$$m(\eta)=\frac{0.70958\eta+0.08891\eta^2-0.01376\eta^3+0.30161\eta^4-0.32837\eta^5}{1+0.12530\eta-0.35273\eta^2+0.06605\eta^3-0.06125\eta^4-0.01978\eta^5} \tag{6.43}$$

$$n(\eta)=\frac{0.93923\eta+1.48352\eta^2+0.90448\eta^3+0.46249\eta^4+0.19181\eta^5}{1+1.57950\eta+0.71489\eta^2+0.41838\eta^3+0.29677\eta^4-0.022257\eta^5} \tag{6.44}$$

$$\theta(\eta)=\frac{1-0.80937\eta-0.21526\eta^2+0.01351\eta^3+0.00412\eta^4+0.00701\eta^5}{1+0.12854\eta-0.02712\eta^2-0.00391\eta^3-0.01074\eta^4+0.00056\eta^5} \tag{6.45}$$

$$\phi(\eta)=\frac{1-0.12123\eta-0.34409\eta^2-0.48574\eta^3-0.00010\eta^4-0.04746\eta^5}{1+1.05982\eta+0.65555\eta^2+0.09425\eta^3+0.02288\eta^4+0.00115\eta^5} \tag{6.46}$$

$$\chi(\eta)=\frac{1-0.14732\eta-0.62596\eta^2-0.16040\eta^3-0.05519\eta^4-0.01107\eta^5}{1+0.91928\eta+0.26633\eta^2+0.07215\eta^3+0.01584\eta^4+0.00046\eta^5} \tag{6.47}$$

6.5 Graphical Results and Tabular Results

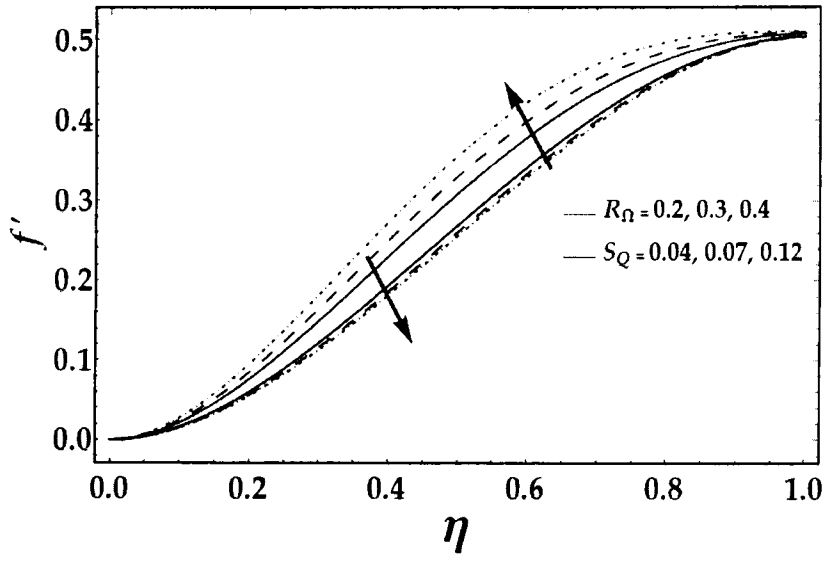

Figure 6.2: Variation of S_Q and R_Ω on $f'(\eta)$.

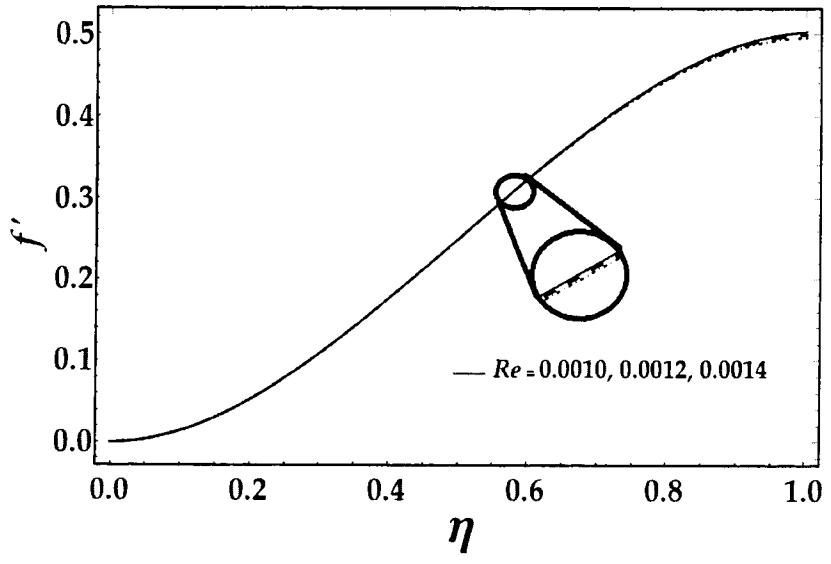

Figure 6.3: Variation of Re on $f'(\eta)$.

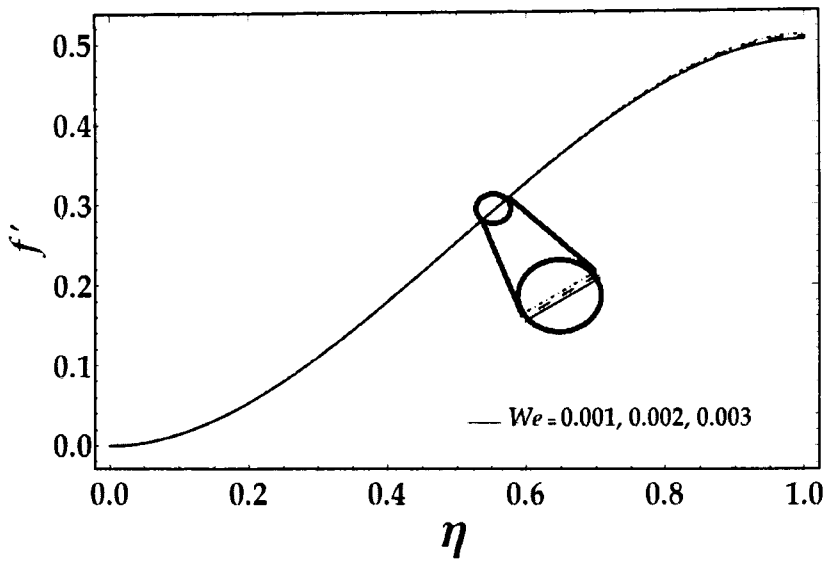

Figure 6.4: Variation of We on $f'(\eta)$.

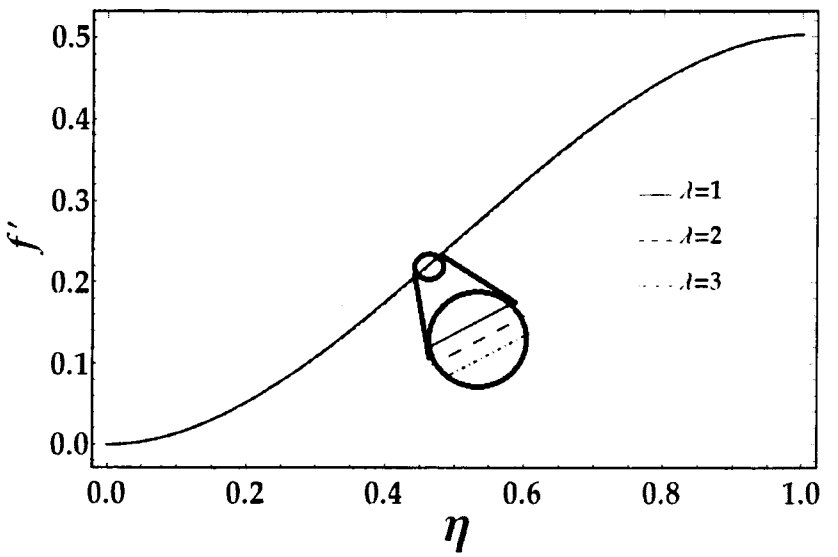

Figure 6.5: Variation of λ on $f'(\eta)$.

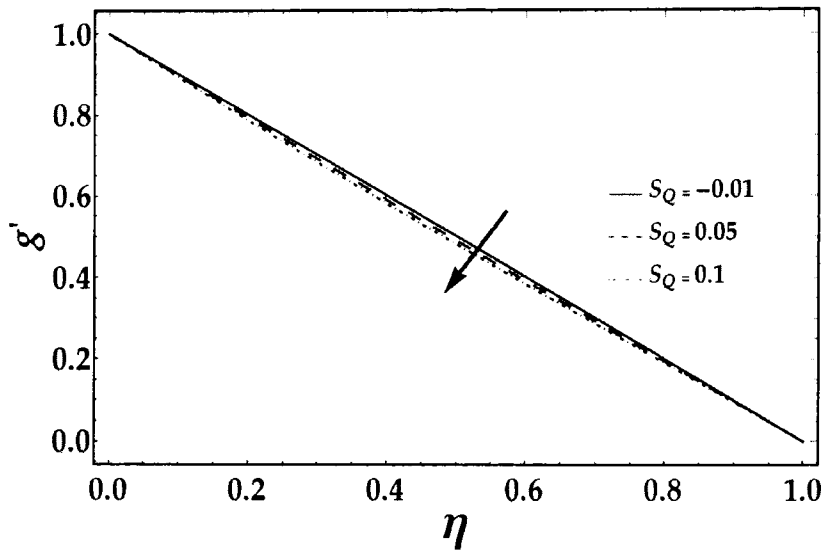

Figure 6.6: Variation of S_Q on the $g'(\eta)$.

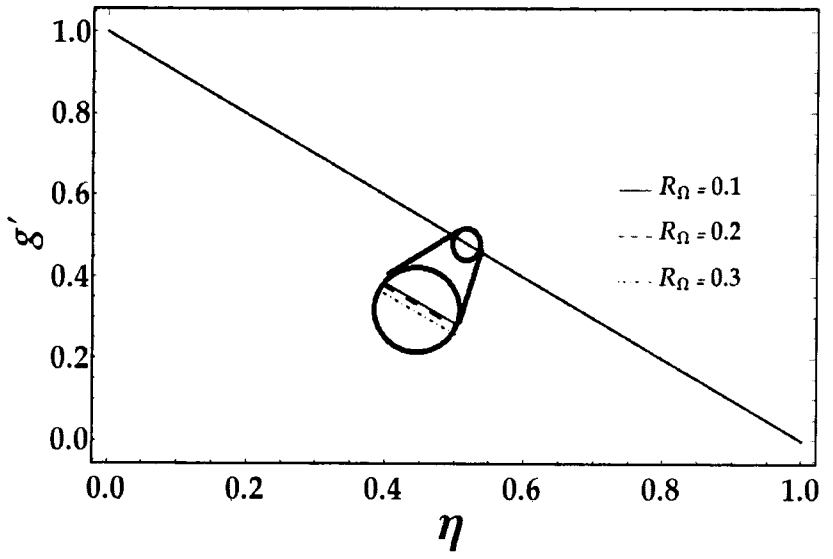

Figure 6.7: Variation of R_Ω on the $g'(\eta)$.

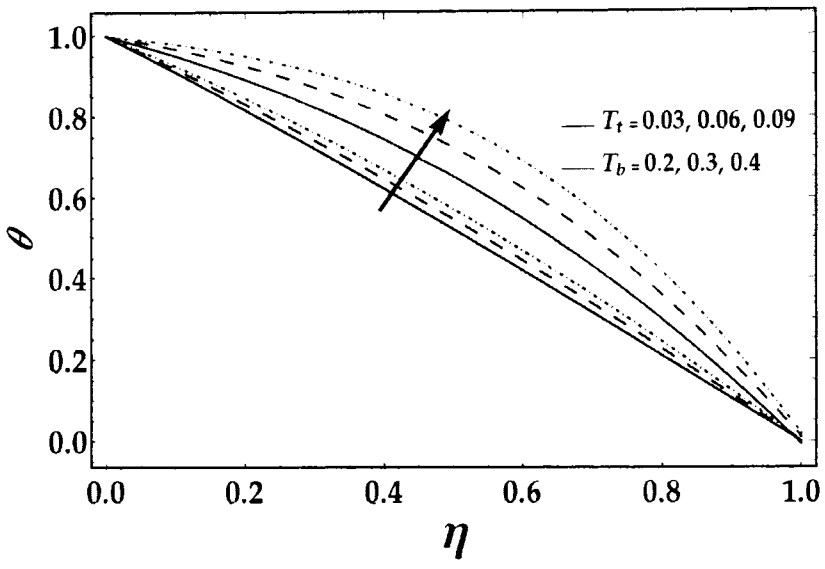

Figure 6.8: Variation of T_t and T_b on the $\theta(\eta)$.

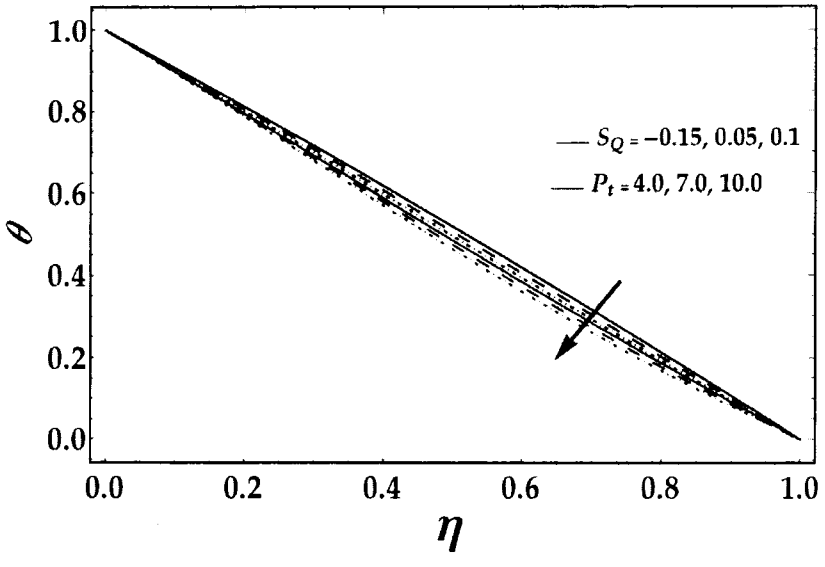

Figure 6.9: Variation of S_Q and P_t on the $\theta(\eta)$.

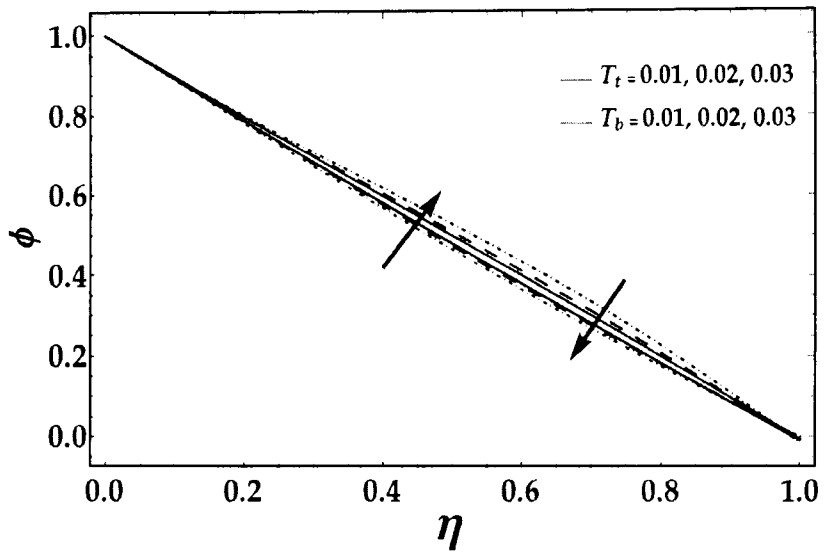

Figure 6.10: Variation of T_t and T_b on the $\phi(\eta)$.

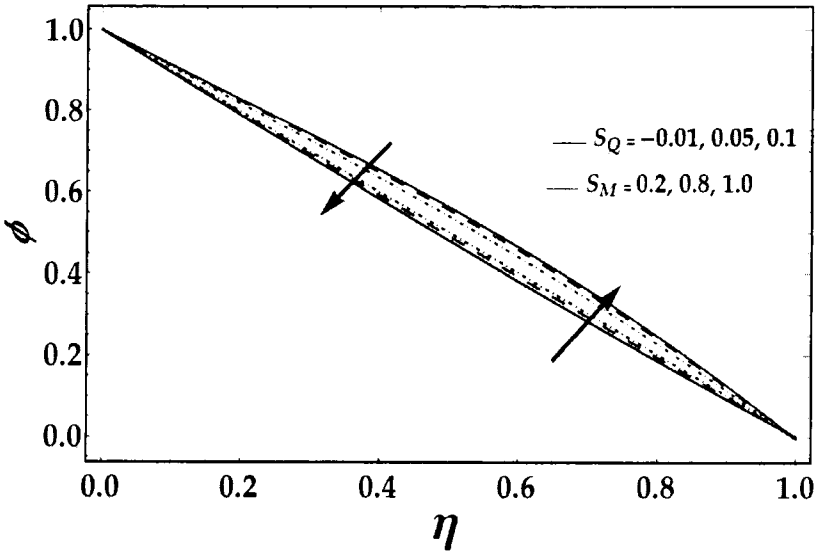

Figure 6.11: Variation of S_Q and S_M on the $\phi(\eta)$.

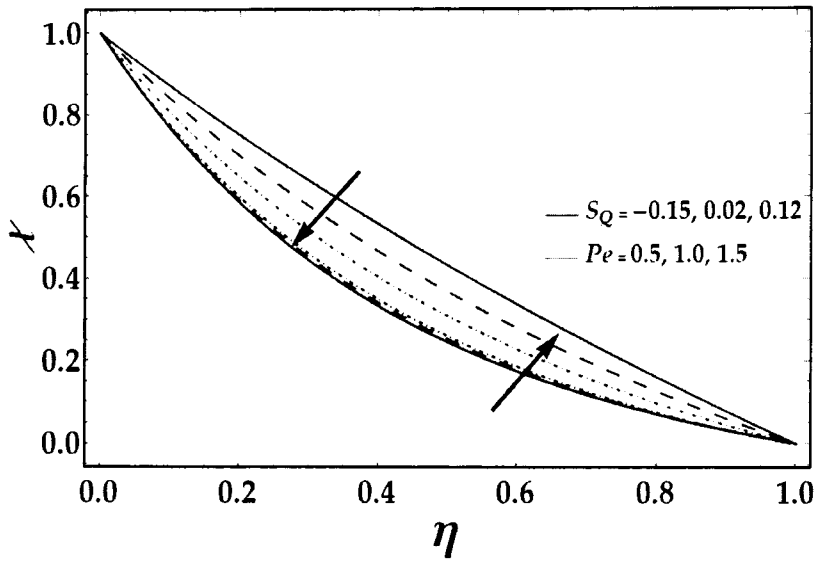

Figure 6.12: Influence of S_Q, Pe on $\chi(\eta)$.

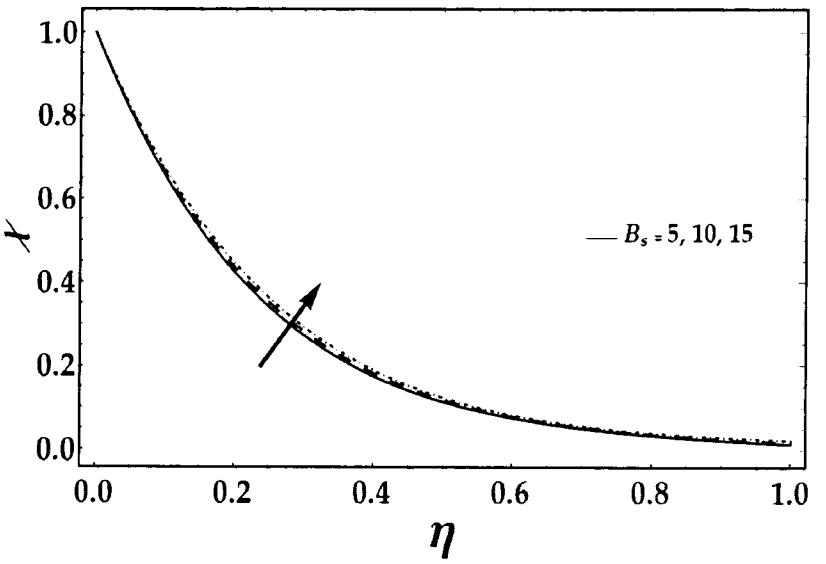

Figure 6.13: Influence of B_s on $\chi(\eta)$.

Table 6.1: Analysis of Nusselt number $\theta'(0)$ for various values T_t, T_b, P_t, S_Q by DTM-Padé $[5\times5]$.

T_t	T_b	P_t	S_Q	$\lambda=0, We=0$	$\lambda=3, We=0.0014$
0.03	0.01	6.8	0.05	-0.894331445910291	-0.8941277793999004
0.06				-0.8037095122926121	-0.8035188663335286
0.09				-0.7198149657681331	-0.7196374670200603
0.05	0.2			-0.39410764468127524	-0.3939963299160305
	0.3			-0.2527760428884648	-0.2526990987319676
	0.4			-0.15733909794397594	-0.1572882408932199
	0.01	4		-0.8991280725547512	-0.8990075291259064
		7		-0.8285960662715828	-0.8283960513827385
		10		-0.7623431624160361	-0.762072979159478
		6.8	-0.01	-0.8055467619687604	-0.8055857980288299
			0.05	-0.8331638701744839	-0.8329688625583156
			0.10	-0.8562584976198991	-0.8558694550669134

Table 6.2: Analysis of Sherwood number $\phi'(0)$ for various values T_t, T_b, S_Q, S_M by DTM-Padé $[5\times5]$.

T_t	T_b	S_Q	S_M	$\lambda=0, We=0$	$\lambda=3, We=0.0014$
0.03	0.01	0.05	1	-1.3206515674569705	-1.3212290607096857
0.06				-2.1810375658926415	-2.182143519538101
0.09				-3.524472568479956	-3.526023984905224
0.05	0.01			-1.8376104521007752	-1.8385494309701467
	0.02			-1.494470255082240	-1.4949112495938333
	0.03			-1.3788394622249018	-1.3791144757696543
	0.01	-0.01		-1.9716481796319092	-1.9714606614525256
		0.05		-1.8376104521007752	-1.8385494309701467
		0.10		-1.7254895229072031	-1.727366226587155
		0.05	0.2	-1.8346779737721937	-1.8356474740015034
			0.8	-1.8368775618025093	-1.837824171426474
			1.0	-1.8376104521007752	-1.8385494309701467

Table 6.3: Analysis of $\chi'(0)$ for various values of S_Q, B_s, P_l by DTM-Padé $[5\times5]$.

S_Q	B_s	P_l	$\lambda=0, We=0$	$\lambda=3, We=0.0014$
-0.01	1	1	-1.6536338714862044	-1.6536062606415687
0.05			-1.6288240938041103	-1.628962928925392
0.10			-1.6081090485862037	-1.6083872620540738
0.05	5		-1.6264756231408841	-1.6264540777338687
	10		-1.623542316208881	-1.6233209170249776
	15		-1.6206115509039687	-1.6201909883290273
	1	0.5	-1.2933454396424895	-1.2933934902581639
		1.0	-1.6288240938041103	-1.628962928925392
		1.5	-2.0028259652004254	-2.0030638099298255

Table 6.4: Torque Values on the fix and moving plates by DTM- Padé $[5\times5]$ for various values of Squeezing Reynolds Number S_Q.

	$\frac{dg(0)}{d\eta}$		$\frac{dg(1)}{d\eta}$	
S_Q	$\lambda=0, We=0$	$\lambda=3, We=0.0014$	$\lambda=0, We=0$	$\lambda=3, We=0.0014$
0.1	-1.092937221430923	-0.8954500024658023	− 0.948663684660318	-0.8968514132478014
0.2	-1.180889912821983	-0.7842736506672865	− 0.901360783950894	-0.7898299005296441

Table 6.5: Torque values of on the fix and moving plates by DTM- Padé $[5\times5]$ for various values of Reynolds Number (Rotational) R_Ω.

	$\frac{dg(0)}{d\eta}$		$\frac{dg(1)}{d\eta}$	
R_Ω	$\lambda=0, We=0$	$\lambda=3, We=0.0014$	$\lambda=0, We=0$	$\lambda=3, We=0.0014$
0.1	− 1.26549257529977	-0.668788920573831	− 0.853300068364298	-0.6266946930246056
0.2	− 1.26527487178758	-0.668350694212925	− 0.854905242597022	-0.6567018469217151

6.6 Discussion

The numerical solutions found using the Differential Transformation method and the Padé approximant are given using graphical and tabular approaches in this section. Numerical simulations were carried out using the computational software *Mathematica 12v*. The physical effects of various components in the momentum equation, magnetic field equation, temperature equation, motile microorganisms' equation, and nanoparticle concentration equation are our key interests. Various physical parameters are deliberated, i.e., effects of squeezing Reynolds number S_Q, rotational Reynolds number R_Ω, Weissenberg number We, Reynolds number Re, porosity parameter λ on the axial and tangential velocity profiles $f'(\eta), g'(\eta)$. Additionally, the impact of different parameters, i.e., squeezing Reynolds number S_Q, Bioconvection Schmidt number B_s, Péclet number Pe, are presented for motile microorganism profile.

Tables (6.1) -(6.3) provide the numerical results for various parameters such as Sherwood number, Nusselt number, and motile density function. Eqs. (3.19)-(3.20) are used to calculate the torque effect on lower and upper circular plates, as indicated in Tables (6.4)-(6.5).

Velocity Distribution

Figures (6.2)-(6.4) illustrated the influence of velocity profile in the axial direction $f'(\eta)$ due to squeezed Reynolds number S_Q, rotational Reynolds number R_Ω, Weissenberg number *We*, Reynolds number Re, and porosity parameter λ. From figure (6.2), one can perceive that by increasing the values of squeezing Reynolds number S_Q and the rotational Reynolds number R_Ω, the axial velocity profile decreases and increases, respectively. The reason behind fluid accelerates by the rotation of the plate, which causes an increment in velocity field for large values of R_Ω. In figure (6.3), it is notice that by increasing the value of Reynolds number, velocity field in axial direction $f'(\eta)$ decreases. In figure (6.4), it is noticed that the Weissenberg number boosts the velocity profile, but the effects are minimal. This increase in axial velocity is the consequence of the increase in relaxation time due to the reduction of resistance in particles of the Williamson fluid. Figure (6.5) shows the impact of the porosity factor λ on axial velocity distribution $f'(\eta)$. It is observed that by enrichment in the value of the porosity parameter λ, velocity profile $f'(\eta)$ decreases. The fluid velocity declines because the viscosity of the fluid increases for the increasing values of the porosity parameter λ.

Figure (6.6) represents the tangential velocity profile $g'(\eta)$ behaviour for squeezed Reynolds number S_Q. It is detected that by boosting the Squeezed Reynolds number S_Q, the tangential velocity distribution declines. A similar mechanism is observed in figure (6.7), i.e., enhancing the values of the rotational Reynolds number, tangential velocity profile decreases.

Temperature Distribution

Figure (6.8) elucidate impact of thermophoresis and Brownian motion parameters T_t, T_b on the temperature profile $\theta(\eta)$. The graph illustrates that by

enhancing the thermophoresis parameter and Brownian motion parameter T_t, T_b, the temperature distribution rises. The physical reason for this is because the fluid temperature is rising as the kinetic energy of the nanoparticles increases. The effects of S_Q and Prandtl number P_t on temperature profile $\theta(\eta)$ displayed in figure (6.9). It is seen that by upgrading the Prandtl number P_t and the squeezing Reynolds number S_Q, the temperature profile $\theta(\eta)$ diminishes. The reason behind this is the thermal conductivity reduces when we increase the value of Prandtl number P_t, which declines temperature profile $\theta(\eta)$.

Nanoparticle Concentration Distribution

Figure (6.10) shows the influence of Brownian motion T_b and thermophoresis parameter T_t on nanoparticle concentration $\phi(\eta)$. It is perceived that the concentration of nanoparticles decays by boosting values of the Brownian parameter T_b, and nanoparticle concentration increases by enhancing values of thermophoresis parameter T_t. Figure (6.11) elaborated impact of Schmidt number S_M and squeezed Reynolds number S_Q on nanoparticle concentration. By enlarging values of squeezing Reynolds number S_Q, nanoparticle concentration $\phi(\eta)$ rises, while the opposed phenomena are detected by enhancing the values of Schmidt number S_M.

Motile Gyrotactic Microorganism Distribution

Figure (6.12) portrays the influence of the Péclet number *Pe*, and squeezed Reynolds number S_Q on the motile microorganism density function $\chi(\eta)$. One can observe that by raising the values of squeezing Reynolds number S_Q, motile gyrotactic microorganism density function enhanced; on the other hand, increasing values of Péclet number *Pe*, causes a decrement in motile microorganism density profile. The physical cause of the above-mentioned physical parameter's behaviour is that as microorganism diffusivity drops, the microorganism's speed reduces. As a

result, as the Péclet number increases, the microorganism density function declines. Figure (6.13) reveals the physical performance of the bioconvection Schmidt number B_s. The density of the motile microorganism function increases when the bioconvection Schmidt number is increased, however the consequence is minor.

Physical Quantities

In Table (6.1-6.3), the numerical findings for the Nusselt number, local Sherwood number and motile density number wall gradient are reported. It is evident that increasing the thermophoresis parameter value causes the Nusselt number to rise, whereas the opposite trend is observed for Sherwood number. Additionally, the Nusselt number decreases when the Brownian motion parameter is increased, and the opposite is true for the Sherwood number. This table demonstrates the extraordinarily good agreement between the numerical shooting approach and the DTM-Padé simulation. Eqs. (3.18) -(3.19) are used to calculate the effects of torque on the upper fixed and lower moving disk, and the DTM-Padé computations are displayed in Table (6.4-6.5). In conclusion, it should be noted that by closer examination, it reveals that, as the squeezing Reynolds number rises, the torque at the upper disk decreases and the torque at the lower disk increases.

Chapter 7

Transport of Motile Gyrotactic Microorganism in a Reiner Rivlin Fluid between a Pair of Rotating Circular Plates

7.1 Introduction

This chapter deals with the unsteady flow in rotating circular plates located at a finite distance filled with Reiner-Rivlin Nano fluid in the presence of gyrotactic microorganism with effects of activation energy and nonlinear thermal radiation. The finalized formulated equations are solved using a semi-numerical technique entitled Differential Transformation Method (DTM) after employing the similarity transformation. Padé approximation is also used with DTM to present the solution of nonlinear coupled ordinary differential equations. The tabular and graphical results are displayed to discuss the physical effects of various features.

7.2 Mathematical Formulation

Flow Assumptions

To formulate the mathematical problem, following assumptions along with assumption of chapter 3 and 4 have been considered. Flow of magnetized viscoelastic Nano fluid saturating space between rotating and squeezing disks is modelled with

- Reiner-Rivlin fluid as base fluid.
- Non linear thermal radiation.

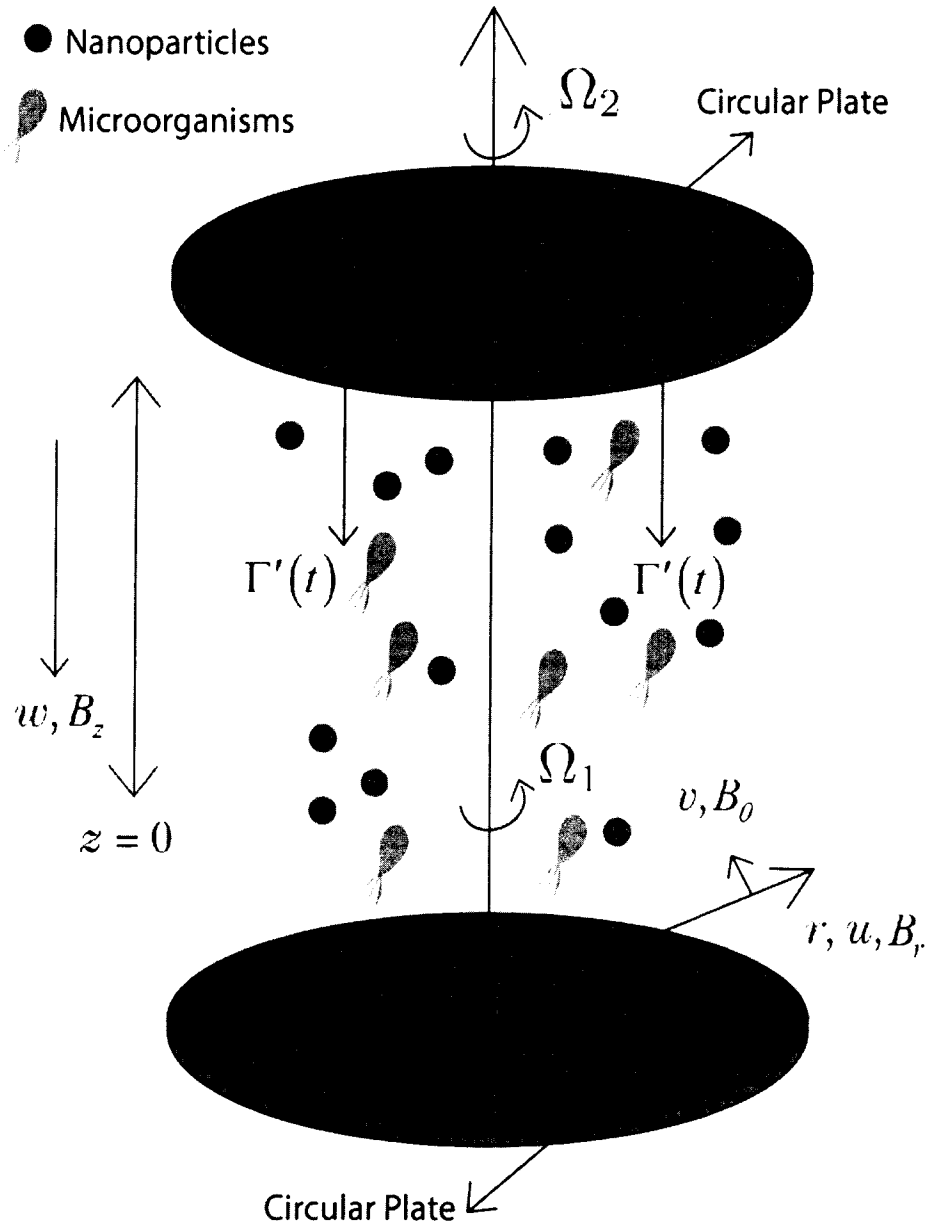

Figure 7.1: A physical structure for Nano fluid flow between parallel circular plates in the existence of motile gyrotactic microorganisms and induced MHD.

Rheological Model for Reiner-Rivlin Fluid fluid

The constitutive equation of Reiner-Rivlin fluid flow is defined as

$$\tau_{ij} = -p\delta_{ij} + \mu e_{ij} + \mu_c e_{ik} e_{kj}, \quad e_{jj} = 0 \tag{7.1}$$

where, τ_{ij} represents stress tensor, p denotes pressure, μ denotes the viscosity

coefficient, μ_c denotes cross-viscosity coefficient, δ_{ij} denotes Kroenke symbol, and deformation rate tensor is represented by $e_{ij} = \left(\partial u_i / \partial x_j\right) + \left(\partial u_j / \partial x_i\right)$. Components of deformation rate tensor are

$$\begin{aligned} &e_{rr} = 2\frac{\partial v_r}{\partial r},\ e_{\theta\theta} = 2\frac{v_r}{r},\ e_{zz} = 2\frac{\partial v_z}{\partial r},\ e_{r\theta} = e_{\theta r} = r\frac{\partial}{\partial r}\left(\frac{v_\theta}{r}\right) = \frac{\partial v_\theta}{\partial r} - \frac{v_\theta}{r}, \\ &e_{z\theta} = e_{\theta z} = \frac{\partial}{\partial z}v_\theta,\ e_{rz} = e_{zr} = \frac{\partial}{\partial z}v_r + \frac{\partial}{\partial \theta}v_z. \end{aligned} \tag{7.2}$$

Assuming the above-mentioned Reiner-Rivlin fluid model, the proposed governing equations for continuity and momentum in direction of r, θ, z read as

$$\frac{1}{r}\frac{\partial}{\partial r}(rv_r) + \frac{1}{r}\frac{\partial v_\theta}{\partial \theta} + \frac{\partial v_z}{\partial z} = 0 \tag{7.3}$$

$$\begin{aligned} \rho\left(\frac{\partial v_r}{\partial t} + v_r\frac{\partial v_r}{\partial r} + \frac{v_\theta}{r}\frac{\partial v_r}{\partial \theta} + v_z\frac{\partial v_r}{\partial z} - \frac{v_\theta}{r}\right) &= -\frac{\partial p}{\partial r} \\ &+ \frac{1}{r}\frac{\partial}{\partial r}(r\tau_{rr}) + \frac{1}{r}\frac{\partial \tau_{r\theta}}{\partial \theta} - \frac{\tau_{\theta\theta}}{r} + \frac{\partial \tau_{rz}}{\partial z} - B_z\frac{\partial B_r}{\partial z} - B_\theta\frac{\partial B_\theta}{\partial z}, \end{aligned} \tag{7.4}$$

$$\begin{aligned} \rho\left(\frac{\partial v_\theta}{\partial t} + v_r\frac{\partial v_\theta}{\partial r} + \frac{v_\theta}{r}\frac{\partial v_\theta}{\partial \theta} + v_z\frac{\partial v_\theta}{\partial z} - \frac{v_r v_\theta}{r}\right) &= -\frac{1}{r}\frac{\partial p}{\partial \theta} \\ &+ \frac{1}{r}\frac{\partial}{\partial \theta}\tau_{\theta\theta} + \frac{1}{r^2}\frac{\partial}{\partial r}(r^2\tau_{r\theta}) + \frac{\partial \tau_{\theta z}}{\partial z} - \frac{\partial B_\theta}{\partial z}B_z - \frac{\partial B_\theta}{\partial \theta}B_r, \end{aligned} \tag{7.5}$$

$$\begin{aligned} \rho\left(\frac{\partial v_z}{\partial t} + v_r\frac{\partial v_z}{\partial r} + \frac{v_\theta}{r}\frac{\partial v_z}{\partial \theta} + v_z\frac{\partial v_z}{\partial z}\right) &= -\frac{\partial p}{\partial z} \\ &+ \frac{\partial \tau_{zz}}{\partial z} + \frac{1}{r}\frac{\partial (r\tau_{rz})}{\partial r}(r\tau_{rz}) + \frac{1}{r}\frac{\partial \tau_{\theta z}}{\partial \theta} - \frac{\partial B_\theta}{\partial z}B_\theta + \frac{\partial B_r}{\partial z}B_r, \end{aligned} \tag{7.6}$$

where

$$\tau_{rr} = -p + 2\mu\frac{\partial u}{\partial r} + \mu_c\left[4\left(\frac{\partial u}{\partial r}\right)^2 + \left(\frac{\partial v}{\partial r} - \frac{v}{r}\right)^2 + \left(\frac{\partial u}{\partial z} + \frac{\partial w}{\partial r}\right)^2\right]$$

$$\tau_{r\theta} = \mu\left(\frac{\partial v}{\partial r} - \frac{v}{r}\right) + \mu_c\left[2\left(\frac{\partial u}{\partial r}\right)\left(\frac{\partial v}{\partial r} - \frac{v}{r}\right) + \left(\frac{\partial v}{\partial r} - \frac{v}{r}\right)\left(2\frac{u}{r}\right) + \left(\frac{\partial v}{\partial z}\right)\left(\frac{\partial u}{\partial z} + \frac{\partial w}{\partial r}\right)\right]$$

$$\tau_{rz} = \mu\left(\frac{\partial u}{\partial z} + \frac{\partial w}{\partial r}\right) + \mu_c\left[2\left(\frac{\partial u}{\partial r}\right)\left(\frac{\partial u}{\partial z} + \frac{\partial w}{\partial r}\right) + \left(\frac{\partial v}{\partial r} - \frac{v}{r}\right)\left(\frac{\partial v}{\partial z}\right) + 2\left(\frac{\partial w}{\partial z}\right)\left(\frac{\partial u}{\partial z} + \frac{\partial w}{\partial r}\right)\right]$$

$$\tau_{\theta\theta} = \mu\left(2\frac{u}{r}\right) + \mu_c\left[\left(\frac{\partial v}{\partial r} - \frac{v}{r}\right)^2 + 4\left(\frac{u}{r}\right)^2 + \left(\frac{\partial v}{\partial z}\right)^2\right]$$

$$\tau_{\theta z} = \tau_{z\theta} = \mu\left(\frac{\partial v}{\partial z}\right) + \mu_c\left[\left(\frac{\partial v}{\partial r} - \frac{v}{r}\right)\left(\frac{\partial u}{\partial z} + \frac{\partial w}{\partial r}\right) + 2\left(\frac{\partial v}{\partial z}\right)\left(\frac{u}{r} + \frac{\partial w}{\partial z}\right)\right]$$

The equation of Magnetic field is

$$\frac{1}{r}\frac{\partial}{\partial r}(rB_r) + \frac{1}{r}\frac{\partial B_\theta}{\partial \theta} + \frac{\partial B_z}{\partial z} = 0 \tag{7.7}$$

$$\frac{\partial B_r}{\partial t} + v_r\frac{\partial B_r}{\partial r} + v_\theta\frac{\partial B_r}{\partial \theta} + v_z\frac{\partial B_r}{\partial z} = -\frac{\partial}{\partial z}(v_r B_z - v_z B_r) + \frac{1}{\delta\mu_2}\left(\frac{\partial^2 B_r}{\partial z^2}\right) \tag{7.8}$$

$$\frac{\partial B_\theta}{\partial t} + v_r\frac{\partial B_\theta}{\partial r} + v_\theta\frac{\partial B_\theta}{\partial \theta} + v_z\frac{\partial B_\theta}{\partial z} = \frac{\partial}{\partial r}(v_r B_\theta - v_\theta B_r) - \frac{\partial}{\partial z}(v_\theta B_z - B_\theta v_z) + \frac{1}{\delta\mu_2}\left(\frac{\partial^2 B_\theta}{\partial z^2}\right) \tag{7.9}$$

$$\frac{\partial B_z}{\partial t} + v_r\frac{\partial B_z}{\partial r} + v_\theta\frac{\partial B_z}{\partial \theta} + v_z\frac{\partial B_z}{\partial z} = \frac{\partial}{\partial t}(v_r B_z - v_z B_r) + \frac{1}{\delta\mu_2}\left(\frac{\partial^2 B_z}{\partial z^2}\right). \tag{7.10}$$

The energy equation reads as

$$\frac{\partial T}{\partial t} + v_r\frac{\partial T}{\partial r} + v_z\frac{\partial T}{\partial z} = \frac{\bar{k}}{(\rho c)_f}\frac{\partial^2 T}{\partial z^2} - \frac{1}{(\rho c)_f}\left(\frac{\partial q_r}{\partial r}\right) + \frac{(\rho c)_p}{(\rho c)_f}\left[D_B\left(\frac{\partial T}{\partial r}\frac{\partial C}{\partial r} + \frac{\partial T}{\partial z}\frac{\partial C}{\partial z}\right) + \frac{D_T}{T_u}\left[\left(\frac{\partial T}{\partial r}\right)^2 + \left(\frac{\partial T}{\partial z}\right)^2\right]\right]. \tag{7.11}$$

In accordance with Roseland approximation radiation heat flux, which is unidirectional (acting axially) takes the form, $q_r = -\frac{4\sigma_e}{3\beta_r}\frac{\partial T^4}{\partial r}$, in which σ_e represents the Stefan–Boltzmann constant and β_r represents the mean absorption coefficient, respectively.

The equation of nanoparticle concentration reads as

$$\frac{\partial C}{\partial t} + v_r\frac{\partial C}{\partial r} + v_z\frac{\partial C}{\partial z} = D_B\frac{\partial^2 C}{\partial z^2} + \frac{D_T}{T_u}\frac{\partial^2 T}{\partial z^2} - k_r^2(C - C_\infty)\left(\frac{T}{T_\infty}\right)^{\bar{n}} e^{-\frac{E_a}{\kappa T}}, \tag{7.12}$$

Where k_r^2 is reaction rate, $\bar{n}$ is rate constant, κ is Boltzmann constant, and E_a is the activation energy.

The microorganism conservation equation reads as

$$\frac{\partial n}{\partial t}+v_r\frac{\partial n}{\partial r}+v_\theta\frac{\partial n}{\partial \theta}+v_z\frac{\partial n}{\partial z}+\frac{\bar{b}W_{mo}}{C_l-C_u}\left[\frac{\partial}{\partial z}\left(n\frac{\partial C}{\partial z}\right)\right]=D_{mo}\left(\frac{\partial^2 n}{\partial z^2}\right). \tag{7.13}$$

The corresponding boundary conditions are

$$v_r=0, v_\theta=\Omega_1 r\frac{D^2}{\Gamma^2(t)}, v_z=0, B_z=B_\theta=0, n=n_l, T=T_l, C=C_l, \text{ at } z=0, \tag{7.14}$$

$$\left.\begin{aligned} &v_r=0, v_\theta=\Omega_2 r\frac{D^2}{\Gamma^2(t)}, B_0=N_0 r\frac{D^2}{\Gamma^2(t)}, B_z=-\frac{\alpha D M_0}{\Gamma(t)},\\ &C=C_u, T=T_u, n=n_u, v_z=-\frac{\alpha D^2}{2\Gamma(t)}, \end{aligned}\right\} \text{ at } z=\Gamma(t). \tag{7.15}$$

7.3 Similarity Transformations

Substituting similarity transformation of chapter five, and using component form of Reiner-Rivlin fluid model in above mentioned governing equations, the following nonlinear, coupled ordinary differential equations (ODE's) with independent variable η are obtained,

$$f^{(iv)}=4R_Q\left[3f''-2\left(\frac{R_\Omega}{S_Q}\right)^2 gg'+2F_T^2\left(mm'''+m'm''\right)-\left(2f-\eta\right)f'''+2F_A^2\left(\frac{R_\Omega}{S_Q}\right)^2 nn'\right]$$
$$-4K\left[\frac{2R_\Omega}{R_Q}g'g''+\frac{R_Q}{R_\Omega}\left[2f'f'''+2\left(f'f'''+ff^{iv}\right)\right]\right] \tag{7.16}$$

$$g''=2S_Q{}^2\left[2g+\eta g'+2gf'-fg'+2F_AF_T\left(mn'+nm'\right)\right]-2K\left[g'(\eta)f''(\eta)-f'(\eta)g''(\eta)\right], \tag{7.17}$$

$$m''=\mathrm{Re}_M\left[m+\eta m'+2mf'-2fm'\right], \tag{7.18}$$

$$n''=\mathrm{Re}_M\left[2n-fn'+\eta n'+2\left(\frac{F_A}{F_T}\right)mg'\right], \tag{7.19}$$

$$\left(1+\frac{4}{3}R_d(1+(T_r-1)\theta)^3\right)\theta''+4Rd(T_r-1)(1+(T_r-1)\theta)^2\theta'^2+S_QP_tf\theta'+T_t\theta'^2+T_b\theta'\phi'=0, \tag{7.20}$$

$$\phi'' + \frac{T_t}{T_b}\theta'' + S_Q S_M f\phi' - S_M \sigma(1+\tilde{\delta}\theta)^{\bar{n}} \exp\left(-\frac{E}{1+\tilde{\delta}\theta}\right)\phi = 0, \tag{7.21}$$

$$\chi'' - S_Q B_s\left(\frac{\eta}{2}\right)\chi' + B_s S_Q f\chi' - P_l\left[\chi'\phi' + (\chi+\Phi)\phi''\right] = 0. \tag{7.22}$$

Where $K = \frac{\mu_c \Omega}{\mu}$ the material parameter of Reiner-Rivlin fluid, $R_d = \frac{4T_u^3\sigma_e}{\beta_r k}$ is radiation parameter.

The boundary conditions said in Eqs. (7.14)- (7.15) reduced as

$$\begin{cases} f'(0)=0, f(0)=0, m(0)=0, g(0)=1, n(0)=1, \theta(0)=1, \chi(0)=1, \phi(0)=1, \\ f(1)=\frac{1}{2}, m(1)=1, g(1)=\dot{\xi}, n(1)=1, \theta(1)=0, \phi(1)=0, \chi(1)=0. \end{cases} \tag{7.23}$$

7.4 Solution Methodolgy

The dimensionless Eqs. (7.16)-(7.22) generated using the similarity transformation and then solved using DTM by using the boundary conditions mentioned in Eq. (7.23). Substituting Differential transformations given in Eqs. (1.1)-(1.11),in which $F(q), G(q), M(q), N(q), \Theta(q), \Phi(q)$ and $X(q)$ are transformed function of $f(\eta), g(\eta), m(\eta), n(\eta), \theta(\eta), \phi(\eta)$ and $\chi(\eta)$ respectively and are expressed as

$$f(\eta) = \sum_{q=0}^{\infty} F(q)\eta^q, \tag{7.24}$$

$$g(\eta) = \sum_{q=0}^{\infty} G(q)\eta^q, \tag{7.25}$$

$$m(\eta) = \sum_{q=0}^{\infty} M(q)\eta^q, \tag{7.26}$$

$$n(\eta) = \sum_{q=0}^{\infty} N(q)\eta^q, \tag{7.27}$$

$$\theta(\eta) = \sum_{q=0}^{\infty} \Theta(q)\eta^q, \tag{7.28}$$

$$\phi(\eta) = \sum_{q=0}^{\infty} \Phi(q)\eta^q, \tag{7.29}$$

$$\chi(\lambda)=\sum_{l=0}^{\infty}\mathrm{X}(q)\eta^{q}. \tag{7.30}$$

By applying differential transform on corresponding boundary conditions, we obtained

$$\left.\begin{array}{lllll} F(0)=0, & F(1)=\frac{1}{2}, & G(0)=1, & M(0)=0, & N(0)=0, \\ \Theta(0)=1, & \Phi(0)=0, & \mathrm{X}(0)=0, & F(2)=\Pi_1, & F(3)=\Pi_2, \\ G(1)=\Pi_3, & M(1)=\Pi_4, & N(1)=\Pi_5, & \Theta(1)=\Pi_6, & \Phi(1)=\Pi_6, \\ \mathrm{X}(1)=\Pi_8 & & & & \end{array}\right\} \tag{7.31}$$

where Π_e $(e=1,\ldots,8)$ are the constants. Substituting transformations given in Eqs. (1.11) -(1.18) into Eqs. (7.16) -(7.22), and solve with support of associated boundary conditions shown in Eq. (7.31), The resulting solutions in the form of series are:

$$F(\eta)=f_1\eta^2+f_2\eta^3+f_3\eta^4+f_4\eta^5+\ldots, \tag{7.32}$$

$$G(\eta)=1-g_1\eta+g_2\eta^2+g_3\eta^3+g_4\eta^4+\ldots, \tag{7.33}$$

$$M(\eta)=m_1\eta+m_2\eta^3+m_3\eta^4+m_4\eta^5+\ldots, \tag{7.34}$$

$$N(\eta)=n_1\eta+n_2\eta^3+n_3\eta^4+n_4\eta^5+\ldots, \tag{7.35}$$

$$\Theta(\eta)=1+\theta_1\eta+\theta_2\eta^2+\theta_3\eta^3+\theta_4\eta^4+\ldots, \tag{7.36}$$

$$\Phi(\eta)=1+\phi_1\eta+\phi_2\eta^2+\phi_3\eta^3+\phi_4\eta^4+\ldots, \tag{7.37}$$

$$\mathrm{X}(\eta)=1+\chi_1\eta+\chi_2\eta^2+\chi_3\eta^3+\chi_4\eta^4+\ldots, \tag{7.38}$$

where, $f_i, g_i, m_i, n_i, \theta_i, \phi_i\ \chi_i$; where $i=(1,2,3,\ldots)$ are constants, and it isn't easy to express them here because of their complex and long numerical values. With the assistance of Mathematica computational software, the equation as mentioned above is solved with 30 iterations. However, it failed to an obtained a reasonable rate of convergence. The convergence rate of certain sequences can be improved with certain techniques. Many researchers used the Padé technique, which was used in the form of a rational fraction, i.e., ratio of two polynomials. The results obtained by DTM, owing to the non-linearity on the governing equations, don't satisfy the boundary conditions

at infinity without applying the Padé approximation. The obtained solution by DTM must then be merged with Padé-approximation, which gives a substantial rate of convergence at infinity. According to one's desired exactness, a higher order of approximation is required. Here, $[5\times5]$ order approximation is applied to Eqs. (7.32) - (7.38), the Padé approximants are as follows.

$$f(\eta)=\frac{1.74424\eta^2-6.38470\eta^3+7.80094\eta^4-2.87313\eta^5+\ldots}{1-2.7754\eta+1.79896\eta^2+0.61264\eta^3-0.04754\eta^4-0.00180\eta^5+\ldots} \quad (7.39)$$

$$g(\eta)=\frac{1-0.46193\eta-0.480814\eta^2-0.03002\eta^3-0.03650\eta^4-0.00872\eta^5+\ldots}{1+0.58051\eta+0.11070\eta^2+0.01490\eta^3+0.00398\eta^4+0.00361\eta^5+\ldots} \quad (7.40)$$

$$m(\eta)=\frac{0.70658\eta-0.05229\eta^2-0.04539\eta^3+0.27273\eta^4-0.32296\eta^5+\ldots}{1-0.07400\eta-0.39757\eta^2+0.11995\eta^3-0.06098\eta^4-0.02778\eta^5+\ldots} \quad (7.41)$$

$$n(\eta)=\frac{0.76783\eta+1.04601\eta^2+0.36514\eta^3+0.42917\eta^4+0.17107\eta^5+\ldots}{1+1.36229\eta+0.03949\eta^2+0.25479\eta^3+0.34003\eta^4-0.21240\eta^5+\ldots} \quad (7.42)$$

$$\theta(\eta)=\frac{1-0.79454\eta-0.24048\eta^2+0.05322\eta^3-0.03268\eta^4+0.01440\eta^5+\ldots}{1.0+0.03887\eta-0.03523\eta^2+0.05099\eta^3-0.03359\eta^4+0.00129\eta^5+\ldots} \quad (7.43)$$

$$\phi(\eta)=\frac{1-1.71536\eta+0.56035\eta^2+0.39145\eta^3-0.35448\eta^4+0.11937\eta^5+\ldots}{1+0.21714\eta-0.06871\eta^2+0.04708\eta^3-0.04350\eta^4-0.00830\eta^5+\ldots} \quad (7.44)$$

$$\chi(\eta)=\frac{1-0.77689\eta+0.66204\eta^2-0.78526\eta^3+0.09975\eta^4-0.19373\eta^5+\ldots}{1+2.48769\eta+2.46292\eta^2+1.10065\eta^3+0.13428\eta^4-0.03765\eta^5+\ldots} \quad (7.45)$$

7.5 Graphical and Tabular Result

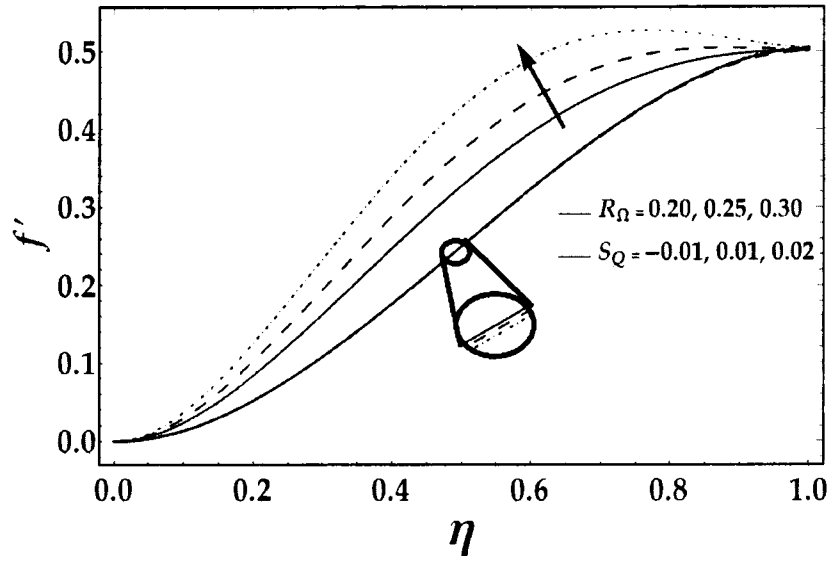

Figure 7.2: Implications of S_Q and R_Ω on velocity distribution (axial) $f'(\eta)$.

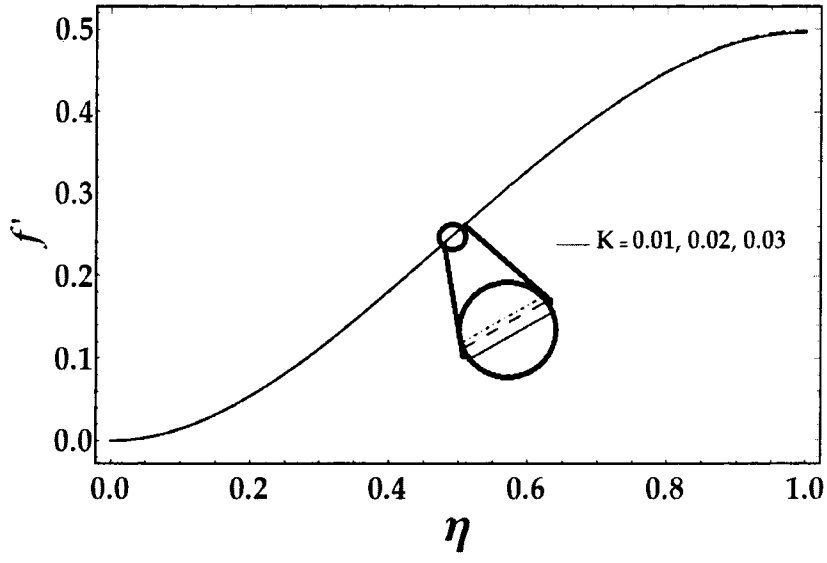

Figure 7.3: Implications of K on velocity distribution (axial) $f'(\eta)$.

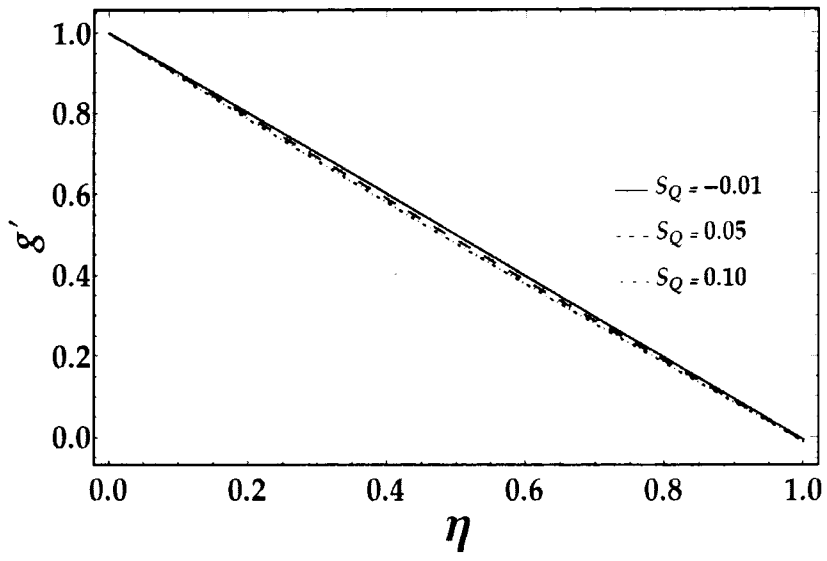

Figure 7.4: Implications of S_Q on velocity distribution (tangential) $g'(\eta)$.

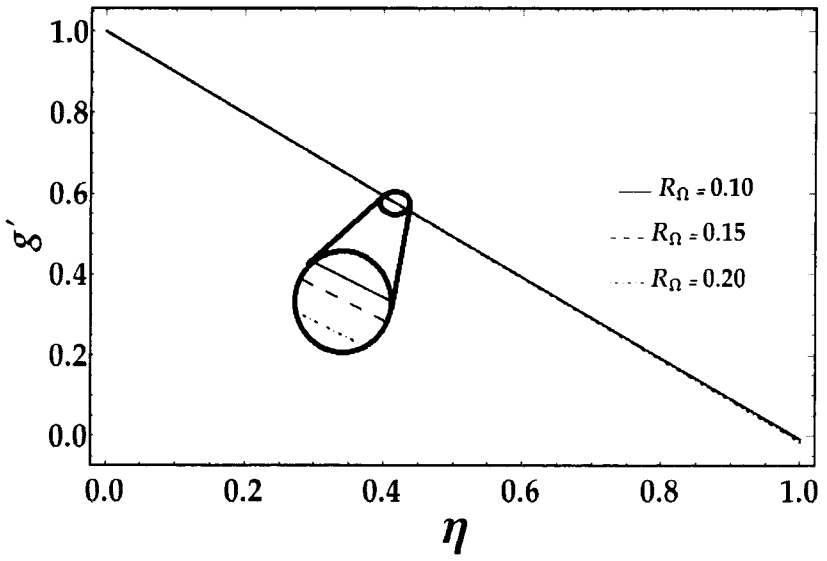

Figure 7.5: Implications of R_Ω on velocity distribution (tangential) $g'(\eta)$.

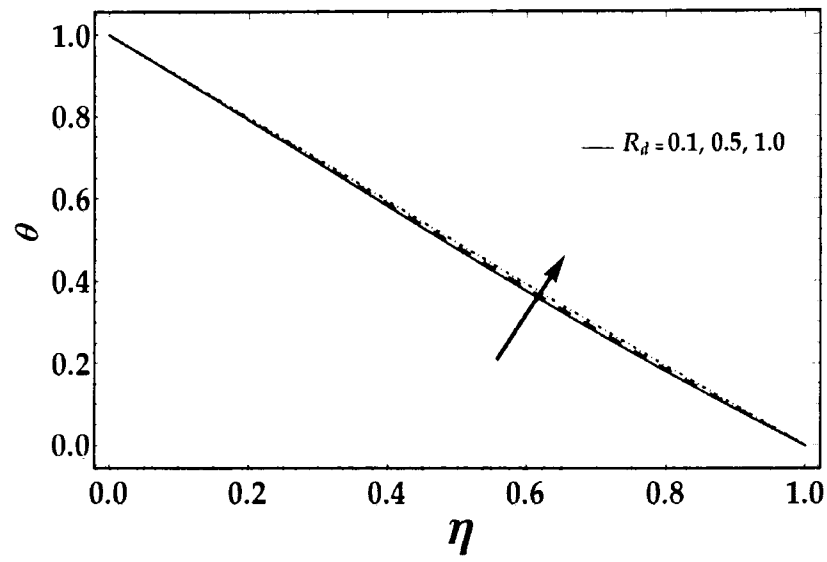

Figure 7.6: Implications of R_d, on temperature function $\theta(\eta)$

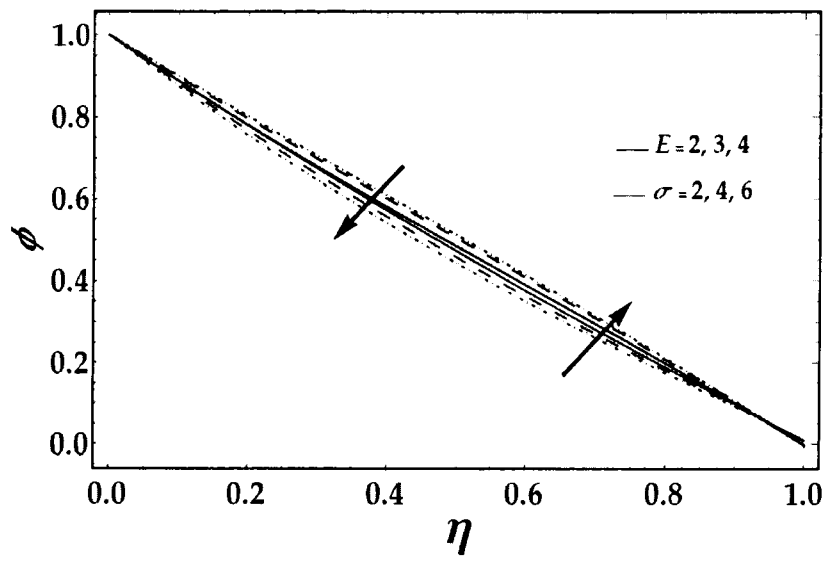

Figure 7.7: Implications of E, σ on concentration function $\phi(\eta)$.

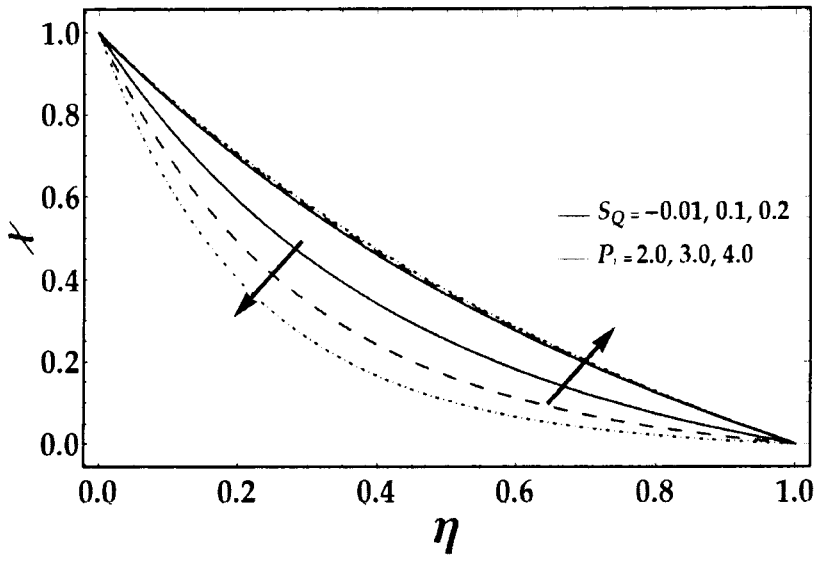

Figure 7.8: Implications of S_Q, P_l on motile microorganism density function $\chi(\eta)$.

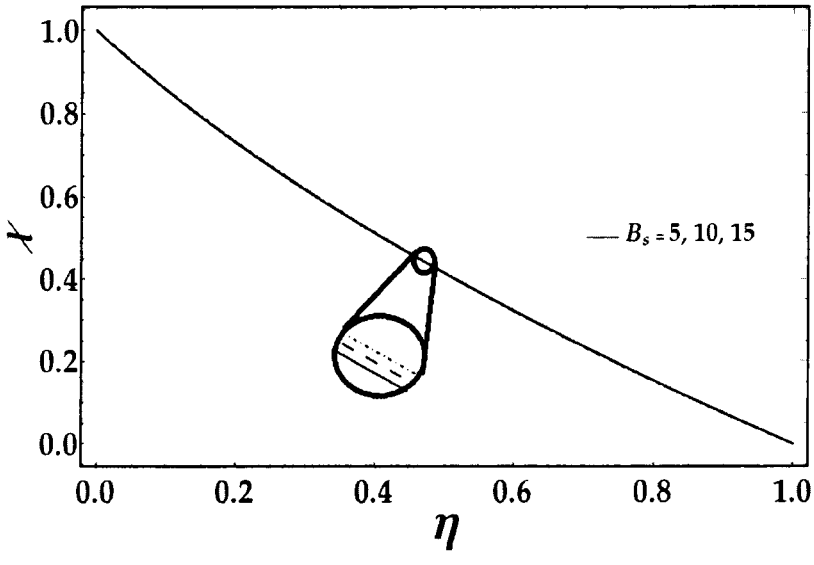

Figure 7.9: Implications of B_s on motile microorganism density function $\chi(\eta)$.

Table 7.1: Comparison of the torque values at the lower and upper plate with previous results [115] when the fluid behaves as Newtonian model $(K = 0)$ and the remaining values are $R_\Omega = 0.3, F_T = 0.5, Bt = 0.6, K = 0, R_d = 0, \sigma = 0$ for various values of S_Q and R_Ω.

	$\frac{dg(0)}{d\eta}$		$\frac{dg(1)}{d\eta}$	
S_Q	**Zhang et al. [115]**	**Present results**	**Zhang et al. [115]**	**Present results**
0.1	-1.0929372214309236	-1.0929372214309236	-0.948663684660318	-0.948663684660318
0.2	-1.180889912821983	-1.180889912821983	-0.9013607839508947	-0.9013607839508947
R_Ω				
0.1	-1.265492575299778	-1.265492575299778	-0.8533000683642988	-0.8533000683642988
0.2	-1.2652748717875888	-1.2652748717875888	-0.8549052425970227	-0.8549052425970227

Table 7.2: Analysis of Nusselt number $\theta'(0)$, for multiple values T_t, T_b, P_t, S_Q by DTM-Padé$[5\times5]$.

				$K=0$	$K=1$
T_t	T_b	P_t	S_Q	**DTM-Padé**	
0.03	0.01	6.8	0.05	-0.8944762272711257	-0.8944824906474336
0.06				-0.8063777250952755	-0.806383306245722
0.09				-0.7253079370829076	-0.7253128728932438
0.05	0.2			-0.37080900827594065	-0.37081139690286175
	0.3			-0.2316716738652042	-0.23167310222667004
	0.4			-0.1411942252519443	-0.14119505897571566
	0.01	4		-0.8998893435594736	-0.899893033465222
		7		-0.8304624112857932	-0.8304683534204742
		10		-0.7656313391774631	-0.7656391365026328
		6.8	-0.01	-0.8068399501595973	-0.8068414709109244
			0.05	-0.8334251602591399	-0.8334257278827505
			0.10	-0.8553872157158188	-0.8553910187144096

Table 7.3: Analysis of Sherwood number $\phi'(0)$ for various values $T_t, T_b, S_Q, S_M, E, \sigma$ by DTM-Padé [5×5]

						$K=0$	$K=0.1$
T_t	T_b	S_Q	S_M	E	σ	**DTM-Padé**	**DTM-Padé**
0.03	0.01	0.05	1	1	1	-1.423723583572087	-1.4237062656685955
0.06						-2.242251830648612	-2.24222066465715
0.09						-3.52021034762737	-3.5201695528198456
0.05	0.01					-1.915474205493601	-1.9154471661812198
	0.02					-1.5921974868312598	-1.5921851742637334
	0.03					-1.4831389820481062	-1.4831315689992728
	0.01	-0.01				-2.0517295527621053	-2.0517273504948057
		0.05				-1.9367842616882913	-1.9268295351904132
		0.10				-1.832060050336652	-1.8320099157048728
		0.05	2			-2.0146398467429014	-2.0241644922138637
			4			-2.2012470588694386	-2.2102937724970664
			6			-2.3744735466373146	-2.3831035839166357
			1	2		-1.8531063430623982	-1.8630765987997622
				3		-1.829718893888726	-1.8397573168178392
				4		-1.821048746320453	-1.8311125640363681
				1	2	-2.01093920918129	-2.020462840246665
					4	-2.19121593549506	-2.2002581288517207
					6	-2.359245916149752	-2.367866612938209

Table 7.4: Analysis of $\chi'(0)$ for various values of S_Q, B_s, P_l by DTM-Padé [5×5]

			$K=0$	$K=0.1$
S_Q	B_s	P_l	**DTM-Padé**	**DTM-Padé**
-0.01	1	1	-2.5484740630681886	-2.5484721652641165
0.05			-2.4422867164206274	-2.442278141197654
0.10			-2.3326945059751685	-2.3545141881576237
0.05	5		-2.4315407355757515	-2.4315225967036653
	10		-2.4300912988489185	-2.430083525231539
	15		-2.4286396339889302	-2.4286422222719586
	1	0.5	-1.6814808605966678	-1.6814680934795112
		1.0	-2.432698678642556	-2.4326722455225793
		1.5	-3.2408290233020116	-3.2407890961974375

Table 7.5: Numerical computations of Torque at a fix circular and upper circular plates by DTM- Padé [5×5] for various values of Squeezing Reynolds Number S_Q.

	$\frac{dg(0)}{d\eta}$		$\frac{dg(1)}{d\eta}$	
S_Q	$K=0$	$K=0.1$	$K=0$	$K=0.1$
0.1	-1.0944523632334688	-1.0885716574469078	-0.9499690408077309	-0.9876461173721226
0.2	-1.1811908734455248	-1.1746346120145237	-0.9071760445081409	-0.9777866647632717

Table 7.6: Numerical computations of Torque at a fix circular and upper circular plates by DTM- Padé [5×5] for multiple values of Rotational Reynolds Number R_Ω.

	$\frac{dg(0)}{d\eta}$		$\frac{dg(1)}{d\eta}$	
R_Ω	$K=0$	$K=0.1$	$K=0$	$K=0.1$
0.1	-1.0470698634685973	-1.0416647863739605	-0.9735621738611226	-0.9805868144292514
0.2	-1.047887492344034	-1.0424472521086106	-0.9736078836468506	-0.9885069828641508

7.6 Discussion

In this segment, graphical and numerical analysis is made on the solutions of resulting nonlinear ordinary differential equations mentioned in Eqs. (7.16)-(7.22). The differential transformation scheme is applied to present the solutions of the foregoing equations. Our principal focus is to inspect the physical characteristics of numerous physical parameters in the momentum equation, induced MHD equations, temperature distribution, motile microorganism density function, and mass transfer equation. For instance, the influence of squeezing and Rotational Reynolds number S_Q, R_Ω Reiner-Rivlin fluid parameter K, Brownian motion T_b, magnetic Reynolds number Re_M, Prandtl number P_t, thermophoresis parameter T_t, Schmidt number S_M, bioconvection number B_s, and Péclet number Pe are examined.

Velocity Distribution

Figures (7.2-7.3) illustrate the influence on velocity profile in the axial direction because of the squeezed Reynolds number S_Q, rotational Reynolds number R_Ω,

and the material parameter of Reiner-Rivlin fluid K. From figure (7.2), one can perceive that increasing the squeezed Reynolds number S_Q axial velocity decreases but increasing rotational Reynolds number R_Ω, the axial velocity profile increases. The physical reason behind this when we increase the value of Squeezing Reynolds number S_Q, the distance between the plates increases, so fluid velocity decreases, and fluid accelerates by rotation of plate when we increase the values of rotational Reynolds number R_Ω. Figure (7.3) depicts that increasing values of the material parameter of Reiner-Rivlin fluid the velocity distribution against axial direction increases.

Figures (7.4)-(7.5) depict the influence of squeezing Reynolds number S_Q and Rotational Reynolds Number R_Ω against tangential velocity distribution. From figure (7.4), it can be ascertained that by enhancing the values of the squeezed Reynolds number S_Q, tangential velocity distribution decreases. Similar phenomena are observed in figure (7.5) i.e., by increasing values of rotational Reynolds number, tangential velocity profile declines.

Temperature Distribution

The effects of radiation parameter R_d on temperature profile are shown in figure (7.6). It is observed that by enhancing the radiation parameter R_d the temperature profile increases. The physical reason behind this is an increase in radiation releases the heat energy from flow; hence there is an increase in temperature.

Concentration Distribution

Figure (7.7) deliberates the influence of reaction rate σ and activation energy E on the nanoparticle concentration. It may be observed that nanoparticle concentration displays a substantial rise by increasing values of E. Since high energy activation and low temperatures impart to a constant reaction rate, the

resulting chemical reaction is therefore slowed down. Consequently, the concentration of solute rises. On the other side, increasing values of σ the nanoparticle concentration decrease.

Motile Gyrotactic Microorganism Distribution

Figure (7.8) portrays the consequences of Péclet number Pe and squeezed Reynolds number S_Q on motile microorganism density function. One can experience that enhancing values of squeezed Reynolds number S_Q tends to boost the microorganism density function while increasing values of Péclet number Pe the motile microorganism density function diminishes. The reason behind this is that the diffusivity of the microorganism reduces, then the speed of the microorganism also decreases. This is the physical fact and resulting in the microorganism density function decreases while increasing the value of Péclet number Pe. Figure (7.9) is plotted to see the physical performance of the Bioconvection Schmidt number B_s. It apparent that enhancing values of bioconvection Schmidt number B_s, motile microorganism density function rises but the consequences are negligible.

Physical Quantities

Table (7.1) shows the numerical comparison with previous results of chapter 2 against the torque values at the upper and the lower plate by taking $K = 0, R_d = 0, \sigma = 0$ in the present results. It is found that the results obtained in the present study are not only correct but also converges rapidly. Furthermore, we can also say that the proposed methodology i.e. DTM-Padé shows promising results against the coupled nonlinear different equations. Tables (7.2-7.6) are developed for different physical parameters against Sherwood number, Nusselt number, and motile density function $\phi'(0), \theta'(0), \chi'(0)$. Moreover, the torque values at the lower plate $dg(0)/d\eta$, and upper plate $dg(1)/d\eta$ are also calculated numerically in these tables.

Chapter 8

Transport of Motile Gyrotactic Microorganism in a Sutterby Fluid between a Pair of Rotating Circular Plates

8.1 Introduction

In this chapter, we analyse unsteady flow confined by parallel circular disks filled with magnetized Sutterby fluid in the presence of nanoparticles and motile gyrotactic microorganism along with the effects of activation energy. The Differential Transformation Method (DTM) is used to obtain the solution of the set of non-linear Ordinary Differential Equations for the flow situation. The Padé approximation is merged with Differential Transformation Method (DTM) to attain the better convergence of coupled, non-linear ODE's. Torque effects on both plates i.e., lower, and upper disks are taken into consideration. The tabular and graphical results are showed to discuss the physical effects.

8.2 Mathematical Formulation

Flow Assumptions

To formulate the mathematical problem, following assumptions along with assumption of chapter 3 and 4 have been considered. Flow of magnetized viscoelastic Nano fluid saturating space between rotating and squeezing disks is modelled with

- Sutterby fluid as base fluid.

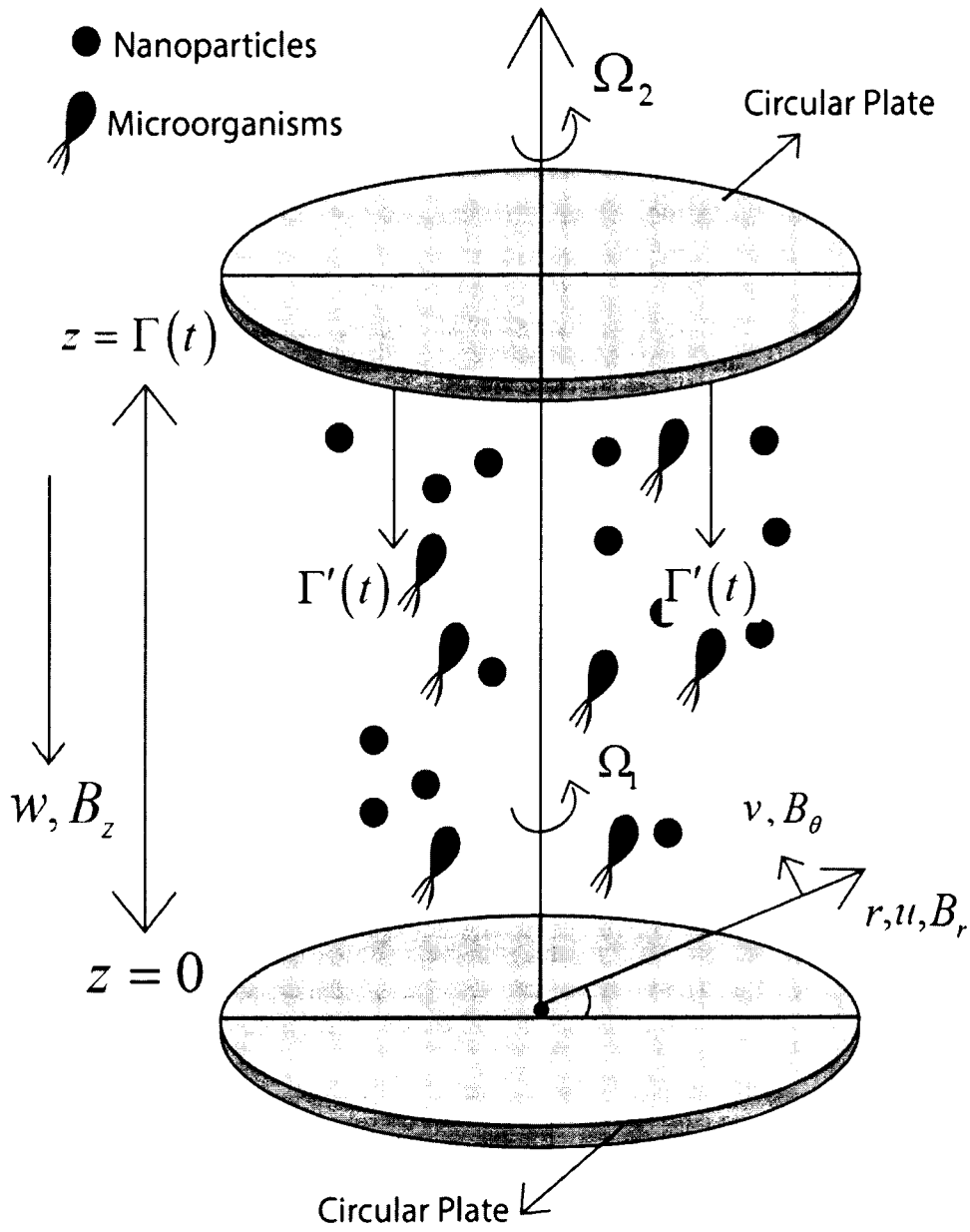

Figure 8.1: A physical structure for Nano fluid flow between parallel circular plates in the existence of motile gyrotactic microorganisms and induced MHD.

Rheological Model for Sutterby Fluid

The etxra stress tenson of sutterby fluid flow is written as

$$\tau = -pI + S, \tag{8.1}$$

where

$$S = \frac{\mu_0}{2}\left[\frac{\sinh^{-1}(\beta_1\gamma)}{\beta_1\gamma}\right]^n A_1.$$

Where τ signifies Cauchy stress tensor, μ_0 signifies viscosity at low share rate, γ signifies share rate, μ_∞ denotes infinity shear rate viscosity, S signifies extra stress tensor, A_1 represents first Rivlin-Erickson rate tensor and define as

$$A_1 = (gradV) + (gradV)^T, \tag{8.2}$$

$$\gamma = \sqrt{\sum_i \sum_j \gamma_{1i}\gamma_{1j}} = \sqrt{\frac{\Lambda}{2}}, \tag{8.3}$$

$$\Lambda = trace\left[(gradV) + (gradV)^T\right]^2. \tag{8.4}$$

By series expansion

$$\sin^{-1}(\beta_1\gamma) \cong \beta_1\gamma - \frac{(\beta_1\gamma)^3}{6}. \tag{8.5}$$

For the sutterby fluid model the viscoisty relation is expressed as

$$\mu = \frac{\mu_0}{2}\left[\frac{\sinh^{-1}(\beta_1\gamma)}{\beta_1\gamma}\right]^n. \tag{8.6}$$

After using Eq. (7.5)-(7.6), the viscosity relation for second order approximation is

$$\mu \cong \mu_0\left[1 - \frac{(\beta_1\gamma)^2}{6}\right]^n \cong \mu_0\left[1 - \frac{n(\beta_1\gamma)^2}{6}\right]. \tag{8.7}$$

This model behaves like visous fluid and Eyring model for various values of n i.e., for $n=0$, Eq. (8.7) reduces to $\mu \cong \mu_0$ (viscous fluid) and for $n=1$, Eq. (8.7) reduces to $\mu \cong \mu_0\left[1-\frac{(\beta_1\gamma)^2}{6}\right]$ which is known as Eyring model.

Assuming the above mentioned Sutterby fluid flow in MHD squeezed film, the continuity and momentum in direction of r,θ,z read as

$$\frac{1}{r}\frac{\partial}{\partial r}(rv_r)+\frac{1}{r}\frac{\partial}{\partial \theta}(v_\theta)+\frac{\partial}{\partial z}(v_z)=0, \tag{8.8}$$

$$\begin{aligned}&\rho\left(\frac{\partial v_r}{\partial t}+v_r\frac{\partial v_r}{\partial r}+\frac{v_\theta}{r}\frac{\partial v_r}{\partial \theta}+v_z\frac{\partial v_r}{\partial z}-\frac{v_\theta}{r}\right)=-\frac{\partial p}{\partial r}\\&+\frac{1}{r}\frac{\partial}{\partial r}(r\tau_{rr})+\frac{1}{r}\frac{\partial \tau_{r\theta}}{\partial \theta}-\frac{\tau_{\theta\theta}}{r}+\frac{\partial \tau_{rz}}{\partial z}-\frac{\partial B_r}{\partial z}B_z-\frac{\partial B_\theta}{\partial z}B_\theta,\end{aligned} \tag{8.9}$$

$$\begin{aligned}&\rho\left(\frac{\partial v_\theta}{\partial t}+v_r\frac{\partial v_\theta}{\partial r}+\frac{v_\theta}{r}\frac{\partial v_\theta}{\partial \theta}+v_z\frac{\partial v_\theta}{\partial z}-\frac{v_r v_\theta}{r}\right)=-\frac{1}{r}\frac{\partial p}{\partial \theta}\\&+\frac{1}{r}\frac{\partial \tau_{\theta\theta}}{\partial \theta}+\frac{1}{r^2}\frac{\partial (r^2\tau_{r\theta})}{\partial r}+\frac{\partial \tau_{\theta z}}{\partial z}-\frac{\partial B_\theta}{\partial z}B_z-\frac{\partial B_\theta}{\partial r}B_r,\end{aligned} \tag{8.10}$$

$$\begin{aligned}&\rho\left(\frac{\partial v_z}{\partial t}+v_r\frac{\partial v_z}{\partial r}+\frac{v_\theta}{r}\frac{\partial v_z}{\partial \theta}+v_z\frac{\partial v_z}{\partial z}\right)=-\frac{\partial p}{\partial z}\\&+\frac{1}{r}\frac{\partial}{\partial r}(r\tau_{rz})+\frac{1}{r}\frac{\partial \tau_{\theta z}}{\partial \theta}+\frac{\partial \tau_{zz}}{\partial z}-\frac{\partial B_\theta}{\partial z}B_\theta+\frac{\partial B_r}{\partial z}B_r,\end{aligned} \tag{8.11}$$

where

$$\tau_{rr}=\mu_0\left[1-\frac{n\beta_1^2\left(2\left(\frac{\partial v_r}{\partial r}\right)^2+\left(\frac{\partial v_r}{\partial z}\right)^2+\left(\frac{\partial v_\theta}{\partial z}\right)^2+\left(\frac{\partial v_\theta}{\partial r}-\frac{v_\theta}{r}\right)^2+2\left(\frac{v_r}{r}\right)^2\right)}{6}\right]2\frac{\partial v_r}{\partial r},$$

$$\tau_{r\theta}=\mu_0\left[1-\frac{n\beta_1^2\left(2\left(\frac{\partial v_r}{\partial r}\right)^2+\left(\frac{\partial v_r}{\partial z}\right)^2+\left(\frac{\partial v_\theta}{\partial z}\right)^2+\left(\frac{\partial v_\theta}{\partial r}-\frac{v_\theta}{r}\right)^2+2\left(\frac{v_r}{r}\right)^2\right)}{6}\right]\left(\frac{\partial v_\theta}{\partial r}-\frac{v_\theta}{r}\right),$$

$$\tau_{rz}=\mu_0\left[1-\frac{n\beta_1^2\left(2\left(\frac{\partial v_r}{\partial r}\right)^2+\left(\frac{\partial v_r}{\partial z}\right)^2+\left(\frac{\partial v_\theta}{\partial z}\right)^2+\left(\frac{\partial v_\theta}{\partial r}-\frac{v_\theta}{r}\right)^2+2\left(\frac{v_r}{r}\right)^2\right)}{6}\right]\frac{\partial v_r}{\partial z},$$

$$\tau_{\theta r}=\mu_0\left[1-\frac{n\beta_1^2\left(2\left(\frac{\partial v_r}{\partial r}\right)^2+\left(\frac{\partial v_r}{\partial z}\right)^2+\left(\frac{\partial v_\theta}{\partial z}\right)^2+\left(\frac{\partial v_\theta}{\partial r}-\frac{v_\theta}{r}\right)^2+2\left(\frac{v_r}{r}\right)^2\right)}{6}\right]\left(\frac{\partial v_\theta}{\partial r}-\frac{v_\theta}{r}\right),$$

$$\tau_{\theta\theta}=-p+\mu_0\left[1-\frac{n\beta_1^2\left(2\left(\frac{\partial v_r}{\partial r}\right)^2+\left(\frac{\partial v_r}{\partial z}\right)^2+\left(\frac{\partial v_\theta}{\partial z}\right)^2+\left(\frac{\partial v_\theta}{\partial r}-\frac{v_\theta}{r}\right)^2+2\left(\frac{v_r}{r}\right)^2\right)}{6}\right]2\left(\frac{v_r}{r}\right),$$

$$\tau_{\theta z}=\mu_0\left[1-\frac{n\beta_1^2\left(2\left(\frac{\partial v_r}{\partial r}\right)^2+\left(\frac{\partial v_r}{\partial z}\right)^2+\left(\frac{\partial v_\theta}{\partial z}\right)^2+\left(\frac{\partial v_\theta}{\partial r}-\frac{v_\theta}{r}\right)^2+2\left(\frac{v_r}{r}\right)^2\right)}{6}\right]\frac{\partial v_\theta}{\partial z},$$

$$\tau_{zr}=\mu_0\left[1-\frac{n\beta_1^2\left(2\left(\frac{\partial v_r}{\partial r}\right)^2+\left(\frac{\partial v_r}{\partial z}\right)^2+\left(\frac{\partial v_\theta}{\partial z}\right)^2+\left(\frac{\partial v_\theta}{\partial r}-\frac{v_\theta}{r}\right)^2+2\left(\frac{v_r}{r}\right)^2\right)}{6}\right]\frac{\partial v_r}{\partial z},$$

$$\tau_{z\theta}=\mu_0\left[1-\frac{n\beta_1^2\left(2\left(\frac{\partial v_r}{\partial r}\right)^2+\left(\frac{\partial v_r}{\partial z}\right)^2+\left(\frac{\partial v_\theta}{\partial z}\right)^2+\left(\frac{\partial v_\theta}{\partial r}-\frac{v_\theta}{r}\right)^2+2\left(\frac{v_r}{r}\right)^2\right)}{6}\right]\frac{\partial v_\theta}{\partial z},$$

$$\tau_{zz}=0,$$

The magnetic field equation in r,θ,z direction along with temperature, concentration of nanoparticle and conservation of microorganism read as

$$\frac{1}{r}\frac{\partial}{\partial r}(rB_r)+\frac{1}{r}\frac{\partial B_\theta}{\partial \theta}+\frac{\partial B_z}{\partial z}=0, \tag{8.12}$$

$$\frac{\partial B_r}{\partial t}+u\frac{\partial B_r}{\partial r}+v\frac{\partial B_r}{\partial \theta}+w\frac{\partial B_r}{\partial z}=-\frac{\partial}{\partial z}(v_r B_z-v_z B_r)+\frac{1}{\delta\mu_2}\left(\frac{\partial^2 B_r}{\partial z^2}\right), \tag{8.13}$$

$$\frac{\partial B_\theta}{\partial t}+u\frac{\partial B_\theta}{\partial r}+v\frac{\partial B_\theta}{\partial \theta}+w\frac{\partial B_\theta}{\partial z}=\frac{\partial}{\partial r}(v_r B_\theta-v_\theta B_r)-\frac{\partial}{\partial z}(v_\theta B_z-B_\theta v_z)+\frac{1}{\delta\mu_2}\left(\frac{\partial^2 B_\theta}{\partial z^2}\right), \tag{8.14}$$

$$\frac{\partial B_z}{\partial t}+u\frac{\partial B_z}{\partial r}+v\frac{\partial B_z}{\partial \theta}+w\frac{\partial B_z}{\partial z}=\frac{\partial}{\partial r}(v_r B_z-v_z B_r)+\frac{1}{\delta\mu_2}\left(\frac{\partial^2 B_z}{\partial z^2}\right), \tag{8.15}$$

$$\frac{\partial T}{\partial t}+v_r\frac{\partial T}{\partial r}+v_z\frac{\partial T}{\partial z}=\tilde{\alpha}\frac{\partial^2 T}{\partial z^2}+\tau\left[D_B\left(\frac{\partial T}{\partial r}\frac{\partial C}{\partial r}+\frac{\partial T}{\partial z}\frac{\partial C}{\partial z}\right)+\frac{D_T}{T_\infty}\left[\left(\frac{\partial T}{\partial r}\right)^2+\left(\frac{\partial T}{\partial z}\right)^2\right]\right]-\frac{1}{(\rho c)_f}\left(\frac{\partial q_r}{\partial r}\right), \tag{8.16}$$

$$\frac{\partial C}{\partial t}+v_r\frac{\partial C}{\partial r}+v_z\frac{\partial C}{\partial z}=D_B\frac{\partial^2 C}{\partial z^2}+\frac{D_T}{T}\frac{\partial^2 T}{\partial z^2}-k_r^2(C-C_\infty)\left(\frac{T}{T_\infty}\right)^{\bar{n}}\exp\left(-\frac{E_a}{1+\kappa T}\right), \tag{8.17}$$

$$\frac{\partial n}{\partial t}+v_r\frac{\partial n}{\partial r}+v_\theta\frac{\partial n}{\partial \theta}+v_z\frac{\partial n}{\partial z}+\frac{\bar{b}W_{mo}}{C_\infty}\left[\frac{\partial}{\partial z}\left(n\frac{\partial C}{\partial z}\right)\right]=D_{mo}\left(\frac{\partial^2 n}{\partial z^2}\right). \tag{8.18}$$

According to our assumptions the initial and boundary conditions for Eqs. (8.8)-(8.18) are

$$u=0, v=\Omega_1 r\frac{D^2}{\Gamma^2(t)}, w=0, B_z=B_\theta=0, C=C_f, T=T_f, n=n_f \quad \text{at} \quad z=0, \tag{8.19}$$

$$\begin{cases} u=0, v=\Omega_2 r\dfrac{D^2}{\Gamma^2(t)}, B_\theta=N_0 r\dfrac{D^2}{\Gamma^2(t)}, B_z=-\dfrac{\beta D M_0}{\Gamma(t)}, w=-\dfrac{\beta D^2}{2\Gamma(t)}, \\ T=T_u, C=C_u, n=n_u, \end{cases} \quad \text{at} \quad z=\Gamma(t). \tag{8.20}$$

8.3 Similarity Transformations

Substituting similarity transformation of chapter five, and using component form of Sutterby fluid model in above mentioned governing equations, the following nonlinear, coupled ordinary differential equations (ODE's) with independent variable η are obtained,

$$f^{(iv)} = \frac{4}{S_Q}\left[3f'' - 2\left(\frac{R_\Omega}{S_Q}\right)^2 gg' + 2F_T^2\left(mm''' + m'm''\right) - \left(2f - \eta\right)f''' + 2F_A^2\left(\frac{R_\Omega}{S_Q}\right)^2 nn'\right]$$

$$-\frac{4n\varepsilon^2}{S_Q}\left[\begin{array}{l}\dfrac{-1}{8S_Q}\left(2g'g''f' + g'^2f''\right) - \dfrac{S_Q}{2\,\mathrm{Re}}\left(f''^3 + 2ff'f''f'''\right) + \dfrac{\mathrm{Re}}{12R_\Omega S_Q}\left(g''^2f'' + g'g''f''' + g'f''g'''\right) \\ + \dfrac{S_Q}{6R_\Omega}\left(2f'f'''^2 + f''^2f^{iv}\right) + \dfrac{\mathrm{Re}}{24S_QR_\Omega}\left(f^{iv}g'^2 + 2g'g''f'''\right) + \dfrac{S_Q\,\mathrm{Re}}{8R_\Omega^{\,3}}\left(2f'f'''^2 + f''^2f^{iv}\right)\end{array}\right] \tag{8.21}$$

$$g''(\eta) = 2S_Q{}^2\left[2g + \eta g' + 2gf' - fg' + 2F_AF_T\left(mn' + nm'\right)\right]$$
$$-\frac{2S_Q{}^2n\varepsilon^2}{R_\Omega{}^2}\left[\frac{R_\Omega}{4S_Q{}^2}g'^2g'' - \frac{2}{3}f'g'f'' - \frac{1}{3}f'^2g'' + \frac{\mathrm{Re}}{12R_\Omega}\left(f'''^2g'' + g'f''f'''\right)\right] \tag{8.22}$$

$$m'' = \mathrm{Re}_M\left[m + \eta m' + 2mf' - 2fm'\right], \tag{8.23}$$

$$n'' = \mathrm{Re}_M\left[2n - fn' + \eta n' + 2\left(\frac{F_A}{F_T}\right)mg'\right], \tag{8.24}$$

$$\left(1 + \frac{4}{3}R_d\right)\theta'' + S_QP_rf\theta' + T_t\theta'^2 + T_b\theta'\phi' = 0, \tag{8.25}$$

$$\phi'' + \frac{T_t}{T_b}\theta'' + S_QS_Mf\phi' - S_M\sigma(1 + \delta\theta)^{\bar{n}}\exp\left(-\frac{E}{1 + \delta\theta}\right)\phi = 0, \tag{8.26}$$

$$\chi'' - S_QB_s\left(\frac{\eta}{2}\right)\chi' + B_sS_Qf\chi' - P_r\left[\chi'\phi' + (\chi + \Phi)\phi''\right] = 0. \tag{8.27}$$

Where $\varepsilon = \Omega_1\beta_1$ the material parameter of Sutterby fluid.

The boundary conditions said in Eqs (8.19) - (8.20) converted to

$$\begin{cases} f(0) = 0 = f'(0), g(0) = 1, m(0) = 0, n(0) = 1, \theta(0) = 1, \chi(0) = 1, \phi(0) = 1, \\ f(1) = \dfrac{1}{2}, g(1) = \dot{\xi}, m(1) = 1, n(1) = 1, \theta(1) = 0, \phi(1) = 0, \chi(1) = 0, \end{cases} \tag{8.28}$$

8.4 Solution Methodolgy

The dimensionless Eqs. (8.21)-(8.27) generated using the similarity transformation and then are solved using DTM using the boundary conditions mentioned in Eq. (8.28). Substituting Differential transformations mentioned in Eqs. (1.1)-(1.11),in

which $F(q), G(q), M(q), N(q), \Theta(q), \Phi(q)$ and $\mathrm{X}(q)$ are transformed function of $f(\eta), g(\eta), m(\eta), n(\eta), \theta(\eta), \phi(\eta)$ and $\chi(\eta)$ respectively and are expressed as

$$f(\eta) = \sum_{q=0}^{\infty} F(q)\eta^q, \tag{8.29}$$

$$g(\eta) = \sum_{q=0}^{\infty} G(q)\eta^q, \tag{8.30}$$

$$m(\eta) = \sum_{q=0}^{\infty} M(q)\eta^q, \tag{8.31}$$

$$n(\eta) = \sum_{q=0}^{\infty} N(q)\eta^q, \tag{8.32}$$

$$\theta(\eta) = \sum_{q=0}^{\infty} \Theta(q)\eta^q, \tag{8.33}$$

$$\phi(\eta) = \sum_{q=0}^{\infty} \Phi(q)\eta^q, \tag{8.34}$$

$$\chi(\eta) = \sum_{q=0}^{\infty} \mathrm{X}(q)\eta^q. \tag{8.35}$$

The differential transform of the corresponding boundary conditions are

$$\left.\begin{array}{lllll} F(0)=0, & F(1)=\frac{1}{2}, & G(0)=1, & M(0)=0, & N(0)=0, \\ \Theta(0)=1, & \Phi(0)=1, & \mathrm{X}(0)=1, & F(2)=\Pi_1, & F(3)=\Pi_2, \\ G(1)=\Pi_3, & M(1)=\Pi_4, & N(1)=\Pi_5, & \Theta(1)=\Pi_6, & \Phi(1)=\Pi_6, \\ \mathrm{X}(1)=\Pi_8 & & & & \end{array}\right\} \tag{8.36}$$

Substituting transformations given in Eqs. (1.1)-(1.11) into Eqs. (8.21)-(8.27), obtained solution with the aid of corresponding boundary conditions given in Eq. (8.36), The resulting series solution are:

$$F(\eta) = f_1\eta^2 + f_2\eta^3 + f_3\eta^4 + f_4\eta^5 + ..., \tag{8.37}$$

$$G(\eta)=1-g_1\eta+g_2\eta^2+g_3\eta^3+g_4\eta^4+..., \tag{8.38}$$

$$M(\eta)=m_1\eta+m_2\eta^3+m_3\eta^4+m_4\eta^5+..., \tag{8.39}$$

$$N(\eta)=n_1\eta+n_2\eta^3+n_3\eta^4+n_4\eta^5+..., \tag{8.40}$$

$$\theta(\eta)=1+\theta_1\eta+\theta_2\eta^2+\theta_3\eta^3+\theta_4\eta^4+..., \tag{8.41}$$

$$\phi(\eta)=1+\phi_1\eta+\phi_2\eta^2+\phi_3\eta^3+\phi_4\eta^4+..., \tag{8.42}$$

$$\chi(\eta)=1+\chi_1\eta+\chi_2\eta^2+\chi_3\eta^3+\chi_4\eta^4+..., \tag{8.43}$$

Where $f_i, g_i, m_i, n_i, \theta_i, \phi_i \chi_i; i(=1,2,3,...)$ is a set of fixed values that is difficult to show here. The above-mentioned equation by replacing the differential transformations is solved with 30 iterations using Mathematica software 12 version. However, a good rate of convergence was not achieved. Various approaches are available which can boost the convergence rate of certain sequences. Many researchers employed the Padé approach, which is defined as the ratio of two polynomials, i.e., the rational fractional form. Due to the non-linearity of the governing equations, the results generated by DTM do not satisfy boundary conditions (BC's) at infinity without the use of the Padé approximation. The DTM solution must then be combined with the Padé-approximant, resulting in a high rate of convergence at infinity. The higher order of approximation is required depending on the desired exactness. we use $[5\times5]$ order approximation is employed to Eqs. (8.37)-(8.43), the Padé approximants are as follows.

$$f(\eta)=\frac{1.50380\eta^2-0.56983\eta^3-0.30957\eta^4+0.01450\eta^5+...}{1+0.29414\eta-0.01741\eta^2-0.00053\eta^3-0.00020\eta^4-0.00017\eta^5+...} \tag{8.44}$$

$$g(\eta)=\frac{1-0.94938\eta-0.05528\eta^2+0.00532\eta^3-0.00107\eta^4+0.00041\eta^5+...}{1+0.05080\eta-0.00466\eta^2+0.00054\eta^3-0.00037\eta^4+0.000001\eta^5+...} \tag{8.45}$$

$$m(\eta)=\frac{0.70127\eta-0.16471\eta^2+0.01670\eta^3+0.22886\eta^4-0.25397\eta^5+\ldots}{1-0.23488\eta-0.30951\eta^2+0.15401\eta^3-0.06434\eta^4-0.016875\eta^5+\ldots} \tag{8.46}$$

$$n(\eta)=\frac{0.92799\eta+1.05985\eta^2+0.47275\eta^3+0.29700\eta^4+0.13981\eta^5+\ldots}{1+1.142086\eta+0.26137\eta^2+0.28733\eta^3+0.23395\eta^4-0.02512\eta^5+\ldots} \tag{8.47}$$

$$\theta(\eta)=\frac{1-0.95542\eta-0.05086\eta^2+0.01017\eta^3-0.00518\eta^4+0.00146\eta^5+\ldots}{1-0.01006\eta-0.00278\eta^2+0.00828\eta^3-0.00443\eta^4-0.000001\eta^5+\ldots} \tag{8.48}$$

$$\phi(\eta)=\frac{1-1.10127\eta+0.08767\eta^2+0.04069\eta^3-0.03182\eta^4+0.01226\eta^5+\ldots}{1-0.01583\eta-0.04098\eta^2+0.0125\eta^3-0.00827\eta^4-0.00049\eta^5+\ldots} \tag{8.49}$$

$$\chi(\eta)=\frac{1-1.41178\eta+0.58200\eta^2-0.20981\eta^3+0.04557\eta^4-0.00436\eta^5+\ldots}{1+0.24883\eta-0.01861\eta^2+0.01883\eta^3+0.00061\eta^4-0.00278\eta^5+\ldots} \tag{8.50}$$

8.5 Graphical and Tabular Results

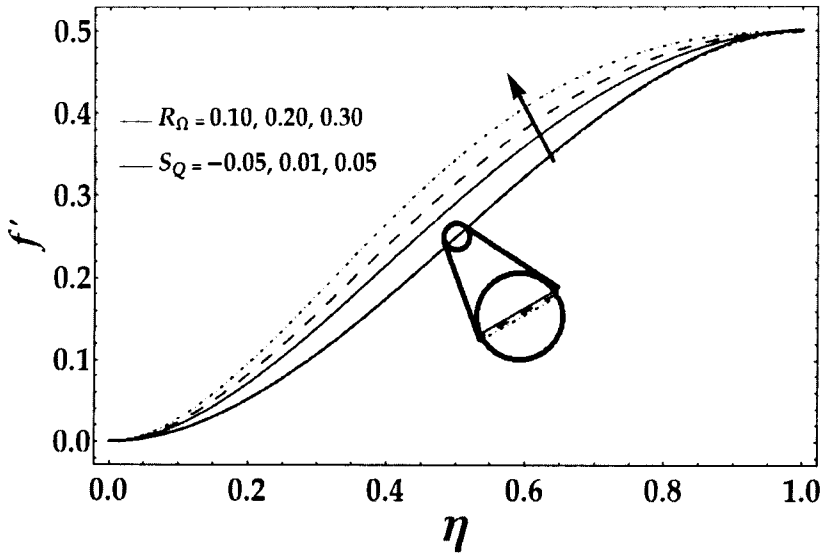

Figure 8.2: Variation of S_Q and R_Ω on $f'(\eta)$.

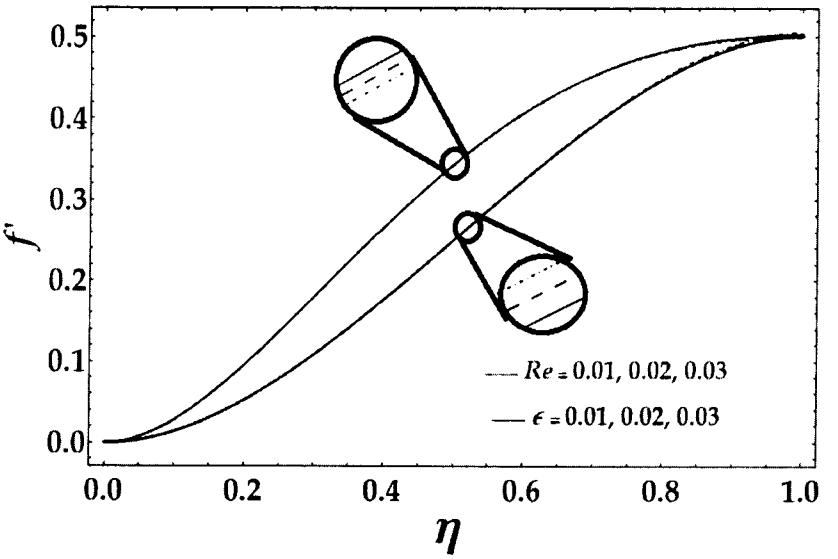

Figure 8.3: Variation of Re and ε on $f'(\eta)$.

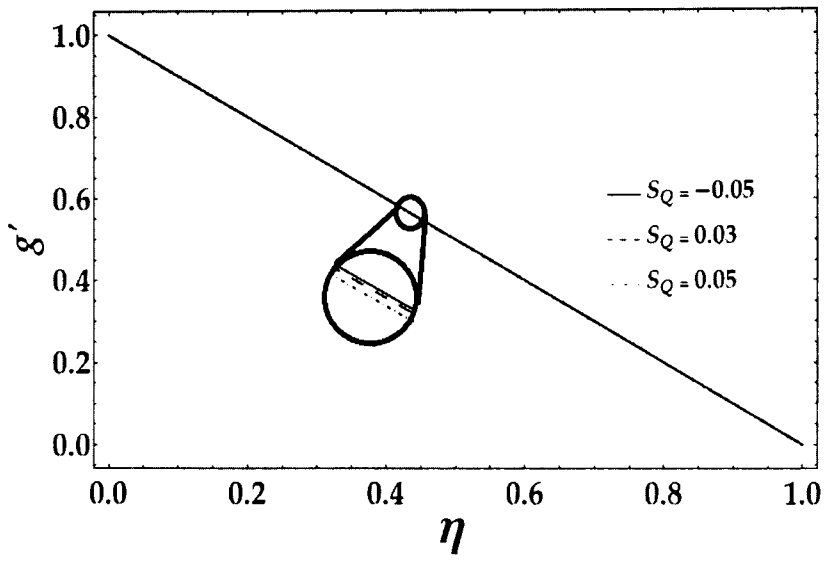

Figure 8.4: Variation of S_Q on the $g'(\eta)$.

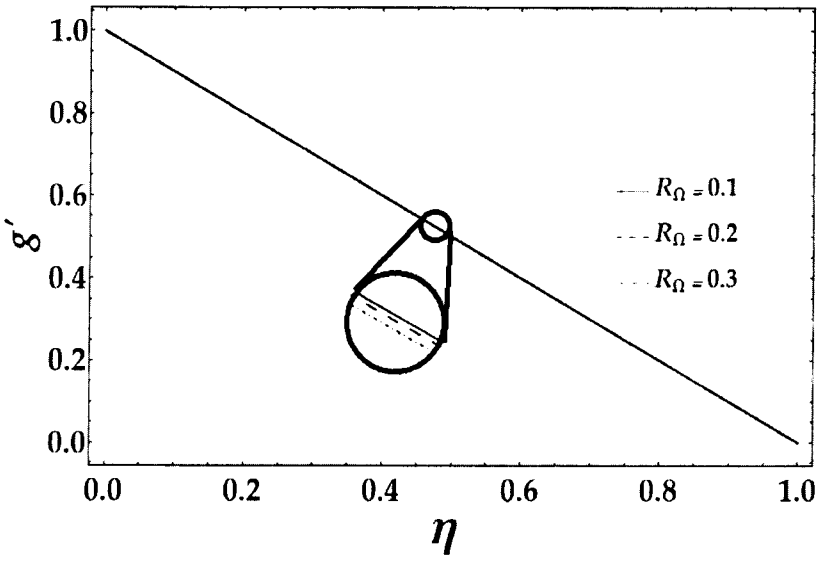

Figure 8.5: Variation of R_Ω on the $g'(\eta)$

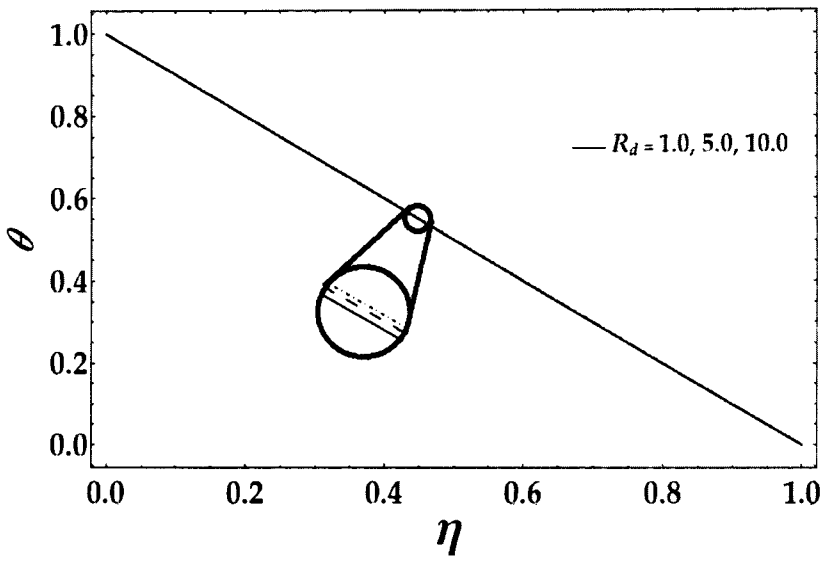

Figure 8.6: Variation of R_d on the $\theta(\eta)$.

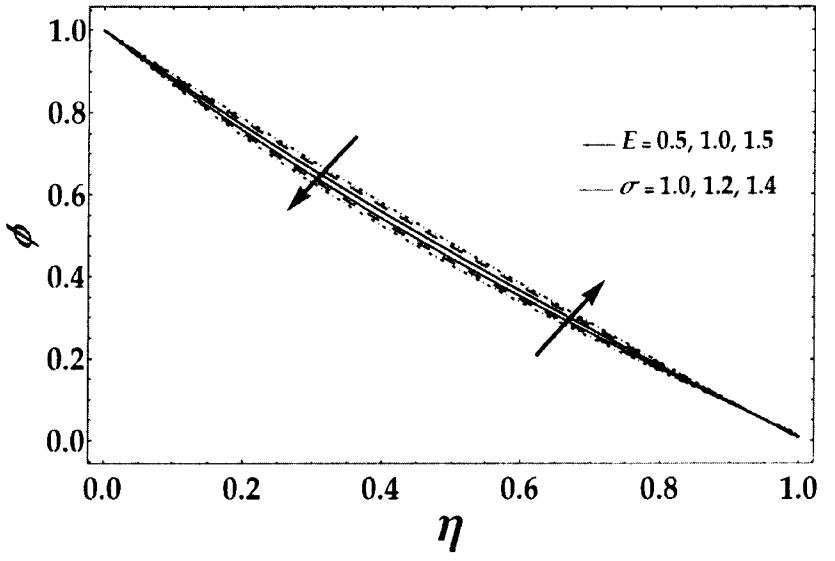

Figure 8.7: Influence of E, σ on $\phi(\eta)$.

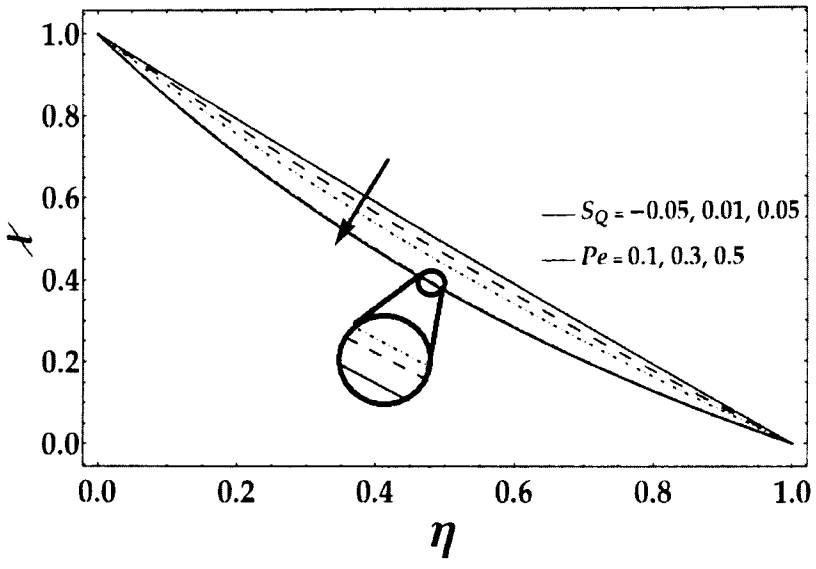

Figure 8.8: Influence of S_Q, Pe on $\chi(\eta)$.

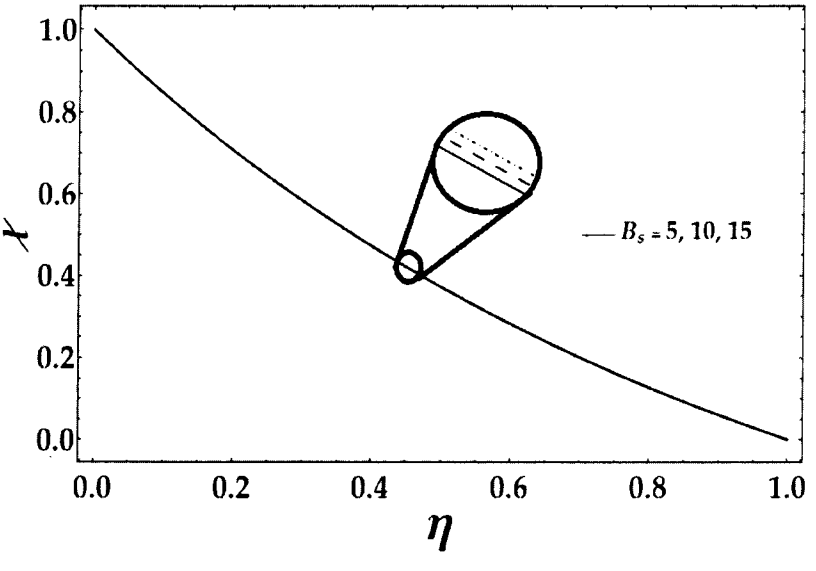

Figure 8.9: Influence of B_s on $\chi(\eta)$.

Table 8.1: Nusselt number $-\theta'(0)$ for various values T_t, T_b, P_t, S_Q, R_d by DTM-Padé $[5\times5]$.

					$N=0, \varepsilon=0$		$N=0.001, \varepsilon=0.01$	
T_t	T_b	P_t	S_Q	R_d	**Shooting Method**	**DTM-Padé**	**Shooting Method**	**DTM-Padé**
0.01	0.01	6.8	0.01	0.1	0.9453581458257031	0.9453581458257031	0.9453580229418479	0.9453580229418479
0.02					0.9129392464647502	0.9129392464647502	0.9168105199062608	0.9168105199062608
0.03					0.885050353876044	0.885050353876044	0.8888640984792582	0.88886421387948
0.01	0.01				0.9453581458257031	0.9453581458257031	0.9453580229418479	0.9453580229418479
	0.02				0.9127247607771866	0.9127247607771866	0.9165850260955254	0.9165850260955254
	0.03				0.8846306434056175	0.8846306434056175	0.8884227981982002	0.8884227981982002
	0.01	4			0.9652550488660355	0.9652550488660355	0.9675928032457709	0.9675928032457709
		7			0.9397439543758035	0.9397439543758035	0.9437839679869379	0.9437839679869379
		10			0.9147012636449525	0.9147012636449525	0.9203987712978005	0.9203987712978005
		6.8	0.01		0.9453581458257031	0.9453581458257031	0.9453580229418479	0.9453580229418479
			0.05		0.962823634655179	0.962823634655179	0.9628229964119813	0.9628229964119814
			0.10		0.9846650661460106	0.9846650661460105	0.9846637459508848	0.9846637459508849
				0.1	0.9453581458257031	0.9453581458257031	0.9453580229418479	0.9453580229418479
				0.2	0.9510070301645854	0.9510070301645854	-0.9510069195680435	0.9510069195680435
				0.3	0.9555976234799036	0.9555976234799036	0.9555975229405811	0.9555975229405811

Table 8.2: Values of $-\phi'(0)$ for various values of T_t, T_b, S_Q, S_M by DTM-Padé [5×5].

						$N=0, \varepsilon=0$		$N=0.001, \varepsilon=0.01$	
T_t	T_b	S_Q	S_M	σ	E	**Shooting Method**	**DTM-Padé**	**Shooting Method**	**DTM-Padé**
0.01	0.01	0.01	2	1.0	0.5	1.435178775912007	1.435178775912007	1.4351845601115252	1.4351845601115252
0.02						-1.5386661248386588	-1.5386661248386588	1.5386815699499619	1.5386815699499619
0.03						1.6915815282592488	1.6915815282592488	1.6916058310008029	1.691605831000803
0.01	0.01					1.435178775912007	1.435178775912007	1.4351845601115252	1.4351845601115252
	0.02					1.4232820562236754	1.4232820562236754	1.4232823835584472	1.4232823835584472
	0.03					1.419093062504203	1.419093062504203	1.4190915732019218	1.4190915732019218
	0.01	0.01				1.435178775912007	1.435178775912007	1.4351845601115252	1.4351845601115252
		0.05				1.4251485442115686	1.4251485442115686	1.4251794413504606	1.425179441350460 6
		0.10				1.4125835930091923	1.4125835930091923	1.4126492708515266	1.4126492708515266
		0.01	2			1.435178775912007	1.435178775912007	1.4351845601115252	1.4351845601115252
			4			1.7668272242531649	1.7668272242531649	1.766826872469483	1.766826872469483
			6			2.061809288257862	2.0618092882578622	2.061802518834794	2.061802518834794
			2	1.0		1.435178775912007	1.435178775912007	1.4351845601115252	1.4351845601115252
				1.2		1.5047236560982666	1.5047236560982666	1.504729257426788	1.504729257426788
				1.4		1.5724569509177595	1.5724569509177595	1.5724623816684822	1.5724623816684822
				1.0	0.5	1.435178775912007	1.435178775912007	1.4351845601115252	1.4351845601115252
					1.0	1.2934921698534982	1.2934921698534982	1.2934983531439321	1.2934983531439321
					1.5	1.2032049045002797	1.2032049045002797	1.203211360514021	1.203211360514021

Table 8.3: Values of $\chi'(0)$ for various values S_Q, B_s, P_l by DTM-Padé $[5\times5]$.

			$N=0, \varepsilon=0$		$N=0.001, \varepsilon=0.01$	
S_Q	B_s	P_l	**Shooting Method**	**DTM-Padé**	**Shooting Method**	**DTM-Padé**
0.01	5	1	1.9920960111923511	1.9920960111923511	1.9920441739686712	1.9920441739686712
0.05			1.9809248574300737	1.9809248574300737	1.9806519209599767	1.9806519209599767
0.10			1.966954532904315	1.966954532904315	1.9664308565984414	1.9664308565984414
0.01	5		1.9920960111923511	1.9920960111923511	1.9920441739686712	1.9920441739686712
	10		1.9913862326581517	1.9913862326581517	1.991250840275269	1.991250840275269
	15		1.9906766098258128	1.9906766098258128	1.9904576936771408	1.9904576936771408
	5	1	1.9920960111923511	1.9920960111923511	1.9920441739686712	1.9920441739686712
		1.2	2.2139723400728952	2.2139723400728952	2.213920738108241	2.213920738108241
		1.4	2.4426103927893497	2.4426103927893497	2.4425593242811856	2.4425593242811856

Table 8.4: Torque Values on the fix and moving plates by DTM- Padé $[5\times5]$ for various values of Squeezing Reynolds Number S_Q.

	$\frac{dg(0)}{d\eta}$		$\frac{dg(1)}{d\eta}$	
S_Q	$\varepsilon=0$	$\varepsilon=0.01$	$\varepsilon=0$	$\varepsilon=0.01$
0.1	-1.092937221430923	-0.8954500024658023	− 0.948663684660318	-0.8968514132478014
0.2	-1.180889912821983	-0.7842736506672865	− 0.901360783950894	-0.7898299005296441

8.6 Discussion

The numerical solutions found by using the Differential Transformation Method in conjunction with the Padé approximant to solve coupled non-linear differential equations for the above-mentioned flow condition are discussed. Nonlinear equations are usually solved using several numerical approaches based on boundary conditions, one of which is set to infinity. Many researchers have created approximate analysis methodologies for non-linear problems while mathematical computational software such as MATHEMATICA, MATLAB, and MAPLE are being used. The Homotopy Perturbation Method (HPM), the HAM, and the Differential Transforming Method (DTM) are some techniques which is used by the various researchers. Some of these methods use special transformations to simplify difficult equations or convert them into systems of equations, and others give solutions in the form of series that are near to the actual solution. The above-mentioned system of equations is solved with help of computational software Mathematica (12v). To ensure that our findings were accurate, we compared our results with shooting method. The physical properties of several components appearing in momentum equation, MHD equation (induced), temperature equation, motile microbe function, and nanoparticle concentration equation are the main focus of our study. Various physical parameter are considered, i.e. effects of squeezing Reynolds number S_Q rotational Reynolds number R_Ω, material parameter ε, Reynolds number Re on the axial and tangential velocity profiles $f'(\eta), g'(\eta)$, and magnetic Reynolds number Re_M on induced magnetic field $m(\eta)$, $n(\eta)$. Additionally, the impact of different parameter i.e. squeezing Reynolds number S_Q, Prandtl number P_t, thermophoresis parameter T_t, Brownian motion T_t, Schmidt number S_M, Bioconvection Schmit number B_s, Péclet number Pe are also discoursed on temperature profile, nanoparticle concentration and motile density function. For graphical results, the following values of different parameters is

selected for analysing the graphical outcomes.

$S_Q = 0.01; R_\Omega = 0.1; Nt = 0.01; Nb = 0.01; Bt = 6; \mathrm{Re}_M = 1; \mathrm{Pr} = 6.8; S_M = 1; B_s = 1; Pe = 0.5;$
$i = 0.01; Re = 0.1; \varepsilon = 0.01;$

Velocity Distribution

Figure (8.2)-(8.3) illuminated that the impact on velocity profile in axial direction due to squeezed Reynolds number S_Q, rotational Reynolds number R_Ω, material parameter ε and Reynolds number Re. As seen in figure (8.2), by rising the squeezing Reynolds number and the rotational Reynolds number the axial velocity profile decreases and increases respectively. In figure (8.3), it is detect that, increasing value of material parameter ε, velocity field in the axial direction increases. This increase in axial velocity is consequence of the increase in relaxation time due to reduction of resistance in particles of the Sutterby fluid. By increasing the value of Reynolds number, the axial velocity profile decreases. The tangential velocity profile behaviour for squeezed Reynolds number is shown in figure (8.4). The tangential velocity distribution decreases when the Squeezed Reynolds number is increased. Similar phenomena are observed in figure (8.5) i.e., temperature profile decreases by increasing the value of rotational Reynolds number.

Temperature Distribution

The influence of radiation parameter on temperature profile is seen in figure (8.6). By increasing value of radiation parameter, temperature profile increases. The physical reason for this is that an increase in radiation causes the heat energy in the flow to be released, resulting in a temperature increase.

Concentration Distribution

Figure (8.7) portrays the influence of rate of chemical reaction and activation energy on nanoparticle concentration. The consequent chemical reaction is retarded because high energy activation and low temperatures produce a steady reaction rate. As a result, the solute's concentration grows.

Motile Gyrotactic Microorganism Distribution

Figure (8.8) portrays the influence of Péclet number Pe and squeezed Reynolds number S_Q on the motile microorganism density function $\chi(\eta)$. One can observed that rising in the values of squeezing Reynolds number S_Q,motile gyrotactic microorganism density function enhanced and enlarging values of Péclet number Pe , performance of motile density of microorganism function opposed. The physical motive of this behaviour of above-mentioned physical parameter is microorganism diffusivity declines then the speed of the microorganism decreases. That's why the microorganism density function decreases while increasing the value of Péclet number Pe. Figure (8.9) establishes the physical performance of Schmidt number S_M . It perceived that by enhancing the value of bioconvection Schmidt number B_s, density of the motile microorganism function rises but the impact is minimal.

Physical Quantities

The numerical results for of different parameters i.e., Sherwood number, Nusselt number, and motile density function are represented in Table (8.1)-(8.3). It is evident that increasing the thermophoresis parameter value causes the Nusselt number to rise, whereas the opposite trend is observed for Sherwood number. Additionally, the Nusselt number decreases when the Brownian motion parameter is increased, and the opposite is true for the Sherwood number. Moreover, the torque values at the lower plate $dg(0)/d\eta$, and upper plate $dg(1)/d\eta$ are also calculated numerically., which is showed in Table (8.4).

Chapter 9

Conclusion and Future Work

9.1 Introduction

This chapter summarizes the main findings of this thesis. We also outline some expected directions for future research on transport of motile gyrotactic microorganism in different fluid models as well as in different geometries.

9.2 Conclusion

The aim of this research work explained in this thesis is to provide mathematical modelling and semi-numerical computation of transport of motile gyrotactic microorganism in a Viscoelastic fluid. For mathematical modelling of nanofluid Buongiorno's model have been taken into consideration. Fluid flow take place through parallel rotating disks. Several flow and heat transfer characteristics like linear and nonlinear thermal radiation, activation energy, Activation energy and porosity are considered. The DTM-Padé approach is used to solve the first order equations derived from the reduced system of nonlinear equations. As the first chapter is preliminary study, which focused on introduction, motivation and objective of this thesis, semi analytic method, and thesis layout. Chapter 2 focus on literature review, governing equations, dimensionless numbers, discussion about viscoelastic fluids and geometry of the problem which is discussed in next 6 chapters (Chapter 3 to 8). From chapter 3 and onward the main published and submitted work is reported. Mathematical model is developed flow the flow situations. Obtained flow problem is then simplified with the help of similarity transformations and then solved with the help of well-known DTM-Padé method. Graphical and tabular discussion is made to discuss the physical parameter occur in the ordinary differential equations. Torque plays important role in the rotating flows. Torque is also calculated for the flow situation.

Mathematical model for nanofluid bioconvection axisymmetric squeezing flow between parallel rotating circular plates is investigated in chapter 3. Rosseland is employed to examine effects of thermal radiation. The key findings of this study shows that with increment in squeezing Reynolds number, both axial and tangential velocity magnitudes decrease. By raising the values of the rotational Reynolds number, the axial velocity distribution increases. Rise in the values of thermophoresis parameter induces significant elevation in nanoparticle concentration values. By Increasing the value of Brownian motion and thermophoresis parameters, fluid temperature is increased due to elevation in the kinetic energy of the nanoparticles. Thermal conductivity reduces when we increase the value of Prandtl number which declines temperature profile. The inclusion of radiative flux therefore produces different results to when it is neglected, and it is important in realistic models of high temperature bioreactors or lubrication systems to include a robust radiative heat transfer model. Speed of the microorganism decreases because the microorganism density function decreases while increasing the Péclet number. The amplification in squeezing effect i.e., greater squeezing Reynolds number, reduces torque at the lower disk whereas it enhances torque at the upper disk.

A mathematical model is devised for flow of magnetized Nano fluid between spinning circular plates containing nanoparticles and gyrotactic microorganisms in chapter 4. A generalized form of magnetic Reynolds number is used for mathematical modelling of nanofluid flow. The key findings of this study show that Magnetic Reynolds number tends to diminish induced magnetic field in axial and tangential direction. Brownian motion reveals the opposite effects on temperature distribution and nanoparticle concentration, while the thermophoresis effects remain similar. Squeezed Reynolds number significantly suppresses the temperature, microorganism, and nanoparticle concentration distribution. Péclet number tends to diminish the microorganism profile, whereas Schmidt number intends to boost the microorganism profile.

In presence of a generalized magnetic field, flow behavior between two spinning circular plates filled with Carreau fluid in suspension of nanoparticles and motile gyrotactic bacteria is discussed in Chapter 5 along with Arrhenius equation. The key findings of this study show that Rotational Reynolds number gives opposite behavior for the axial and tangential velocity distribution. The shear-thinning fluid viscosity decline with shear strain because of big velocity as collate to Newtonian and shear-thickening fluids. In axial and tangential velocity distribution, velocity is decreasing by increasing value of squeezed Reynolds number. Activation energy enhances while the reaction rate suppresses the nanoparticle concentration. Péclet number reduces the microorganism profile, whereas squeezed Reynolds number and bioconvection number intend to enhance the microorganism profile.

The unsteady flow confined by parallel rotating circular plates in porous media filled with Williamson Nano fluid is discussed in chapter 6. The impact of the porosity parameter is considered as well. The key finding of this study are shows that on axial and tangential velocity profiles, the rotational Reynolds number shows a reverse trend. As the squeezing Reynolds number increases, the axial and tangential velocity profiles decrease. Increasing the squeezing Reynolds number increases nanoparticle concentration and motile microorganism profile. The motile microorganism profile is decreased when Péclet number increased, whereas microorganism profile increased when bio convection Schmidt number increased.

The unsteady flow between rotating circular plates located at finite distance filled with Reiner-Rivlin Nano fluid analyzed in chapter 7. The Reiner-Rivlin Nano fluid is incompressible and electrically conducting. Moreover, Nano fluid also accommodates motile gyrotactic microorganisms under effect of activation energy and thermal radiation. The key finding of study are shows that opposite behavior is experienced for the rotational Reynolds number on tangential and axial velocity distribution. Enhancing value of squeezing Reynolds number, tangential and axial velocity distribution decreases. The thermal radiation parameter enhances temperature distribution. Nanoparticle concentration and motile density increase by enhancing

value of squeezing Reynolds number. Increasing values of Activation energy tends to intensify the nanoparticle concentration profile. The microorganism profile declines by increasing values of Péclet number, but microorganism profile rises by enlarging bio convection number.

The unsteady flow confined by parallel circular disks filled with magnetized Sutterby fluid in presence of nanoparticles and motile gyrotactic microorganism discussed in chapter 8. Impact of Arrhenius Kinetics also considered in this study. The key findings of this study show that on axial and tangential velocity profiles, the rotational Reynolds number shows a reverse trend. The axial and tangential velocity profiles reduce as the value of the squeezing Reynolds number increases. The temperature profile rises as the thermophoresis and Brownian motion parameters are increased. The temperature distribution rises as the radiation parameters is increased. Energy parameter and rate of chemical reaction indicate opposing patterns for nanoparticle concentration. The microorganism profile decreases as the Péclet number increases, whereas the microorganism profile increases as the bio convection number increases.

9.3 Future Work

Useful information is provided by flow phenomena investigated in this thesis about the swimming of motile gyrotactic microorganism in parallel rotating disk. By applying it to many real-world scenarios, current exploration's qualities and benefits have been clearly demonstrated. But there are still a lot of difficulties to overcome to achieve complete predictive capabilities for swimming of motile gyrotactic microorganism in different fluids. In this thesis, struggle is made to perform investigations with more complex simulation models and more improved measurements. Here, some notions and directions for future work are.

Entropy Generation: The work investigated in this thesis focused on transport of nanoparticle. future plane is to extend this work for case of swimming of motile gyrotactic microorganism in viscoelastic fluid along with entropy generation.

Microchannel and Microtube: The actual configurations incorporated in current thesis are parallel rotating disk. Because microchannel and micro tube geometries have several technical and industrial uses, it is planned to further this study in the future.

Homotopy Analysis Method: In current study, differential transform method is used for solving nonlinear coupled differential equations. Another mathematical model that was built by the transport of a motile, gyrotactic bacterium using HAM will be solved in a future proposal.

ss: In current study, uniform distribution of nanoparticle is chosen. The extension of our work on particle random distribution, which might lead to stochastic modelling, is a future suggestion.

References

[1] Dillon, R., Fauci, L., & Gaver, D., 3rd. (1995). A microscale model of bacterial swimming, chemotaxis and substrate transport. *Journal of Theoretical Biology, 177*(4), 325–340. doi:10.1006/jtbi.1995.0251.

[2] Hopkins, M. M., & Fauci, L. J. (2002). A computational model of the collective fluid dynamics of motile micro-organisms. *Journal of Fluid Mechanics, 455*, 149–174. doi:10.1017/s0022112001007339.

[3] Turkyilmazoglu, M. (2014). Unsteady convection flow of some nanofluids past a moving vertical flat plate with heat transfer. *Journal of Heat Transfer, 136*(3), 031704. doi:10.1115/1.4025730.

[4] Sk, M. T., Das, K., & Kundu, P. K. (2016). Multiple slip effects on bioconvection of nanofluid flow containing gyrotactic microorganisms and nanoparticles. *Journal of Molecular Liquids, 220*, 518–526. doi:10.1016/j.molliq.2016.04.097.

[5] Motsa, S. S., & Animasaun, I. L. (2016). Paired quasi-linearization analysis of heat transfer in unsteady mixed convection nanofluid containing both nanoparticles and gyrotactic microorganisms due to impulsive motion. *Journal of Heat Transfer, 138*(11), 114503. doi:10.1115/1.4034039.

[6] Mallikarjuna, B., Rashad, A. M., Chamkha, A. J., & Abdou, M. M. M. (2018). Mixed bioconvection flow of a nanofluid containing gyrotactic microorganisms past a vertical slender cylinder. *Frontiers in Heat and Mass Transfer, 10*. doi:10.5098/hmt.10.21.

[7] Sudhagar, P., Kameswaran, P. K., & Kumar, B. R. (2019). Gyrotactic microorganism effects on mixed convective nanofluid flow past a vertical

cylinder. *Journal of Thermal Science and Engineering Applications*, *11*(4), 041018. doi:10.1115/1.4044185.

[8] Khan, S. U., & Ali, H. M. (2020). Swimming of gyrotactic microorganisms in unsteady flow of Eyring-Powell nanofluid with variable thermal features: Some bio-technology applications. *Int J Thermophys*, (11).

[9] Kotha, G., Kolipaula, V. R., Venkata Subba Rao, M., Penki, S., & Chamkha, A. J. (2020). Internal heat generation on bioconvection of an MHD nanofluid flow due to gyrotactic microorganisms. European Physical Journal Plus, 135(7). doi:10.1140/epjp/s13360-020-00606-2.

[10] Basha, H. T., & Sivaraj, R. (2021). Numerical simulation of blood nanofluid flow over three different geometries by means of gyrotactic microorganisms: Applications to the flow in a circulatory system. *Proceedings of the Institution of Mechanical Engineers, Part C: Journal of Mechanical Engineering Science*, *235*(2), 441–460. doi:10.1177/0954406220947454.

[11] Awais, M., Awan, S. E., Raja, M., & Shoaib, M. (2021). Effects of gyrotactic organisms in bio-convective nano-material with heat immersion, stratification, and viscous dissipation. *Arab J Sci Eng*, *46*(6), 5907–5920.

[12] Raju, C. S. K., Hoque, M. M., & Sivasankar, T. (2017). Radiative flow of Casson fluid over a moving wedge filled with gyrotactic microorganisms. *Advanced Powder Technology: The International Journal of the Society of Powder Technology*, *28*(2), 575–583. doi:10.1016/j.apt.2016.10.026.

[13] Saleem, S., Rafiq, H., Al-Qahtani, A., El-Aziz, M. A., Malik, M. Y., & Animasaun, I. L. (n.d.). Magneto Jeffrey nanofluid bioconvection over a rotating vertical cone due to gyrotactic microorganism. *Math Probl Eng*, *2019*, 1–11.

[14] Kotnurkar, A. S., & Giddaiah, S. (2019). Bioconvection peristaltic flow of nano Eyring–Powell fluid containing gyrotactic microorganism. *SN Applied Sciences*, *1*(10). doi:10.1007/s42452-019-1281-y.

[15] Nima, N. I., Salawu, S. O., Ferdows, M., Shamshuddin, M. D., Alsenafi, A., & Nakayama, A. (2020). Melting effect on non-Newtonian fluid flow in gyrotactic microorganism saturated non-darcy porous media with variable fluid properties. *Applied Nanoscience*, *10*(10), 3911–3924. doi:10.1007/s13204-020-01491-y.

[16] Khan, S. U., Al-Khaled, K., & Khan, M. I. (2020). Convective nonlinear thermally developed flow of thixotropic nanoliquid configured by Riga surface with gyrotactic microorganism and activation energy: A bio-technology and thermal extrusion model. *International Communications in Heat and Mass Transfer*, *119*(104966), 104966. doi:10.1016/j.icheatmasstransfer.2020.104966.

[17] Sohail, M., Naz, R., & Raza, R. (2019). Application of double diffusion theories to Maxwell nanofluid under the appliance of thermal radiation and gyrotactic microorganism. *Multidiscipline Modeling in Materials and Structures*, *16*(2), 256–280. doi:10.1108/mmms-05-2019-0101.

[18] Choi, S. U., & Eastman, J. A. (1995). Enhancing thermal conductivity of fluids with nanoparticles. *Argonne National Lab*, 99–105.

[19] Buongiorno, J. (2006). Convective transport in nanofluids. *Journal of Heat Transfer*, *128*(3), 240–250. doi:10.1115/1.2150834.

[20] Bird, R. B., Armstrong, R. C., Hassager, O., & Curtiss, C. F. (1987). *Dynamics of polymeric liquids, volume 2: Kinetic theory* (2nd ed.). Nashville, TN: John Wiley & Sons.

[21] Carreau, P. J. (1972). Rheological equations from molecular network theories. *Transactions of the Society of Rheology*, *16*(1), 99–127. doi:10.1122/1.549276.

[22] Yahaya, R. I., Arifin, N. M., & Isa, S. S. P. M. (2019). Stability analysis of MHD Carreau fluid flow over a permeable shrinking sheet with thermal radiation. *Sains Malaysiana*, *48*(10), 2285–2295.

[23] Eid, M. R., Mahny, K. L., Dar, A., & Muhammad, T. (2020). Numerical study for Carreau nanofluid flow over a convectively heated nonlinear stretching surface with chemically reactive species. *Physica A*, *540*(123063), 123063. doi:10.1016/j.physa.2019.123063.

[24] Santoshi, P. N., Reddy, G. V. R., & Padma, P. (2019). Numerical study of Carreau nanofluid flow under slips. *International Journal of Applied and Computational Mathematics*, *5*(5).

[25] Khan, M., Salahuddin, T., Malik, M. Y., & Khan, F. (2020). Change in internal energy of Carreau fluid flow along with Ohmic heating: A Von Karman application. *Physica A*, *547*(123440), 123440. doi:10.1016/j.physa.2019.123440.

[26] Bilal, S., Shafqatullah, Alshomrani, A. S., Malik, M. Y., Kausar, N., Khan, F., & Khalil-ur-Rehman. (2018). Analysis of Carreau fluid in the presence of thermal stratification and magnetic field effect. *Results in Physics*, *10*, 118–125. doi:10.1016/j.rinp.2018.05.005.

[27] Khan, M., Azam, M., & Alshomrani, A. S. (2017). On unsteady heat and mass transfer in Carreau nanofluid flow over expanding or contracting cylinder with convective surface conditions. *Journal of Molecular Liquids*, *231*, 474–484. doi:10.1016/j.molliq.2017.02.033.

[28] Khan, M., Salahuddin, T., Yousaf, M. M., Khan, F., & Hussain, A. (2020). Variable diffusion and conductivity change in 3D rotating Williamson fluid flow along with magnetic field and activation energy. *International Journal of Numerical Methods for Heat & Fluid Flow*, *30*(5), 2467–2484. doi:10.1108/hff-02-2019-0145.

[29] Raza, R., Mabood, F., Naz, R., & Abdelsalam, S. I. (2021). Thermal transport of radiative Williamson fluid over stretchable curved surface. *Thermal Science and Engineering Progress*, *23*(100887), 100887. doi:10.1016/j.tsep.2021.100887.

[30] Khan, M. S., Rahman, M. M., Arifuzzaman, S. M., Biswas, P., & Karim, I. (2017). Williamson fluid flow behaviour of mhd convective-radiative Cattaneo–Christov heat flux type over a linearly stretched-surface with heat generation and thermal-diffusion. *Frontiers in Heat and Mass Transfer*, 9(1), 1-12. doi:10.5098/hmt.9.15.

[31] Amanulla, C. H., Nagendra, N., & Suryanarayana Reddy, M. (2017). Mhd flow and heat transfer in a Williamson fluid from a vertical permeable cone with thermal and momentum slip effects: A mathematical study. *Frontiers in Heat and Mass Transfer*, *8*, 1-11. doi:10.5098/hmt.8.40.

[32] Hamid, A., Khan, M., & Alghamdi, M. (2019). Numerical simulation for transient flow of Williamson fluid with multiple slip model in the presence of chemically reacting species. *International Journal of Numerical Methods for Heat & Fluid Flow*, *29*(11), 4445–4461. doi:10.1108/hff-02-2019-0151.

[33] Shamsi, M. R., Akbari, O. A., Marzban, A., Toghraie, D., & Mashayekhi, R. (2017). Increasing heat transfer of non-Newtonian nanofluid in rectangular microchannel with triangular ribs. *Physica. E, Low-Dimensional Systems & Nanostructures*, *93*, 167–178. doi:10.1016/j.physe.2017.06.015.

[34] Nadeem, S., Haq, R. U., & Khan, Z. H. (2014). Numerical solution of non-Newtonian nanofluid flow over a stretching sheet. *Applied Nanoscience*, *4*(5), 625–631. doi:10.1007/s13204-013-0235-8.

[35] Shankar, U., Naduvinamani, N. B., & Basha, H. (2020). Effect of magnetized variable thermal conductivity on flow and heat transfer characteristics of unsteady Williamson fluid. *Nonlinear Engineering*, *9*(1), 338–351. doi:10.1515/nleng-2020-0020.

[36] Goudarzi, S., Shekaramiz, M., Omidvar, A., Golab, E., Karimipour, A., & Karimipour, A. (2020). Nanoparticles migration due to thermophoresis and Brownian motion and its impact on Ag-MgO/water hybrid nanofluid natural convection. *Powder Technology*, *375*, 493–503. doi:10.1016/j.powtec.2020.07.115

[37] Ghalandari, M., Mirzadeh Koohshahi, E., Mohamadian, F., Shamshirband, S., & Chau, K. W. (2019). Numerical simulation of nanofluid flow inside a root canal. *Engineering Applications of Computational Fluid Mechanics*, *13*(1), 254–264. doi:10.1080/19942060.2019.1578696.

[38] Sheikholeslami, M., & Vajravelu, K. (2017). Nanofluid flow and heat transfer in a cavity with variable magnetic field. *Applied Mathematics and Computation*, *298*, 272–282. doi:10.1016/j.amc.2016.11.025.

[39] Sheikholeslami, M., & Ganji, D. D. (2015). Nanofluid flow and heat transfer between parallel plates considering Brownian motion using DTM. *Computer Methods in Applied Mechanics and Engineering*, *283*, 651–663. doi:10.1016/j.cma.2014.09.038.

[40] Biswal, U., Chakraverty, S., Ojha, B. K., & Hussein, A. K. (2021). Numerical simulation of magnetohydrodynamics nanofluid flow in a semi-porous channel

with a new approach in the least square method. International Communications in Heat and Mass Transfer, 121(105085), 105085. doi:10.1016/j.icheatmasstransfer.2020.105085.

[41] Zhang, X., Gu, H., & Fujii, M. (2007). Effective thermal conductivity and thermal diffusivity of nanofluids containing spherical and cylindrical nanoparticles. *Experimental Thermal and Fluid Science*, *31*(6), 593–599. doi:10.1016/j.expthermflusci.2006.06.009.

[42] Fakour, M., Vahabzadeh, A., & Ganji, D. D. (2015). Study of heat transfer and flow of nanofluid in permeable channel in the presence of magnetic field. *Propulsion and Power Research*, *4*(1), 50–62. doi:10.1016/j.jppr.2015.02.005.

[43] Zhu, J., Wang, S., Zheng, L., & Zhang, X. (2017). Heat transfer of nanofluids considering nanoparticle migration and second-order slip velocity. *Applied Mathematics and Mechanics*, *38*(1), 125–136. doi:10.1007/s10483-017-2155-6.

[44] Alamri, S. Z., Ellahi, R., Shehzad, N., & Zeeshan, A. (2019). Convective radiative plane Poiseuille flow of nanofluid through porous medium with slip: An application of Stefan blowing. *Journal of Molecular Liquids*, *273*, 292–304. doi:10.1016/j.molliq.2018.10.038.

[45] Lu, D., Ramzan, M., ul Huda, N., Chung, J. D., & Farooq, U. (2018). Nonlinear radiation effect on MHD Carreau nanofluid flow over a radially stretching surface with zero mass flux at the surface. *Scientific Reports*, *8*(1). doi:10.1038/s41598-018-22000-w.

[46] Amanulla, C. H., Wakif, A., Boulahia, Z., Suryanarayana Reddy, M., & Nagendra, N. (2018). Numerical investigations on magnetic field modeling for Carreau non-Newtonian fluid flow past an isothermal sphere. *Journal of the*

Brazilian Society of Mechanical Sciences and Engineering, *40*(9). doi:10.1007/s40430-018-1385-0.

[47] Amanulla, C. H., Wakif, A., Boulahia, Z., Suryanarayana Reddy, M., & Nagendra, N. (2018). Numerical investigations on magnetic field modeling for Carreau non-Newtonian fluid flow past an isothermal sphere. *Journal of the Brazilian Society of Mechanical Sciences and Engineering*, *40*(9). doi:10.1007/s40430-018-1385-0.

[48] Khan, I., Ullah, S., Malik, M. Y., & Hussain, A. (2018). Numerical analysis of MHD Carreau fluid flow over a stretching cylinder with homogenous-heterogeneous reactions. *Results in Physics*, *9*, 1141–1147. doi:10.1016/j.rinp.2018.04.022.

[49] Mustafa, M. (2017). MHD nanofluid flow over a rotating disk with partial slip effects: Buongiorno model. *International Journal of Heat and Mass Transfer*, *108*, 1910–1916. doi:10.1016/j.ijheatmasstransfer.2017.01.064.

[50] Pandey, A. K., & Kumar, M. (2016). Effect of viscous dissipation and suction/injection on MHD nanofluid flow over a wedge with porous medium and slip. *Alexandria Engineering Journal*, *55*(4), 3115–3123. doi:10.1016/j.aej.2016.08.018.

[51] Eldesoky, I. M., Abdelsalam, S. I., El-Askary, W. A., El-Refaey, A. M., & Ahmed, M. M. (2019). Joint effect of magnetic field and heat transfer on particulate fluid suspension in a catheterized wavy tube. *BioNanoScience*, *9*(3), 723–739. doi:10.1007/s12668-019-00651-x.

[52] Elmaboud, Y. A., & Abdelsalam, S. I. (2019). DC/AC magnetohydrodynamic-micropump of a generalized Burger's fluid in an annulus. *Physica Scripta*, *94*(11), 115209. doi:10.1088/1402-4896/ab206d.

[53] Abdelsalam, S. I., Velasco-Hernández, J. X., & Zaher, A. Z. (2021). Electromagnetically modulated self-propulsion of swimming sperms via cervical canal. *Biomechanics and Modeling in Mechanobiology, 20*(3), 861–878. doi:10.1007/s10237-020-01407-3.

[54] Bestman, A. R. (1991). Radiative heat transfer to flow of a combustible mixture in a vertical pipe. *International Journal of Energy Research, 15*(3), 179–184. doi:10.1002/er.4440150305.

[55] Anuradha, S., & Yegammai, M. (2017). MHD radiative boundary layer flow of nanofluid past a vertical plate with effects of binary chemical reaction and activation energy. *Glob J Pure Appl Math, 13*, 6377–6392.

[56] Irfan, M., Khan, W. A., Khan, M., & Gulzar, M. M. (2019). Influence of Arrhenius activation energy in chemically reactive radiative flow of 3D Carreau nanofluid with nonlinear mixed convection. *The Journal of Physics and Chemistry of Solids, 125*, 141–152. doi:10.1016/j.jpcs.2018.10.016.

[57] Khan, M. I., Irfan, M., Khan, W. A., Waqas, M., & Rashid, S. (2020). Activation energy analysis in entropy optimized reactive flow. *Applied Nanoscience, 10*(8), 2673–2683. doi:10.1007/s13204-020-01305-1.

[58] Kumar, K. G., Baslem, A., Prasannakumara, B. C., Majdoubi, J., Rahimi-Gorji, M., & Nadeem, S. (2020). Significance of Arrhenius activation energy in flow and heat transfer of tangent hyperbolic fluid with zero mass flux condition. *Microsystem Technologies*. 1–10.

[59] Khan, M. I., Irfan, M., Khan, W. A., Waqas, M., & Rashid, S. (2020). Activation energy analysis in entropy optimized reactive flow. *Applied Nanoscience, 10*(8), 2673–2683. doi:10.1007/s13204-020-01305-1.

[60] Khan, S. A., Nie, Y., & Ali, B. (2020). Multiple slip effects on MHD unsteady viscoelastic nano-fluid flow over a permeable stretching sheet with radiation using the finite element method. *SN Applied Sciences*, *2*(1). doi:10.1007/s42452-019-1831-3.

[61] Raju, C. S. K., Mamatha, S. U., Rajadurai, P., & Khan, I. (2019). Nonlinear mixed thermal convective flow over a rotating disk in suspension of magnesium oxide nanoparticles with water and EG. *European Physical Journal Plus*, *134*(5). doi:10.1140/epjp/i2019-12552-y.

[62] Sheikholeslami, M., & Rokni, H. B. (2018). Numerical simulation for impact of Coulomb force on nanofluid heat transfer in a porous enclosure in presence of thermal radiation. *International Journal of Heat and Mass Transfer*, 118, 823–831. https://doi.org/10.1016/j.ijheatmasstransfer.2017.11.041.

[63] Muhammad, T., Waqas, H., Khan, S. A., Ellahi, R., & Sait, S. M. (2021). Significance of nonlinear thermal radiation in 3D Eyring–Powell nanofluid flow with Arrhenius activation energy. *Journal of Thermal Analysis and Calorimetry*, *143*(2), 929–944. doi:10.1007/s10973-020-09459-4.

[64] Aziz, A., Jamshed, W., Aziz, T., Bahaidarah, H. M. S., & Ur Rehman, K. (2021). Entropy analysis of Powell–Eyring hybrid nanofluid including effect of linear thermal radiation and viscous dissipation. *Journal of Thermal Analysis and Calorimetry*, *143*(2), 1331–1343. doi:10.1007/s10973-020-10210-2.

[65] Mahanthesh, B., Mackolil, J., Radhika, M., Al-Kouz, W., & Siddabasappa. (2021). Significance of quadratic thermal radiation and quadratic convection on boundary layer two-phase flow of a dusty nanoliquid past a vertical plate. *International Communications in Heat and Mass Transfer*, *120*(105029), 105029. doi:10.1016/j.icheatmasstransfer.2020.105029.

[66] Jawad, M., Saeed, A., Khan, A., Gul, T., Zubair, M., & Shah, S. A. A. (2020). Unsteady bioconvection Darcy-Forchheimer nanofluid flow through a horizontal channel with impact of magnetic field and thermal radiation. *Heat Transfer*, (htj.22026). doi:10.1002/htj.22026.

[67] Majeed, A., Zeeshan, A., Amin, N., Ijaz, N., & Saeed, T. (2020). Thermal analysis of radiative bioconvection magnetohydrodynamic flow comprising gyrotactic microorganism with activation energy. *Journal of Thermal Analysis and Calorimetry*. doi:10.1007/s10973-020-10207-x.

[68] Amanulla, C. H., Wakif, A., Boulahia, Z., Suryanarayana Reddy, M., & Nagendra, N. (2018). Numerical investigations on magnetic field modeling for Carreau non-Newtonian fluid flow past an isothermal sphere. *Journal of the Brazilian Society of Mechanical Sciences and Engineering*, *40*(9). doi:10.1007/s40430-018-1385-0.

[69] Kalaivanan, R., Vishnu Ganesh, N., & Al-Mdallal, Q. M. (2020). An investigation on Arrhenius activation energy of second grade nanofluid flow with active and passive control of nanomaterials. *Case Studies in Thermal Engineering*, *22*(100774), 100774. doi:10.1016/j.csite.2020.100774.

[70] Shah, Z., Kumam, P., & Deebani, W. (2020). Radiative MHD Casson Nanofluid Flow with Activation energy and chemical reaction over past nonlinearly stretching surface through Entropy generation. *Scientific Reports*, *10*(1), 4402. doi:10.1038/s41598-020-61125-9.

[71] Reddy, S. R. R., Bala Anki Reddy, P., & Rashad, A. M. (2020). Activation energy impact on chemically reacting eyring–Powell nanofluid flow over a stretching cylinder. *Arabian Journal for Science and Engineering*, *45*(7), 5227–5242. doi:10.1007/s13369-020-04379-9.

[72] Kotresh, M. J., Ramesh, G. K., Shashikala, V. K. R., & Prasannakumara, B. C. (2021). Assessment of Arrhenius activation energy in stretched flow of nanofluid over a rotating disc. *Heat Transfer*, *50*(3), 2807–2828. doi:10.1002/htj.22006.

[73] Abdelmalek, Z., Ullah Khan, S., Waqas, H., A. Nabwey, H., & Tlili, I. (2020). Utilization of second order slip, activation energy and viscous dissipation consequences in thermally developed flow of third grade nanofluid with gyrotactic microorganisms. *Symmetry*, *12*(2), 309. doi:10.3390/sym12020309.

[74] Makinde, O. D., Mahanthesh, B., Gireesha, B. J., Shashikumar, N. S., Monaledi, R. L., & Tshehla, M. S. (2018). MHD nanofluid flow past a rotating disk with thermal radiation in the presence of aluminum and titanium alloy nanoparticles. *Defect and Diffusion Forum*, *384*, 69–79. doi:10.4028/www.scientific.net/ddf.384.69.

[75] Reddy, P. S., Jyothi, K., & Reddy, M. S. (2018). Flow and heat transfer analysis of carbon nanotubes-based Maxwell nanofluid flow driven by rotating stretchable disks with thermal radiation. *Journal of the Brazilian Society of Mechanical Sciences and Engineering*, *40*(12), 1–16.

[76] Waqas, H., Farooq, U., Muhammad, T., Hussain, S., & Khan, I. (2021). *Thermal effect on bioconvection flow of Sutterby nanofluid between two rotating disks with motile microorganisms. Case Studies in Thermal Engineering.*

[77] Latiff, N. A., Uddin, M. J., & Ismail, A. I. M. (2016). Stefan blowing effect on bioconvective flow of nanofluid over a solid rotating stretchable disk. *Propulsion and Power Research*, *5*(4), 267–278. doi:10.1016/j.jppr.2016.11.002.

[78] Bég, O. A., Kabir, M. N., Uddin, M. J., Izani Md Ismail, A., & Alginahi, Y. M. (2021). Numerical investigation of Von Karman swirling bioconvective nanofluid transport from a rotating disk in a porous medium with Stefan blowing

and anisotropic slip effects. *Proceedings of the Institution of Mechanical Engineers, Part C: Journal of Mechanical Engineering Science*, *235*(19), 3933–3951. doi:10.1177/0954406220973061.

[79] Tuz Zohra, F., Uddin, M. J., Basir, M. F., & Ismail, A. I. M. (2020). Magnetohydrodynamic bio-nano-convective slip flow with Stefan blowing effects over a rotating disc. *Proceedings of the Institution of Mechanical Engineers Part N Journal of Nanomaterials Nanoengineering and Nanosystems*, *234*(3–4), 83–97. doi:10.1177/2397791419881580.

[80] Zohra, F. T., Uddin, M. J., & Ismail, A. I. M. (2019). Magnetohydrodynamic bio-nanoconvective Naiver slip flow of micropolar fluid in a stretchable horizontal channel. *Heat Transfer, Asian Research*, *48*(8), 3636–3656. doi:10.1002/htj.21560.

[81] Raju, C. S. K., Hoque, M. M., & Sivasankar, T. (2017). Radiative flow of Casson fluid over a moving wedge filled with gyrotactic microorganisms. *Advanced Powder Technology: The International Journal of the Society of Powder Technology, Japan*, *28*(2), 575–583. doi:10.1016/j.apt.2016.10.026.

[82] Saleem, S., Rafiq, H., Al-Qahtani, A., El-Aziz, M. A., Malik, M. Y., & Animasaun, I. L. (2019). Magneto Jeffrey nanofluid bioconvection over a rotating vertical cone due to gyrotactic microorganism. *Mathematical Problems in Engineering, 2019.*

[83] Kotnurkar, A. S., & Giddaiah, S. (2019). Bioconvection peristaltic flow of nano Eyring–Powell fluid containing gyrotactic microorganism. *SN Applied Sciences*, *1*(10). doi:10.1007/s42452-019-1281-y.

[84] Nima, N. I., Salawu, S. O., Ferdows, M., Shamshuddin, M. D., Alsenafi, A., & Nakayama, A. (2020). Melting effect on non-Newtonian fluid flow in gyrotactic microorganism saturated non-darcy porous media with variable fluid properties. *Applied Nanoscience*, *10*(10), 3911–3924. doi:10.1007/s13204-020-01491-y.

[85] Khan, S. U., Al-Khaled, K., & Khan, M. I. (2020). Convective nonlinear thermally developed flow of thixotropic nanoliquid configured by Riga surface with gyrotactic microorganism and activation energy: A bio-technology and thermal extrusion model. *International Communications in Heat and Mass Transfer*, *119*(104966), 104966. doi:10.1016/j.icheatmasstransfer.2020.104966.

[86] Sohail, M., Naz, R., & Raza, R. (2019). Application of double diffusion theories to Maxwell nanofluid under the appliance of thermal radiation and gyrotactic microorganism. *Multidiscipline Modeling in Materials and Structures*, *16*(2), 256–280. doi:10.1108/mmms-05-2019-0101.

[87] Maleque, K. (2013). Effects of binary chemical reaction and activation energy on MHD boundary layer heat and mass transfer flow with viscous dissipation and heat generation/absorption. International Scholarly Research Notices, 2013.

[88] Awad, F. G., Motsa, S., & Khumalo, M. (2014). Heat and mass transfer in unsteady rotating fluid flow with binary chemical reaction and activation energy. *PloS One*, *9*(9), e107622. doi:10.1371/journal.pone.0107622.

[89] Zaib, A., Rashidi, M. M., Chamkha, A., & Bhattacharyya, K. (2017). Numerical solution of second law analysis for MHD Casson nanofluid past a wedge with activation energy and binary chemical reaction. *International Journal of Numerical Methods for Heat & Fluid Flow*, 00–00. doi:10.1108/hff-02-2017-0063.

[90] Hamid, A., Hashim, & Khan, M. (2018). Impacts of binary chemical reaction with activation energy on unsteady flow of magneto-Williamson nanofluid. *Journal of Molecular Liquids, 262,* 435–442. doi:10.1016/j.molliq.2018.04.095.

[91] Umar, M., Akhtar, R., Sabir, Z., Wahab, H. A., Zhiyu, Z., Imran, A., ... & Raja, M. A. Z. (2019). Numerical treatment for the three-dimensional Eyring-Powell fluid flow over a stretching sheet with velocity slip and activation energy. Advances in Mathematical Physics, 2019.

[92] Abbas, T., Hayat, T., Ayub, M., Bhatti, M. M., & Alsaedi, A. (2019). Electromagnetohydrodynamic Nano fluid flow past a porous Riga plate containing gyrotactic microorganism. Neural Computing and Applications, 31(6), 1905-1913.

[93] Waqas, H., Imran, M., Muhammad, T., Sait, S. M., & Ellahi, R. (2020). On bio-convection thermal radiation in Darcy–Forchheimer flow of Nano fluid with gyrotactic motile microorganism under Wu's slip over stretching cylinder/plate. International Journal of Numerical Methods for Heat & Fluid Flow.

[94] Usman, A. H., Rano, S. A., & Humphries, U. W. (2021). Activity of viscoelastic nanofluid film sprayed on a stretching cylinder with Arrhenius activation energy and entropy generation. *J Adv Res Micro Nano Eng, 3*(1), 12–24.

[95] Khan, U., Zaib, A., Ishak, A., Sherif, E. S. M., Waini, I., Chu, Y. M., & Pop, I. (2022). Radiative mixed convective flow induced by hybrid nanofluid over a porous vertical cylinder in a porous media with irregular heat sink/source. Case Studies in Thermal Engineering, 30, 101711.

[96] Khan, U., Zaib, A., Bakar, S. A., Roy, N. C., & Ishak, A. (2021). Buoyancy effect on the stagnation point flow of a hybrid nanofluid toward a vertical plate in a saturated porous medium. Case Studies in Thermal Engineering, 27, 101342.

[97] Chu, Y.-M., Khan, M. I., Khan, N. B., Kadry, S., Khan, S. U., Tlili, I., & Nayak, M. K. (2020). Significance of activation energy, bio-convection and magnetohydrodynamic in flow of third grade fluid (non-Newtonian) towards stretched surface: A Buongiorno model analysis. *International Communications in Heat and Mass Transfer*, *118*(104893), 104893. doi:10.1016/j.icheatmasstransfer.2020.104893.

[98] Chu, Y. M., Nazir, U., Sohail, M., Selim, M. M., & Lee, J. R. (2021). Enhancement in thermal energy and solute particles using hybrid nanoparticles by engaging activation energy and chemical reaction over a parabolic surface via finite element approach. *Fractal and Fractional,* 5(3), 119.

[99] Ijaz Khan, M., Qayyum, S., Nigar, M., Chu, Y. M., & Kadry, S. (2020). Dynamics of Arrhenius activation energy in flow of Carreau fluid subject to Brownian motion diffusion. *Numerical Methods for Partial Differential Equations.*

[100] Bhatti, M. M., & Michaelides, E. E. (2021). Study of Arrhenius activation energy on the thermo-bioconvection nanofluid flow over a Riga plate. *Journal of Thermal Analysis and Calorimetry*, *143*(3), 2029–2038. doi:10.1007/s10973-020-09492-3.

[101] Arain, M. B., Bhatti, M. M., Zeeshan, A., & Alzahrani, F. S. (2021). Bioconvection Reiner-Rivlin nanofluid flow between rotating circular plates with induced magnetic effects, activation energy and squeezing phenomena. *Mathematics*, *9*(17), 2139. doi:10.3390/math9172139.

[102] Shahid, A., Huang, H. L., Bhatti, M. M., & Marin, M. (2022). Numerical computation of magnetized bioconvection nanofluid flow with temperature-dependent viscosity and Arrhenius kinetic. *Mathematics and Computers in Simulation*, *200*, 377–392. doi:10.1016/j.matcom.2022.04.032.

[103] Shafiq, A., Sindhu, T. N., & Khalique, C. M. (2020). Numerical investigation and sensitivity analysis on bioconvective tangent hyperbolic nanofluid flow towards stretching surface by response surface methodology. *Alexandria Engineering Journal*, *59*(6), 4533–4548. doi:10.1016/j.aej.2020.08.007.

[104] Shafiq, A., Hammouch, Z., Naz Sindhu, T., & Baleanu, D. (2020). Statistical approach of mixed convective flow of third-grade fluid towards an exponentially stretching surface with convective boundary condition. In *Special Functions and Analysis of Differential Equations* (pp. 307–319). Chapman and Hall/CRC.

[105] Lu, D., Ramzan, M., ul Huda, N., Chung, J. D., & Farooq, U. (2018). Nonlinear radiation effect on MHD Carreau nanofluid flow over a radially stretching surface with zero mass flux at the surface. *Scientific Reports*, *8*(1). doi:10.1038/s41598-018-22000-w.

[106] Amanulla, C. H., Wakif, A., Boulahia, Z., Suryanarayana Reddy, M., & Nagendra, N. (2018). Numerical investigations on magnetic field modeling for Carreau non-Newtonian fluid flow past an isothermal sphere. *Journal of the Brazilian Society of Mechanical Sciences and Engineering*, *40*(9). doi:10.1007/s40430-018-1385-0.

[107] Khan, I., Shafquatullah, Malik, M. Y., Hussain, A., & Khan, M. (2017). Magnetohydrodynamics Carreau nanofluid flow over an inclined convective heated stretching cylinder with Joule heating. *Results in Physics*, *7*, 4001–4012. doi:10.1016/j.rinp.2017.10.015.

[108] Khan, I., Ullah, S., Malik, M. Y., & Hussain, A. (2018). Numerical analysis of MHD Carreau fluid flow over a stretching cylinder with homogenous-heterogeneous reactions. *Results in Physics*, *9*, 1141–1147. doi:10.1016/j.rinp.2018.04.022.

[109] Sardar, H., Khan, M., & Ahmad, L. (2019). Local non-similar solutions of convective flow of Carreau fluid in the presence of MHD and radiative heat transfer. *Journal of the Brazilian Society of Mechanical Sciences and Engineering*, *41*(2). doi:10.1007/s40430-018-1561-2.

[110] Salahuddin, T., Hussain, A., Malik, M. Y., Awais, M., & Khan, M. (2017). Carreau nanofluid impinging over a stretching cylinder with generalized slip effects: Using finite difference scheme. *Results in Physics*, *7*, 3090–3099. doi:10.1016/j.rinp.2017.07.036.

[111] Bhatti, M. M., Ellahi, R., Zeeshan, A., Marin, M., & Ijaz, N. (2019). Numerical study of heat transfer and Hall current impact on peristaltic propulsion of particle-fluid suspension with compliant wall properties. *Modern Physics Letters. B, Condensed Matter Physics, Statistical Physics, Applied Physics*, *33*(35), 1950439. doi:10.1142/s0217984919504396.

[112] Bovand, M., Rashidi, S., Esfahani, J. A., Saha, S. C., Gu, Y. T., & Dehesht, M. (2016). Control of flow around a circular cylinder wrapped with a porous layer by magnetohydrodynamic. *Journal of Magnetism and Magnetic Materials*, *401*, 1078–1087. doi:10.1016/j.jmmm.2015.11.019.

[113] Bhatti, M. M., Riaz, A., Zhang, L., Sait, S. M., & Ellahi, R. (2021). Biologically inspired thermal transport on the rheology of Williamson hydromagnetic nanofluid flow with convection: an entropy analysis. *Journal of Thermal Analysis and Calorimetry*, *144*(6), 2187–2202. doi:10.1007/s10973-020-09876-5.

[114] Bhatti, M. M., Riaz, A., Zhang, L., Sait, S. M., & Ellahi, R. (2021). Biologically inspired thermal transport on the rheology of Williamson hydromagnetic nanofluid flow with convection: an entropy analysis. *Journal of*

Thermal Analysis and Calorimetry, *144*(6), 2187–2202. doi:10.1007/s10973-020-09876-5.

[115] Zhang, L., Arain, M. B., Bhatti, M. M., Zeeshan, A., & Hal-Sulami, H. (2020). Effects of magnetic Reynolds number on swimming of gyrotactic microorganisms between rotating circular plates filled with nanofluids. *Applied Mathematics and Mechanics*, *41*(4), 637–654. doi:10.1007/s10483-020-2599-7.

[116] Fosdick, R. L., & Rajagopal, K. R. (1980). Thermodynamics and stability of fluids of third grade. *Proceedings of the Royal Society of London*, *369*(1738), 351–377. doi:10.1098/rspa.1980.0005.

[117] Rashidi, M. M., Hayat, T., Keimanesh, M., & Hendi, A. A. (2013). New analytical method for the study of natural convection flow of a non-Newtonian fluid. *International Journal of Numerical Methods for Heat & Fluid Flow*, *23*(3), 436–450. doi:10.1108/09615531311301236.

[118] Bhatti, M. M., & Michaelides, E. E. (2021). Study of Arrhenius activation energy on the thermo-bioconvection nanofluid flow over a Riga plate. *Journal of Thermal Analysis and Calorimetry*, *143*(3), 2029–2038. doi:10.1007/s10973-020-09492-3.